CALIFORNIA INSTITUTE OF TECHNOLOGY

ELECTRON TUBE AND MICROWAVE LABORATORY

BANDWIDTH LIMITATIONS AND SYNTHESIS PROCEDURES FOR NEGATIVE RESISTANCE AND VARIABLE REACTANCE AMPLIFIERS

by

Richard M. Aron

Technical Report No. 15

August 1960

A REPORT ON RESEARCH CONDUCTED UNDER

CONTRACT WITH THE OFFICE OF NAVAL RESEARCH

BANDWIDTH LIMITATIONS AND SYNTHESIS PROCEDURES FOR NEGATIVE RESISTANCE AND VARIABLE REACTANCE AMPLIFIERS

by

Richard M. Aron

Technical Report 15

CALIFORNIA INSTITUTE OF TECHNOLOGY
Pasadena, California

A Technical Report to the Office of Naval Research

Contract Nonr 220(13)

August 1960

ABSTRACT

The bandwidth limitation on the reflection coefficient of circuits containing a reactance limited negative conductance such as a tunnel diode is derived, and the insertion loss method of modern network theory is adapted to the synthesis of low pass ladder equivalents of amplifiers containing these elements. Amplifiers which have a considerable bandwidth advantage over simple single tuned circuits, and which approach the ultimate bandwidth limit as rapidly as possible as the number of passive components is increased, are demonstrated.

Fundamental bandwidth limitations of three-frequency nonlinear reactance amplifiers, parametric amplifiers, and non-inverting upconverters are also found. A low pass ladder equivalent circuit and the insertion loss method are shown to be useful tools for synthesis of these amplifiers. Considerable bandwidth advantage over single-tuned circuits is again demonstrated. Syntheses which yield the ultimate bandwidth as the number of circuit elements is increased are found.

These synthesis methods and the reverse predistortion technique are used to synthesize stable amplifiers whose bandwidth capability increases almost linearly with the number of active elements employed.

Relationships between physically achievable amplifier circuits and the low pass equivalents are shown, and the general compatibility of presently available active elements with these circuits is considered.

TABLE OF CONTENTS

Partial list of symbols and subscripts i

I Introduction 1

1.1 The Tunnel Diode and Other Negative Resistance Devices 3

1.2 Nonlinear Reactance Amplifiers 7

1.3 The Lossless Low Pass Ladder Network 9

II Ladder Networks with Tunnel Diodes in Terminations 11

2.0 Introduction 11

2.1 Ladder Network Synthesis Procedure--A Review 16

2.2 Normalized Bandwidth of Basic Ladder Network with One Active Termination 23

2.3 Four Low Pass Amplifier Configurations 31

2.4 Three Configurations with Tunnel Diodes in Both Terminations 45

2.5 Band Pass Equivalents 50

2.6 Sensitivity to Element Variation and Approximate Loss Calculations 56

2.7 Warm Up Stability 62

2.8 Compatibility of Tunnel Diode Packaging Elements with Basic Configurations 69

III Gain and Bandwidth in Nonlinear Reactance Amplifiers 77

3.0 Introduction 77

3.1 Basic Equations of Nonlinear Reactance Amplifiers 78

3.2 Required Symmetry and Ladder Network Representation 90

3.3 Physical Configurations which Approximate Low Pass Ladder Networks in One or Two Frequency Bands 95

3.4 The Non-Inverting Upconverter 103

3.5 Fundamental Parametric Amplifier Bandwidth Limitations 108

3.6 Degenerate and Pseudo-Degenerate Cases 116

3.7 Some Non-Degenerate Cases 127

3.8 Comparison of Non-Degenerate and Pseudo-Degenerate Results 132

3.9 Configurations and Noise Figure 134

IV Synthesis of Negative Resistance Amplifiers with Several Active Elements by Predistortion 139

4.0 Introduction 139

4.1 Integral Limitations and Noise Figure 144

4.2 Uniform Predistortion Synthesis of Tunnel Diode Bandpass Amplifiers 152

4.3 Predistortion Synthesis of Multi-Element Parametric Amplifiers 166

V Summary and Suggestions for Further Work 172

References 176

Partial List of Symbols

A	power attenuation ratio
η	modulation factor for sinusoidal reactance
B	noise bandwidth
C	capacitance or capacitive reactance slope
C_T	differential capacitance of tunnel diode or an equivalent reactance limited element
df	small frequency interval
ϵ	Tchebysheff ripple factor
F	noise figure
G	conductance
$-G_T$	differential conductance of a tunnel diode or equivalent active element
I	complex current coefficient
K	Boltzmann factor in noise expressions
L	inductance or inductive reactance slope
L_p	series inductance of a tunnel diode
ω	angular frequency
ω_c	angular bandwidth not specifically connected with a single response function
ω_B	Butterworth angular bandwidth
ω_T	Tchebysheff angular bandwidth
ω_o	signal frequency of time varying reactance amplifier
$\omega_i = \omega_{+1}$	idler frequency of non-inverting upconverter
ω_{-1}	idler frequency of parametric amplifier (negative)
Ω_p	angular frequency of time varying reactance
$\Omega_o, \Omega_i, \Omega_{+1}, \Omega_{-1}$	band center frequencies of $\omega_o, \omega_i, \omega_{+1}$, and ω_{-1} bands
P_G	power gain

q	charge or complex charge coefficient
q_o	normalized loss factor of elements in a uniform loss network
ρ	voltage reflection coefficient
ρ_{Bo}	midband Butterworth ρ
ρ_{To}	midband Tchebysheff ρ
$\overline{\rho}_T$	RMS Tchebysheff ρ over the equal ripple band
$s = i\omega$	complex angular frequency variable
s_{pm}	complex location of m^{th} pole
s_{on}	complex location of n^{th} zero
T	transmission, voltage gain between two elements normalized so that $\|T\|^2$ is power gain
T' or T_q	transmission under positive or negative loss conditions
$\overline{T}_T$	RMS Tchebysheff T over the equal ripple band
τ	noise temperature
τ_s	source noise temperature
V	complex voltage coefficient
Y	admittance
Y_c	characteristic admittance
Z	impedance
Z_c	characteristic impedance

Partial List of Subscripts

A, A' B, B' C, C' D	tunnel diode amplifier types
B	Butterworth
c	characteristic
G	gain
T	tunnel diode or Tchebysheff
L	load
p	pump, pole
s	source

CHAPTER I

INTRODUCTION

The recent discovery of the tunnel diode and the maser, and the re-emergence of the principles of parametric amplification with nonlinear reactances have led to a reconsideration of the performance capability of negative resistance amplifiers. The characteristics of available nonlinear reactors and negative resistance devices serve as boundary conditions limiting the performance of systems containing them. There is a need to translate these characteristics into equations and tables in order to facilitate their engineering application. In the past attention has been focused mainly on noise performance. This present work places the analytic emphasis on bandwidth in attempting to give a theoretical but practical evaluation of the system performance of these devices in terms of gain, bandwidth, noise figure, and circuit complexity.

The approach here is to give first order synthesis procedures for designing wide band amplifiers. Only physical amplifier configurations which allow synthesis in terms of simple low-pass ladder equivalent circuits are considered. In each problem presented the relation between the basic low pass ladder equivalent circuit and the physical configuration of an amplifier is pointed out. This should be sufficient to allow the first order design of a physical amplifier from a knowledge of the elements in the low pass equivalent.

In no case in this work, however, is the synthesis of a low pass equivalent ever carried to the point where all its elements are determined. The object is to obtain as much information as possible

about the bandwidth capabilities of the active elements. In this light, only those parameters of the equivalent circuit which correlate explicitly with the essential properties of the active elements are actually calculated. The physical realizability of the other elements required in the equivalent circuit is guaranteed indirectly by the synthesis technique used.

For the design engineer then, the synthesis problem still lies ahead. He can only find here synthesis procedures to be used and the results he may obtain in terms of the properties of the active elements and circuit complexity. It is hoped that the information contained in this work will increase his understanding of the capabilities of tunnel diode and nonlinear reactance amplifiers. It is also hoped that the results given will allow him to make a good preliminary choice of an amplifier configuration which will meet his first order requirements in terms of bandwidth and noise figure. He will then be in a position to do an intensive analysis and synthesis directly in terms of a single configuration. In doing this he can remove any approximations which have been required in this more extensive than intensive work to treat physical truths with mathematical simplicity.

A brief review of basic information on negative resistance and nonlinear reactance amplifiers is presented here first. Some of the problems which will be approached in succeeding chapters are suggested, and some reason for the choice of the low pass ladder network formalism is given.

1.1 The Tunnel Diode and Other Negative Resistance Devices

The tunnel diode (1,2) is a very heavily doped semiconductor P-N junction. Under low forward bias conditions, current carrying electrons may traverse the depletion layer which is normally forbidden to them on energy band considerations, by quantum mechanical tunneling. A typical current voltage characteristic arising from the process is shown in Figure 1.1. The shape of this curve and the resulting differential negative conductance have no theoretical frequency variation for frequencies under 10^{+13} cps. The high doping levels and extremely narrow depletion layer give rise to appreciable capacitance in parallel with the effective conductance of the junction. This capacitance is the essential bandwidth limiting factor of this device. Taking into account ohmic losses and series inductance arising in packaging, we use the equivalent circuit shown in Figure 1.2 for the tunnel diode (2). The noise generator I_{TN}^2 in parallel with $-G_T$ has been found experimentally to be correctly given by the shot noise formula (3)

$$I_{TN}^2 = 2e\, I_o\, df \tag{1.1}$$

Several other negative resistance devices such as the maser and the reflex klystron have models which are bandpass equivalents of the internal tunnel diode. The analogies are close enough so that no more need be said about them.

The negative conductance can be used as a two-terminal amplifier. However, the maximum gain bandwidth is always achieved by isolating the generator from the load with a circulator. Under these conditions

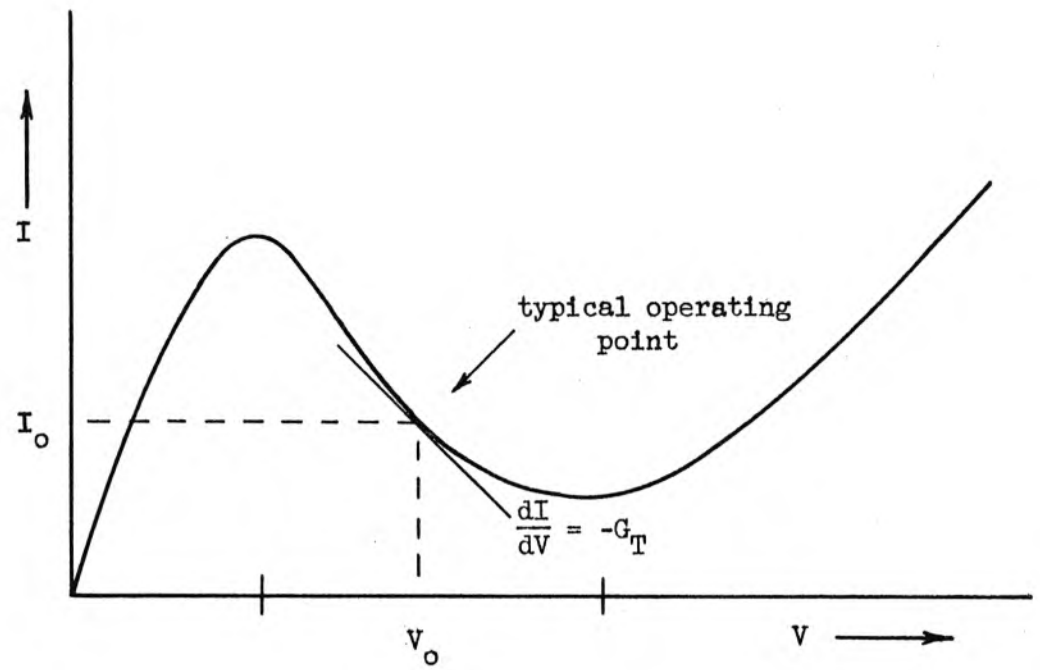

Figure 1.1 Typical current voltage characteristics of a tunnel diode

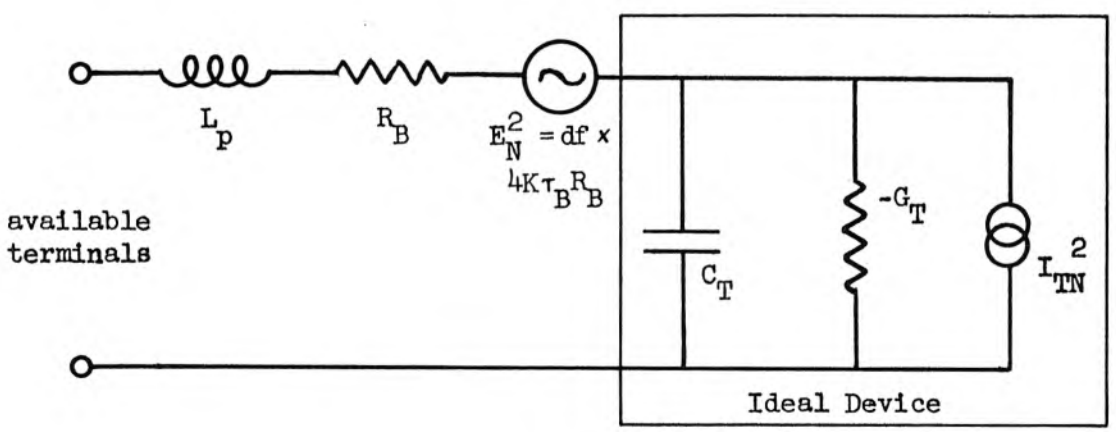

Figure 1.2 An equivalent circuit of a tunnel diode

the power reflection coefficient

$$\rho\rho^* = \left| \frac{Y_o^* - Y}{Y_o + Y} \right|^2 \tag{1.2}$$

defined at the negative conductance is the power gain. Under single tuning conditions the shunt capacitance of the tunnel diode limits the half power gain bandwidth of the reflection to

$$\omega_{3DB} \cong \frac{2G_T}{C_T} \frac{1}{|\rho_o|} \tag{1.3}$$

giving rise to the common voltage gain-bandwidth product. As will be shown in Chapter II, a more fundamental limitation on bandwidth is (4,5) $\int_0^\infty \ell n\ |\rho|\ d\omega = \frac{\pi G_T}{C_T}$. One can predict, then, a maximum bandwidth for constant reflection ρ_o,

$$\omega_c = \frac{\pi G_T}{C_T} \frac{1}{\ell n\ \rho_o} \tag{1.4}$$

The disparity between equations 1.3 and 1.4 is the motivation for the wideband tunnel diode amplifier syntheses in Chapter II. In this chapter amplifiers with and without circulators are considered and the bandwidth and noise figure properties of several configurations are discussed. Fundamental limitations and practical difficulties due to the series inductance of the tunnel diode package are also presented and discussed in Chapter II.

In many potential applications the ultimate bandwidth of a single tunnel diode may be too small at the required gain level. One must then think of amplifiers containing multiple active elements. While single negative conductance amplifiers containing perfect circulators may be easily cascaded, it is more difficult in general to guarantee the

stability of a cascade of stages containing only reciprocal elements. One approach taken by Carlin (6) involves the synthesis of amplifier stages whose input and output characteristic impedancesare real and constant at all frequencies, so-called constant resistance networks. He has shown that each stage has a power gain bandwidth integral limitation

$$\int_0^\infty \ell n\, P_G^{1/2}\, d\omega \leq \frac{\pi G_T}{2C_T} \tag{1.5}$$

These so-called constant resistance stages will not be simple configurations such as ladder networks or their band pass equivalents. They must be networks of the lattice or twin or shunt tee variety, and may be physically difficult to achieve at high frequencies. In addition, they must contain at least two conductances. If one of these is required to be passive, it may have a seriously degrading effect on the noise figure.

Another approach commonly taken to the multiple element problem is the design of iterative circuits by image parameter theory. This technique, however, lends itself better to analysis than to synthesis procedures. The gain or transmission of the overall circuit including terminations may be evaluated in terms of the propagation constant and characteristic impedance of the basic section which are simply calculated. The reverse or synthesis process, however, cannot be carried out except by trial and error, making the terminating sections difficult to design.

In Chapter IV a synthesis of multiple element amplifiers by "negative predistortion", a technique suggested by Weinberg (7) is

considered. Syntheses which give 60% of the bandwidth limitation given in equation 1.5 are found and the method is apparently capable of achieving the full integral limitation. The problems arising from reflections in these circuits as well as the noise figure properties are also discussed. The synthesis is in terms of band pass ladder networks which contain one tunnel diode per section. These are definitely simpler than Carlin's networks and should be physically achievable in all frequency ranges.

1.2 Nonlinear Reactance Amplifiers

The power flow relations for a nonlinear reactance in the presence of excitation at two frequencies whose ratio is an irrational fraction, and all the multiple sum and difference frequencies have been given by Manley and Rowe (8). In Chapter III we will consider two devices in which only three of this infinite set are of major importance. In both cases Ω_p will be considered the pump frequency supplied by a local oscillator. The signal frequency, $\omega_o < \Omega_p$ as well as Ω_p, are considered positive, while the third frequency may be either positive, $\omega_{+1} = \omega_o + \Omega_p$ or negative, $\omega_{-1} = \omega_o - \Omega_p$, depending on whether the device is to be called, respectively, a non-inverting upconverter or a parametric amplifier.

The non-inverting upconverter obeys the power relations

$$\frac{P_o}{\omega_o} = -\frac{P_{+1}}{\omega_{+1}}$$

$$\frac{P_o}{\omega_o} = \frac{P_p}{\Omega_p} \qquad (1.6)$$

The device is unconditionally stable when imbedded in a linear passive network and may give a maximum power gain

$$P_G = \frac{\omega_{+1}}{\omega_o} = \frac{\omega_o + \Omega_p}{\omega_o} \tag{1.7}$$

It is essentially a two port amplifier. The nonlinear reactance used as a three frequency parametric amplifier obeys the power relations

$$\frac{P_o}{\omega_o} = -\frac{P_{-1}}{\omega_{-1}}$$
$$\frac{P_o}{\omega_o} = -\frac{P_p}{\Omega_p} \tag{1.8}$$

The fact that P_o and P_{-1} may be simultaneously negative allows unlimited gain. In circuit terms this capability must appear as a negative real part to the input immittance at the reactance terminals at both ω_o and ω_{-1}.

The discussions of nonlinear reactance amplifiers in this work are restricted to circuits containing nonlinear capacitances or elastances whose time variation due to the pump excitation at Ω_p is explicitly defined as

$$C_o(1 + \eta \cos \Omega_p t + \theta_p)$$

or

$$S_o(1 + \eta \cos \Omega_p t + \theta_p) .$$

The choice as to which of these representations is best suited to a given physical nonlinear reactance will depend on whether the parasitic and packaging elements fit better into a parallel or series equivalent circuit. The nonlinear capacitance of the back biased semiconductor

diode, for instance, is usually associated with series inductance and resistance and the S_o representation will be preferable. Results for the two other types of nonlinear reactances can be obtained from a consideration of these two and the application of the duality principle. One may expect the bandwidth of parametric amplifiers and upconverters to be limited in some way by the D.C. parameter C_o or S_o. In Chapter III the same assumptions which are made by virtually all workers in the field of three frequency parametric amplifiers and upconverters lead to equivalent circuits for these devices. It is shown that the parametric amplifier does have a gain bandwidth limitation in the form of equation 1.4. It is also shown that under some circumstances it may be treated with complete analogy to the tunnel diode, but that these conditions do not necessarily lead to a synthesis that gives the greatest possible bandwidth for the least circuit complexity. In Chapter IV the conditions under which multiple element parametric amplifiers can be synthesized by negative predistortion are related.

1.3 The Lossless Low-Pass Ladder Network

The lossless low-pass ladder network has many advantages as a basis for synthesis. It and its equivalents are realizable either exactly or approximately in any frequency range with lumped, semi-distributed and mixed elements. One bandpass approximant, the coupled resonator circuit, can be built with coupled cavities or loaded transmission lines and waveguides for operation at very high frequencies. In addition the coupled resonator circuit allows a useful and somewhat arbitrary impedance level transformation not achievable in other circuits. The second major advantage of the lossless ladder network in

design is the fact that the synthesis may be carried out simply and directly starting from the poles or zeros of a desired response function. Physical realizability and stability arguments will remove any arbitrary choices in most of the active networks. The simplicity of the method will become clear in Section 2.1.

An infinite variety of response functions are of course achievable in ladder networks. Certain response shapes, however, have been proven optimum for achieving desirable gain versus frequency relations with the least circuit complexity. In some cases these optimum response functions are also optimum for approaching the reflection coefficient bandwidth limitations most rapidly as a function of circuit complexity.

CHAPTER II

LADDER NETWORKS WITH TUNNEL DIODES IN TERMINATIONS

2.0 Introduction

The bandwidth over which gain can be obtained from a tunnel diode can be associated qualitatively with the bandwidth over which its essential reactance can be canceled by an external immittance. The accuracy required of this cancellation must depend in some measure on the gain desired. The ladder network has been successfully applied in the past to impedance matching problems involving the cancelation of reactance associated with passive conductances (9). This success, plus the fact that the well known methods of passive ladder network synthesis can be applied to the active network problem, suggests the synthesis of tunnel diode amplifiers from the basic low pass configurations shown in Figure 2.1 A,B,C and D.

The power gain of all these configurations may be associated with the reflection and transmission power gains of the low pass circuit shown in Figure 2.2 A and B. This circuit provides a unified approach to the synthesis of the networks in the four basic configurations. In addition practical questions of stability, stability under variation of the circuit elements, and "warm up" stability, may be answered in terms of the basic circuit. The transformation of this basic low pass circuit into a band pass equivalent aids in the construction of the band pass equivalents of the four amplifier configurations.

The unification provided by the basic network does not extend to the calculation of amplifier noise figure. This will be done separately for the various configurations. The reciprocity theorem (10) for networks containing bilateral elements will prove of extreme utility. This

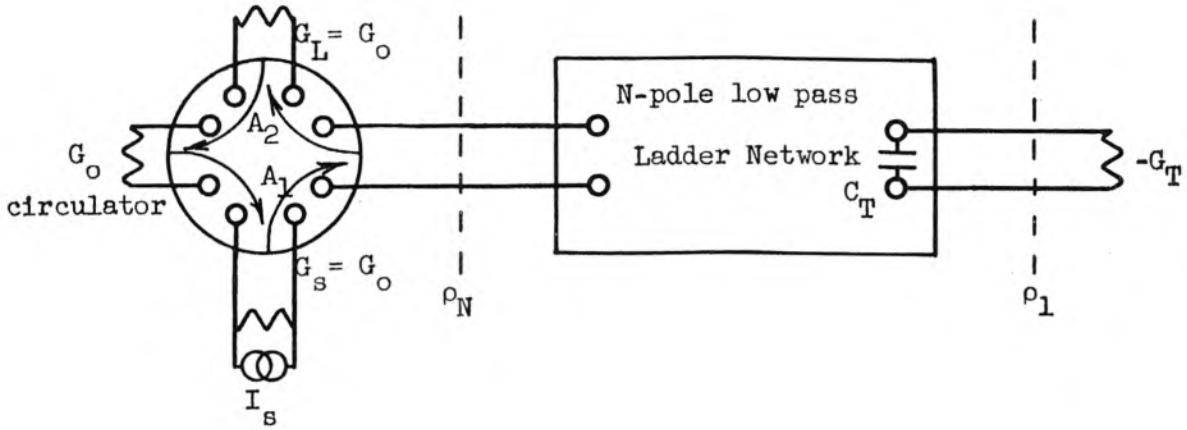

A. Reflection amplifier with circulator

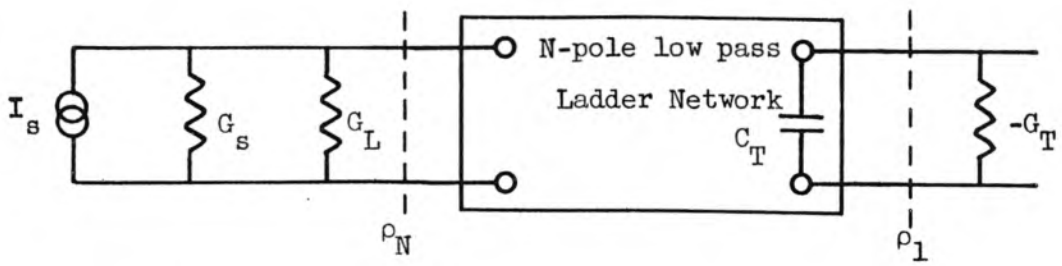

B. Bilateral reflection amplifier

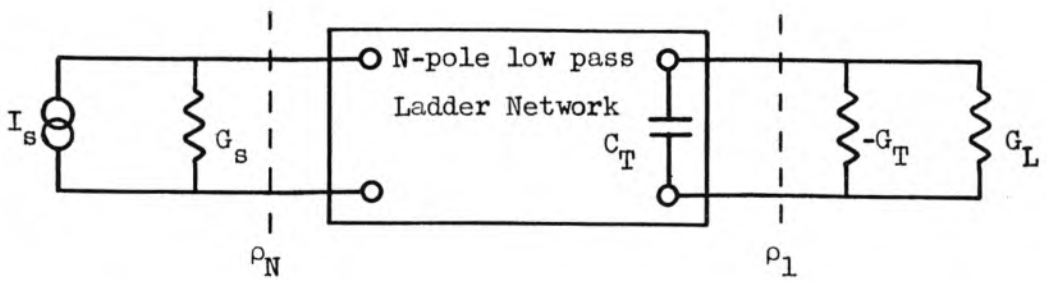

C. Transmission amplifier, load in parallel with tunnel diode

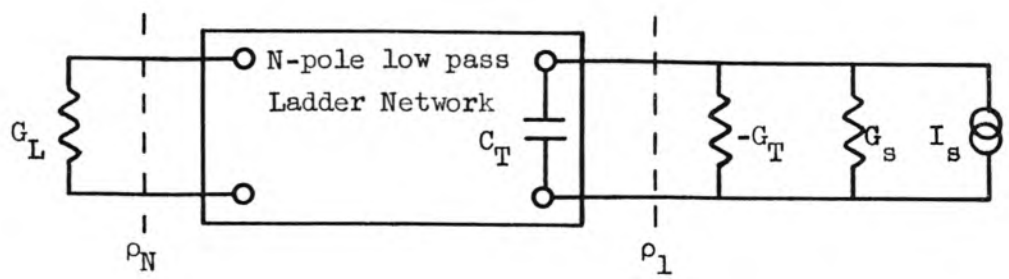

D. Transmission amplifier, source in parallel with tunnel diode

Figure 2.1 Four low-pass ladder network amplifiers containing a tunnel diode in one termination

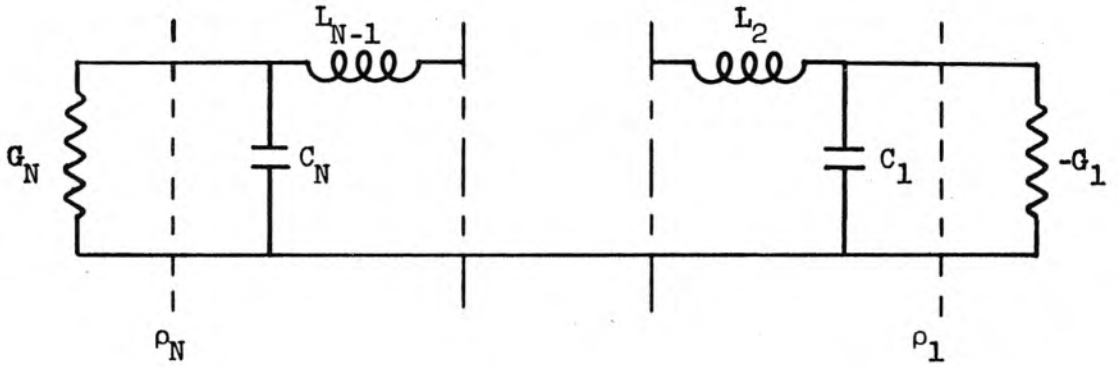

Figure 2.2a Basic low pass ladder network with an odd number of reactive elements

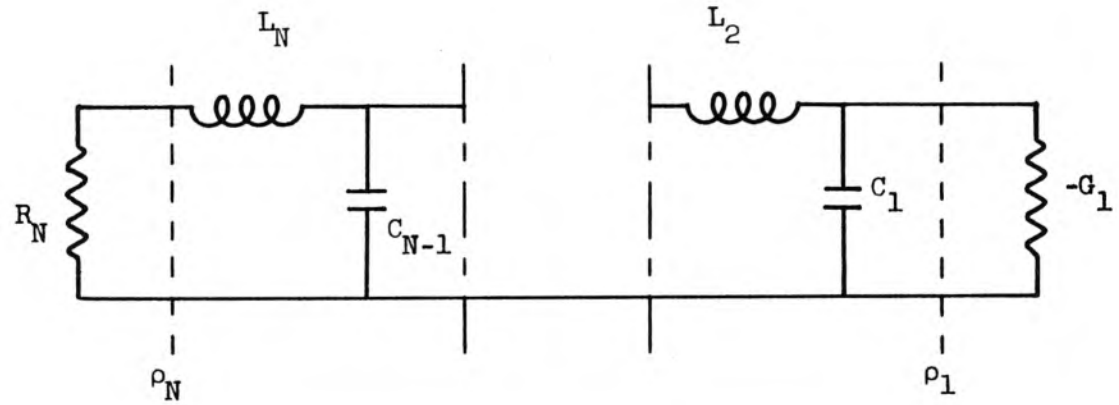

Figure 2.2b Basic low pass ladder network with an even number of reactive elements

theorem states that the ratio of power delivered to resistor 1 to power available from resistor 2, P_{G12}, is equal to the ratio of power delivered to resistor 2 to power available from resistor 1, P_{G21}.

$$P_{G12} = P_{G21} \tag{2.1}$$

While the power available in a frequency range df from a passive conductance at temperature τ_R is well known to be $K\tau_R\, df$, a definition may also be made for negative conductances through the artificial use of an impedance negator as shown in Figure 2.3 A and B. The power flowing out of the impedance negator is the negative of the power flowing out of its termination. It is therefore appropriate to associate with $-G_T$ and I_{TN}^2 a negative available noise power

$$\frac{1}{-4G_T}\frac{dI_{TN}^2}{df}\,df = K(-\tau_T)df$$

$$\tau_T = \frac{dI_{TN}^2}{df}\frac{1}{4K\,G_T} \tag{2.2}$$

While the basic circuit approach deals with an idealized tunnel diode containing only a negative conductance $-G_T$ in parallel with a capacitance C_T, presently available tunnel diodes also have series inductance and resistance associated with packaging and bulk material resistivity. The last section of this chapter will consider the compatibility of these elements with the basic configurations as well as any new fundamental limitations which the inductance places on tunnel diode amplifiers.

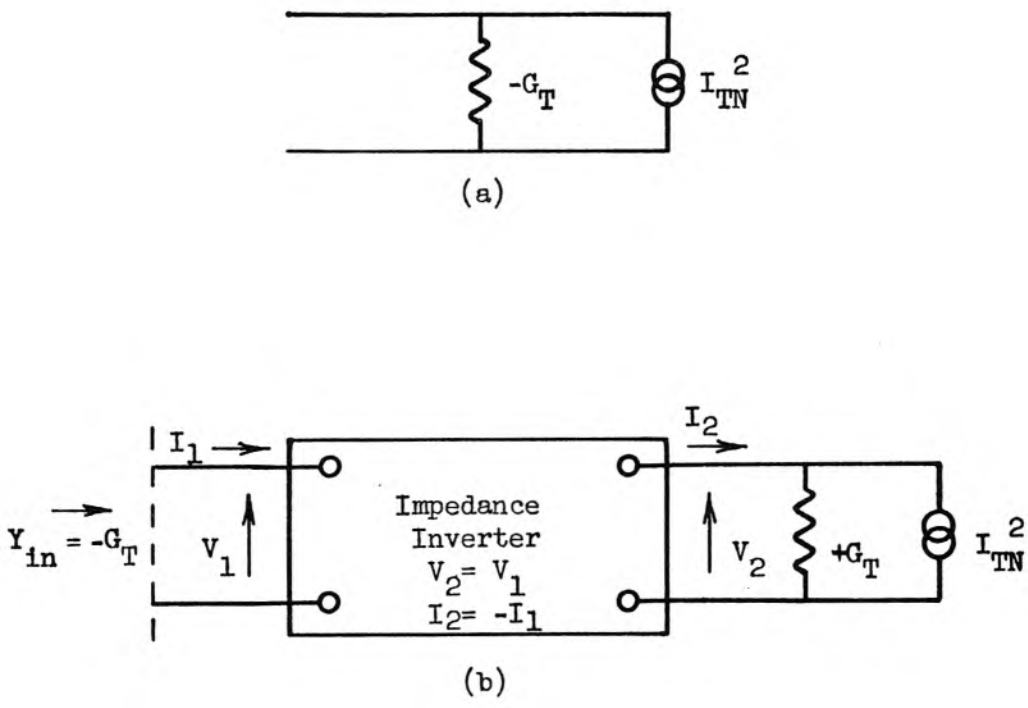

Figure 2.3 Illustrating the equivalence between

(a) a noisy negative conductance, and

(b) a noiseless impedance negator terminated in a noisy positive conductance

2.1 Ladder Network Synthesis Procedure--A Review

Before considering the analysis of the basic network in Figure 2.2, let us review some of the nomenclature and techniques of ladder network synthesis (11). Transmission gain is defined as the ratio of power delivered to one termination to power available from another and is written as

$$T(i\omega)\ T(-i\omega) = T(s)\ T(-s)\Big|_{i\omega} \tag{2.3}$$

The ratio of power reflected to power available from a termination is

$$\rho(i\omega)\ \rho(-i\omega) = \rho(s)\ \rho(-s)\Big|_{i\omega} \tag{2.4}$$

The reflection coefficient between arbitrary admittances Y_a and Y_b must be defined as

$$\rho(i\omega) = \frac{Y_a^*(i\omega) - Y_b(i\omega)}{Y_a(i\omega) + Y_b(i\omega)} \tag{2.5}$$

and is analytic in the s plane only when Y_a is real. When Y_a is not real analyticity may be restored by writing Y_a and Y_b as ratios of polynomials in $i\omega$ and removing any phase rotation factors:

$$\begin{aligned}\rho(i\omega) &= \frac{\dfrac{N_a^*(i\omega)}{D_a^*(i\omega)} - \dfrac{N_b(i\omega)}{D_b(i\omega)}}{\dfrac{N_a(i\omega)}{D_a(i\omega)} + \dfrac{N_b(i\omega)}{D_b(i\omega)}} \\ &= \frac{N_a(-s)\ D_b(s) - N_b(s)\ D_a(-s)}{N_a(s)\ D_b(s) + N_b(s)\ D_a(s)}\Bigg|_{i\omega} \quad \frac{D_a(i\omega)}{D_a^*(i\omega)}\end{aligned} \tag{2.6}$$

For lossless networks conservation of energy yields

$$\rho(s)\ \rho(-s)\Big|_{i\omega} + \ T(s)\ T(-s)\Big|_{i\omega} = \ 1 \tag{2.7}$$

and therefore for all values of s

$$\rho(s)\ \rho(-s) + T(s)\ T(-s) \ = \ 1 \tag{2.8}$$

The reciprocity theorem indicates that $T(i\omega)\ T(-i\omega)$ is the same in either direction when the network contains bilateral elements. When one of the terminations of the ladder network is negative, $T(i\omega)\ T(-i\omega)$ must also be negative. To avoid confusion, however, the sign and absolute value will be used here.

Equation 2.6 greatly simplfies the synthesis of lossless ladders operating between passive terminations by giving $\rho(i\omega)$ almost directly in terms of the transmission gain. Equation 2.5 gives

$$\frac{Y_b}{Y_a} = \frac{1 - \rho(s)}{1 + \rho(s)} \tag{2.9}$$

when Y_a is real, and the continued fraction expansion of Y_b/Y_a yields directly the ladder network elements normalized to Y_a. Some choice must be exercised in choosing the poles and zeros of $\rho(s)$. In networks with passive terminations the numbers of poles and zeros of $\rho(s)$ are equal and must equal the number of reactances to appear in the low pass ladder. The elements of the ladder will be physically realizable if all the poles of $\rho(s)$ are in the left half plane, LHP, but its zeros can be chosen anywhere. In all cases the zeros of $\rho(s)$ defined at one termination are the negatives of the zeros of $\rho(s)$ defined at the other termination. Equation 2.5 can be used to show that the change in the sign of a termination simply inverts the reflection coefficient and interchanges the poles and zeros.

$$\frac{Y_a^* - Y_b}{Y_a + Y_b} \xrightarrow{Y_a^* \to -Y_a} \frac{Y_a + Y_b}{Y_a^* - Y_b} \tag{2.10}$$

Thus, the zeros of the reflection coefficient at the active element must be chosen in the LHP to guarantee that all other network elements are positive. The poles of $\rho(s)$ are arbitrary but must be chosen in the LHP for stability.

It was indicated in the introduction that the bandwidth limitation on the reflection coefficient at a negative conductance $-G$ in parallel with a capacitance C obeys the limitation

$$\int_0^\infty \ell n \, |\rho(\omega)| \, d\omega = \frac{\pi G}{C} \tag{2.11}$$

The frequency range over which ρ is large can be maximized by minimizing the contribution of $\ell n \, \rho(\omega)$ to the integral elsewhere. Thus outside the desired bandwidth of the reflection it is desirable to have

$$|\rho(\omega)|^2 = 1 \qquad |T(\omega)|^2 = 0 \tag{2.12}$$

Fortunately, something is known of synthesizable response functions which have desirable properties in the light of equations 2.11 and 2.12. Of all transmission response functions synthesizable with an N pole ladder network, the Tchebysheff transmission response has the property that it gives the fastest possible rate of cutoff of $|T(i\omega)|^2$ outside the passband consistent with a prescribed maximum deviation of $|T(i\omega)|^2$ and $|\rho(i\omega)|^2$ from their maximum values $|T_{To}|^2$ and $|\rho_{To}|^2$ within the passband (12). The Tschebysheff response functions

are written as

$$|T_T(i\omega)|^2 = \frac{|T_{To}|^2}{1 + \epsilon^2 T_N^2(\omega/\omega_T)}$$

$$|\rho_T(i\omega)|^2 = \frac{\rho_{To}^2 + \epsilon^2 T_N^2 (\frac{\omega}{\omega_T})}{1 + \epsilon^2 T_N^2 (\frac{\omega}{\omega_T})} \qquad (2.13)$$

in which

$$T_N^2(\frac{\omega}{\omega_T}) = \cos^2 N \cos^{-1} \frac{\omega}{\omega_T} \qquad \omega < \omega_T$$

$$\cosh^2 N \cosh^{-1} \frac{\omega}{\omega_T} \qquad \omega > \omega_T$$

and

$$T_{To}^2 = 1 - \rho_{To}^2$$

This response is also commonly called equal ripple response with ϵ known as the ripple factor and ω_T the ripple bandwidth. $1 + \epsilon^2 T_N^2(\frac{\omega}{\omega_T})$ is a polynomial of order $2N$ in ω/ω_T. Typical reflection response shapes and pole zero locations for $N = 2$ and 3 are shown in Figure 2.4. Because of its oscillatory nature and because it may lead to extremely nonlinear transmission phase characteristics, the Tchebysheff response is often dismissed in favor of the Butterworth response. This transmission response has the maximum number of zero frequency derivatives at the band center consistent with the number of poles allowed (12). The Butterworth response functions are written as

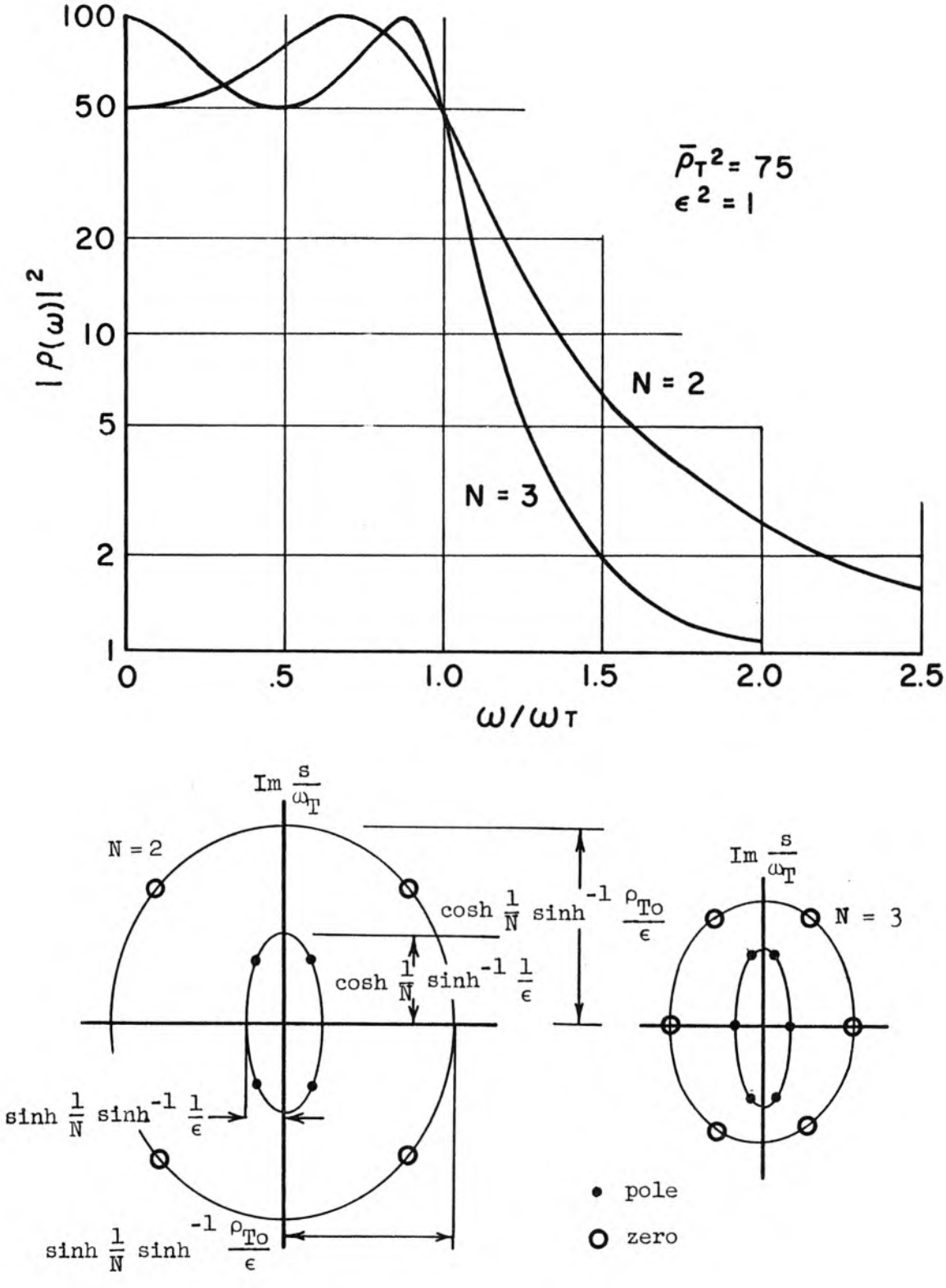

Figure 2.4 Tchebysheff reflection gain versus frequency and pole zero locations for $|\bar{\rho}_T|^2 = 75$, $\epsilon = 1$, N = 2 and 3

$$|T_B(i\omega)|^2 = \frac{|T_{Bo}|^2}{1 + (\frac{\omega}{\omega_B})^{2N}}$$

$$|\rho_B(i\omega)|^2 = \frac{|\rho_{Bo}|^2 + (\frac{\omega}{\omega_B})^{2N}}{1 + (\frac{\omega}{\omega_B})^{2N}} \qquad (2.14)$$

in which $|T_{Bo}|^2 = \left| 1 - |\rho_{Bo}|^2 \right|$. The Butterworth response, also called maximally flat response, is a special case of the Tchebysheff with $\epsilon = 0$. The Butterworth normalization frequency ω_B , however, is the 3 db bandwidth of the transmission function. It may be said of the Butterworth transmission response then, that it has the fastest rate of cutoff at the band edge consistent with the flattest possible gain at midband. Typical Butterworth reflection response characteristics and pole zero locations for $N = 2$ and 3 are shown in Figure 2.5.

The Butterworth and Tchebysheff responses will form the basis for the synthesis not only of the one and two element tunnel diode amplifiers discussed in this chapter but also for the nonlinear reactance amplifiers to be discussed in Chapter III and the multi-element amplifiers to be synthesized in Chapter IV. The analytic expressions for poles and zeros of these response functions will be required for all further work and are given below in equations 2.15 through 2.18 (13).

Butterworth poles:

$$\frac{s_{pBm}}{\omega_B} = (-1)^m \sin(2m+1)\frac{\pi}{2N} + i\cos(2m+1)\frac{\pi}{2N} \qquad (2.15)$$

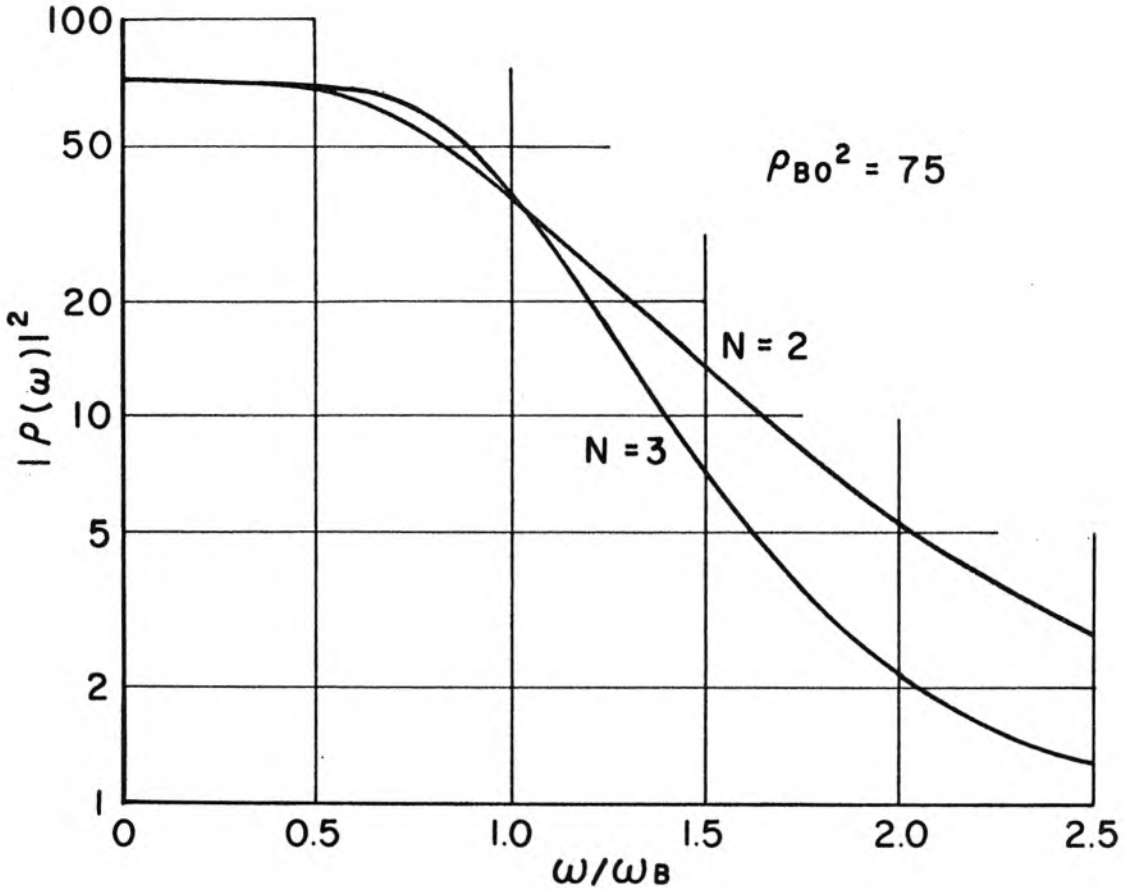

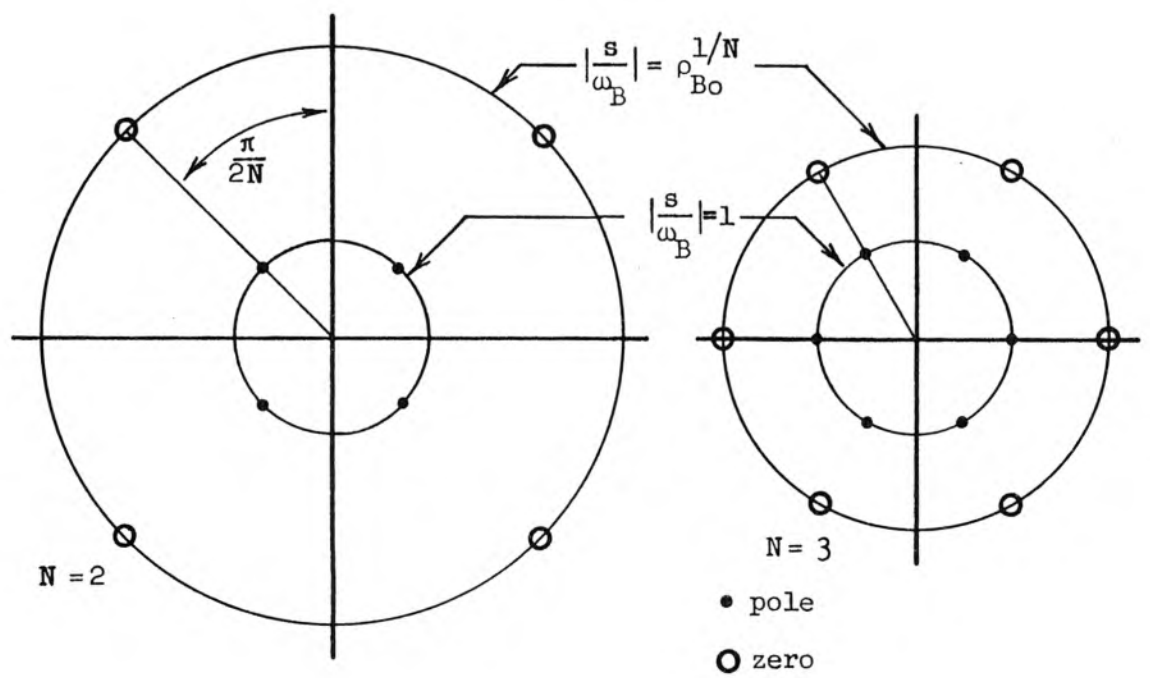

Figure 2.5 Butterworth reflection gain versus frequency and pole zero locations for $|\rho_{Bo}|^2 = 75$, N = 2 and 3

Butterworth reflection zeros:

$$\frac{s_{oBm}}{\omega_B} = \rho_{Bo}^{1/N}\left[(-1)^m \sin(2m+1)\frac{\pi}{2N} + i\cos(2m+1)\frac{\pi}{2N}\right] \tag{2.16}$$

Tchebysheff poles

$$\frac{s_{pTm}}{\omega_T} = \begin{array}{l}(-1)^m\left(\sinh\frac{1}{N}\sinh^{-1}\frac{1}{\epsilon}\right)\left(\sin(2m+1)\frac{\pi}{2N}\right) \\ +j\left(\cosh\frac{1}{N}\sinh^{-1}\frac{1}{\epsilon}\right)\left(\cos(2m+1)\frac{\pi}{2N}\right)\end{array} \tag{2.17}$$

Tchebysheff reflection zeros

$$\frac{s_{oTm}}{\omega_T} = \begin{array}{l}(-1)^m\left(\sinh\frac{1}{N}\sinh^{-1}\frac{\rho_{To}}{\epsilon}\right)\left(\sin(2m+1)\frac{\pi}{2N}\right) \\ +j\left(\cosh\frac{1}{N}\sinh^{-1}\frac{\rho_{To}}{\epsilon}\right)\left(\cos(2m+1)\frac{\pi}{2N}\right)\end{array} \tag{2.18}$$

2.2 Normalized Bandwidth of Basic Ladder Network with One Active Termination

It is appropriate to think of the circuit parameters G_1 and C_1 in the basic low pass ladder network of Figure 2.2 as determining the bandwidth normalization factors ω_B and ω_T since these two elements will be directly associated with the terminations of the four amplifier configurations. The frequency normalization can be found directly from the knowledge of the poles and zeros of $\rho_1(s)$ without carrying out the detailed continued fraction expansion of the ladder by considering the evaluation of $\oint \ell n\,[-\rho_1(s)]ds$ on the two contours shown in Figure 2.6.

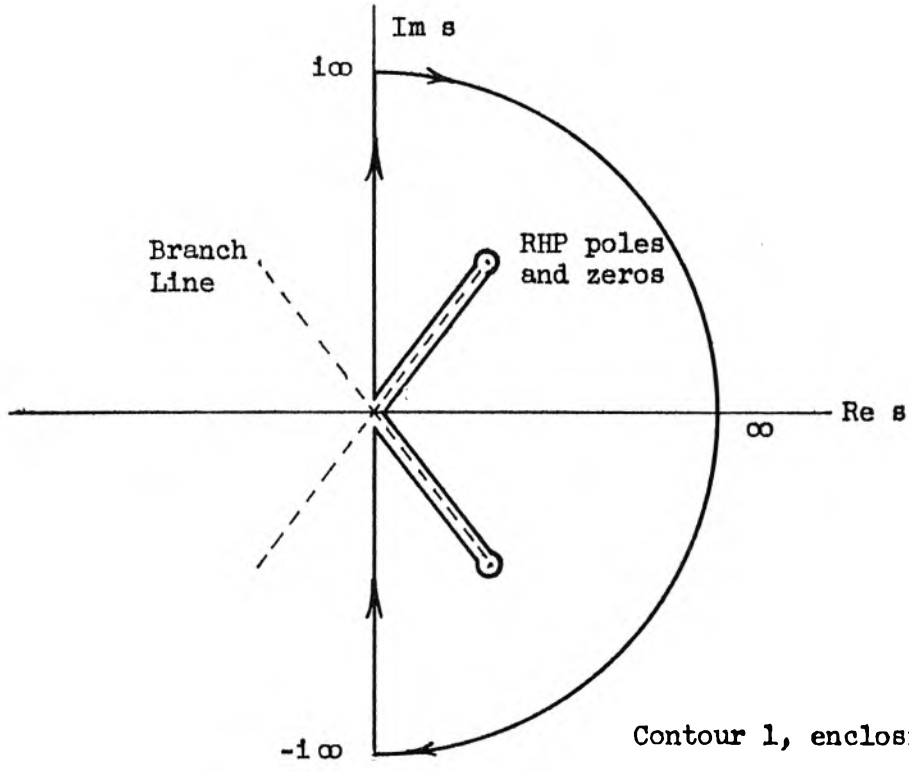

Contour 1, enclosing the RHP

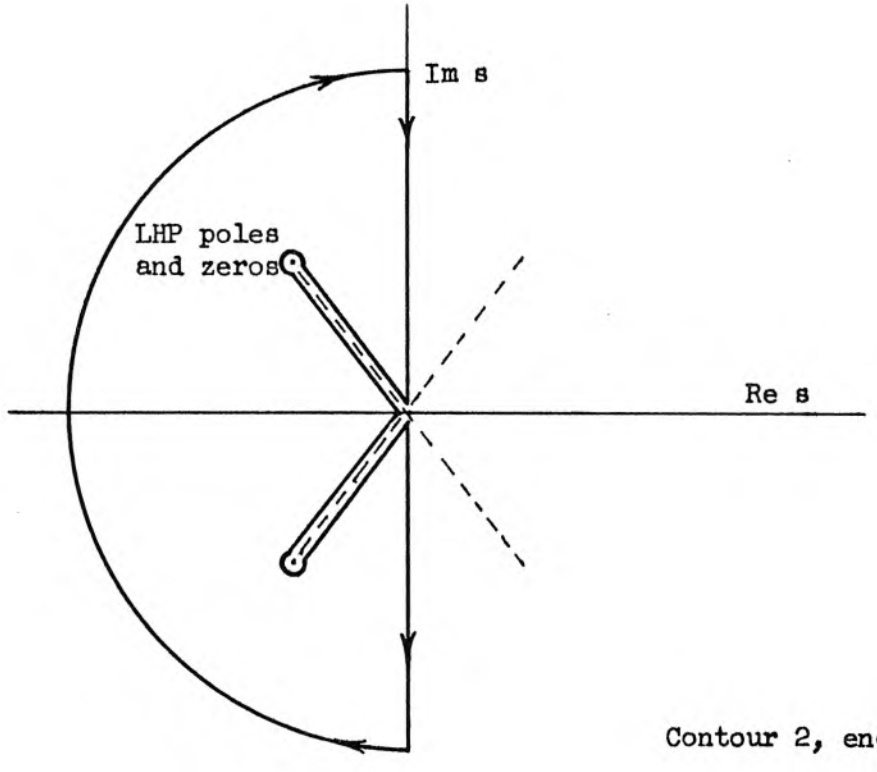

Contour 2, enclosing the LHP

Figure 2.6 Integral contours in s plane for functions with logarithmic singularities

From Figure 2.2 the asymptotic dependence of $\rho_1(s)$ can be evaluated.

$$\lim_{s \to \infty} - \rho_1(s) = \frac{1 + \frac{G_1}{sC_1}}{1 - \frac{G_1}{sC_1}}$$

$$\lim_{s \to \infty} \ell n - \rho_1(s) = \frac{2G_1}{sC_1} \tag{2.19}$$

On contour 1

$$\int_{-i\infty}^{i\infty} \ell n - \rho_1(s) ds = \frac{2\pi i G_1}{C_1} + 2\pi i \sum_{RHP_m} \left(s_{om} - s_{pm} \right) \tag{2.20}$$

Since for stability and physical realizability $\sum_{RHP_m} s_{om} - s_{pm} = 0$, and since $\arg \rho_1$ is an odd function of s, this gives the fundamental limitation

$$\int_0^{\infty} \ell n \left| \rho_1(\omega) \right| d\omega = \frac{\pi G_1}{C_1} \tag{2.21}$$

and on contour 2

$$- \int_{-i\infty}^{i\infty} \ell n - \rho_1(s) ds = \frac{2\pi i G_1}{C_1} + 2\pi i \sum_{LHP_m} \left(s_{om} - s_{pm} \right) \tag{2.22}$$

In Equation 2.22 the left half plane singularities of $\rho_1(s)$ appear and are taken as negative. The addition of equations 2.20 and 2.22 gives

$$\frac{2G_1}{C_1} = \sum_{LHP_m} \left(s_{pm} - s_{om} \right) + \sum_{RHP_m} \left(s_{pm} - s_{om} \right) \tag{2.23}$$

The RHP summation has been shown zero for stable physically realizable response. The LHP summation can be evaluated for the Butterworth and Tchebysheff roots given in equations 2.15 through 2.18 (13). Closed form expressions for these summations lead to

$$\frac{G_1}{\omega_B C_1} = \frac{1}{2 \sin \frac{\pi}{2N}} \left(\rho_{Bo}^{1/N} - 1\right) \tag{2.24}$$

$$\frac{G_1}{\omega_T C_1} = \frac{1}{2 \sin \frac{\pi}{2N}} \left(\sinh \frac{1}{N} \sinh^{-1} \frac{\rho_{To}}{\epsilon} - \sinh \frac{1}{N} \sinh^{-1} \frac{1}{\epsilon}\right) \tag{2.25}$$

For infinite N equation 2.24 becomes

$$\frac{G_1}{\omega_B C_1} = \frac{\ell n\, \rho_{Bo}}{\pi}$$

which agrees with equation 1.4 . Figure 2.7 shows $\omega_B C_1/G_1$ as a function of ρ_{Bo} for several values of N . Figure 2.8 shows $\omega_T C_1/G_1$ as a function of $\bar{\rho}_T$, the approximate root mean square average reflection coefficient over the Tchebysheff ripple band. Approximately three decibel ripple was assumed and ϵ^2 taken as 1. The curves of $\omega_T C_1/G_1$ for smaller ϵ do not lie between the Butterworth and $\epsilon = 1$ curve. Curves of $\omega_{3DB} C_1/G_1$ for $\epsilon < 1$, do, however, lie between the Butterworth and $\epsilon = 1$ curves. The asymptotic values of the Butterworth and Tchebysheff bandwidths are the same for $\rho_{Bo} = \bar{\rho}_T$.

Similar arguments may be applied to $\rho_{N(s)}$ to calculate $G_N/\omega_B C_N$ and $G_N/\omega_T C_N$ or $R_N/\omega_B L_N$ and $R_N/\omega_T L_N$ as shown in Figure 2.2. The zeros and poles of $\rho_{N(s)}$ are in opposite half planes giving

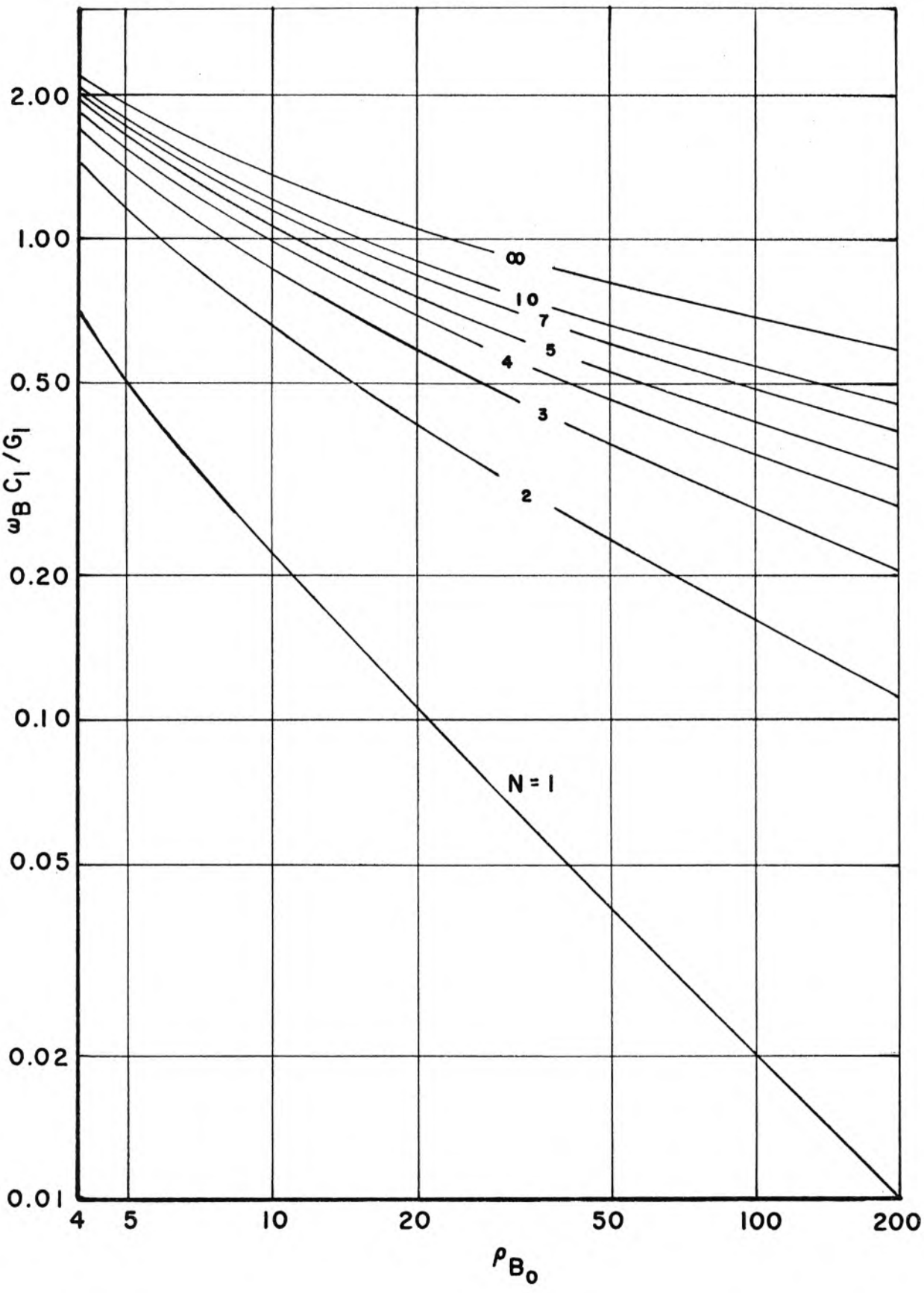

Figure 2.7 Normalized half power bandwidth for Butterworth Response versus ρ_{B_0}

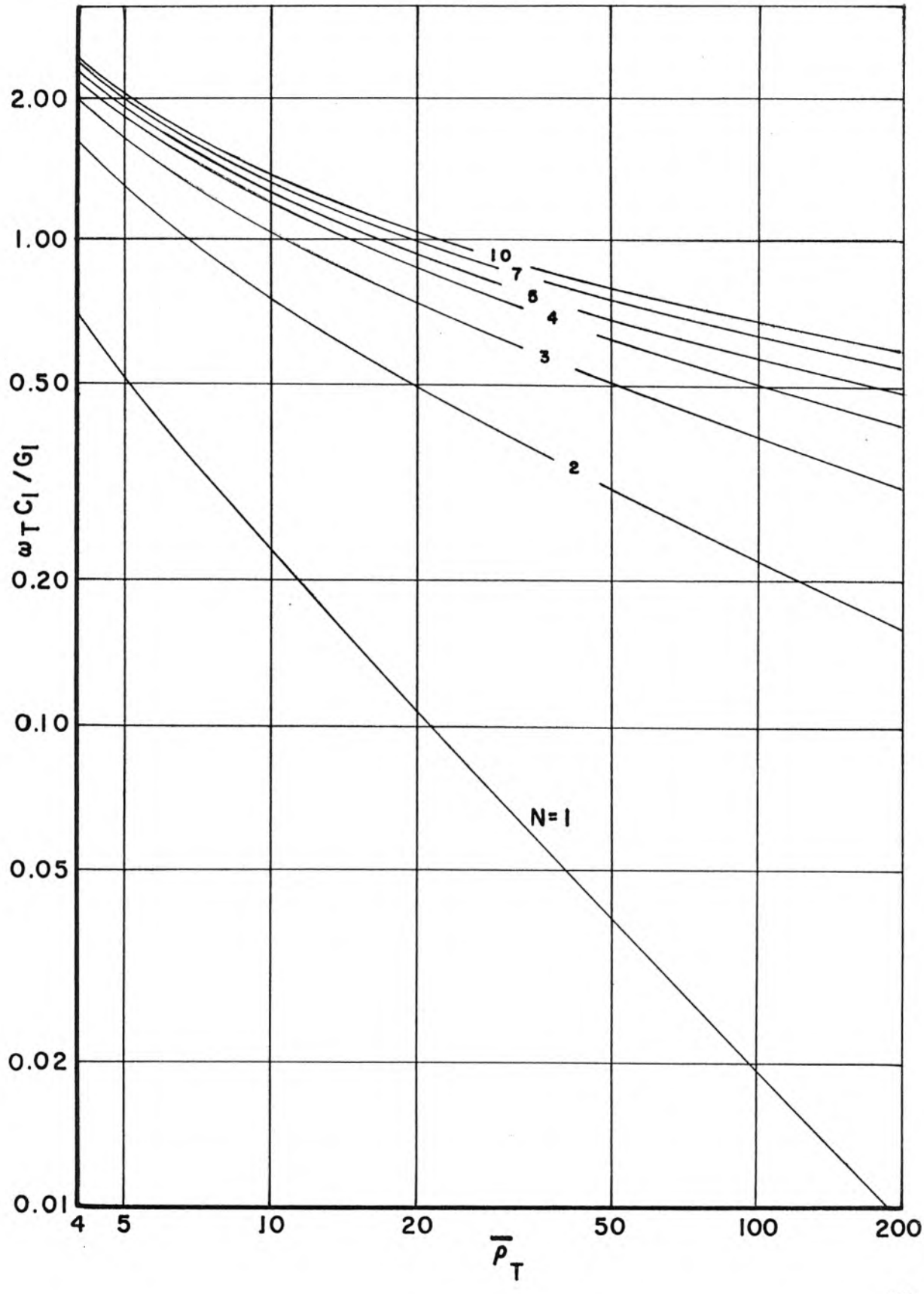

Figure 2.8 Normalized Tchebysheff ripple bandwidth for $\epsilon = 1$ versus $\overline{\rho}_T$

$$\left.\frac{G_N}{\omega_B C_N}\right|_{N_{odd}} \qquad \left.\frac{R_N}{\omega_B L_N}\right|_{N_{even}} = \frac{1}{2\sin\frac{\pi}{2N}}\left(\rho_{Bo}^{1/N}+1\right) = \frac{G_1}{\omega_B C_1} + \frac{1}{\sin\frac{\pi}{2N}} \tag{2.26}$$

$$\left.\frac{G_N}{\omega_T C_N}\right|_{N_{odd}} \qquad \left.\frac{R_N}{\omega_T L_N}\right|_{N_{even}} = \frac{1}{2\sin\frac{\pi}{2N}}\left(\sinh\frac{1}{N}\sinh^{-1}\frac{\rho_{To}}{\epsilon} + \sinh\frac{1}{N}\sinh^{-1}\frac{1}{\epsilon}\right)$$

$$= \frac{G_1}{\omega_T C_T} + \frac{\sinh\frac{1}{N}\sinh^{-1}\frac{1}{\epsilon}}{\sin\frac{\pi}{2N}} \tag{2.27}$$

The quantities G_N/G_1 and $1/R_N G_1$ can be determined from the zero frequency reflection coefficient on which the inductors and capacitors have no effect. Stability criteria manifested in the requirement that the poles of ρ_1 be in the LHP require G_N/G_1 or $1/R_N G_1$ to be greater than unity. Using equation 2.5 to obtain these quantities from the zero frequency reflection and using equations 2.11 to find the Tchebysheff zero frequency reflection from ρ_{To} and ϵ, one finds for odd N,

$$\left.\frac{G_N}{G_1}\right|_B = \frac{|\rho_{Bo}|+1}{|\rho_{To}|-1}$$

$$\left.\frac{G_N}{G_1}\right|_T = \frac{|\rho_{To}|+1}{|\rho_{To}|-1} \tag{2.28}$$

and for even N,

$$\left.\frac{1}{R_N G_1}\right|_B = \frac{|\rho_{Bo}| + 1}{|\rho_{Bo}| - 1}$$

$$\left.\frac{1}{R_N G_1}\right|_T = \frac{\sqrt{\rho_{To}^2 + \epsilon^2} + \sqrt{1 + \epsilon^2}}{\sqrt{\rho_{To}^2 + \epsilon^2} - \sqrt{1 + \epsilon^2}}$$

Because of the reciprocity under a change in sign of G_N as exhibited by equation 2.10, the network of Figure 2.2 with active response may be completely synthesized in terms of an equivalent passive circuit. The reciprocal of the active Butterworth response is

$$\frac{1 + (\frac{\omega}{\omega_B})^{2N}}{\rho_{Bo}^2 + (\frac{\omega}{\omega_B})^{2N}} = \frac{(\frac{1}{\rho_{Bo}})^2 + (\frac{\omega}{\omega_B'})^{2N}}{1 + (\frac{\omega}{\omega_B'})^{2N}}, \quad \omega_B' = \omega_B \rho_{Bo}^{1/N} \tag{2.29}$$

Reciprocal Tchebysheff response is

$$\frac{1 + \epsilon^2 T_N^2(\frac{\omega}{\omega_T})}{\rho_{To}^2 + \epsilon^2 T_N^2(\frac{\omega}{\omega_T})} = \frac{\frac{1}{\rho_{To}^2} + \epsilon'^2 T_N^2 (\frac{\omega}{\omega_T})}{1 + \epsilon'^2 T_N^2 (\frac{\omega}{\omega_T})}, \quad \epsilon'^2 = \frac{\epsilon^2}{\rho_{To}^2} \tag{2.30}$$

Tables or closed form expressions (14,15) for the elements of lossless Butterworth and Tchebysheff filters are generally given for the case where the zeros and poles are in the same or opposite plane, as we require, and equations 2.29 and 2.30 put the reciprocal of active responses into the normal passive network form. Tchebysheff and Butterworth responses for both active and passive terminations may also be

obtained with lossy reactances in the filter. Tables of network elements given for passive responses as a function of element loss factors cannot, however, be used to synthesize lossy networks with an active termination.

2.3 Four Low Pass Amplifier Configurations

The bandwidth normalizations for the basic network of Figure 2.2 have been found in terms of the time constants of the terminations for Butterworth and Tchebysheff reflection responses. The bandwidth and noise figure of the four amplifier configurations in Figure 2.1 which all use this same basic network can now be determined. For brevity, these amplifiers will be called Type A, B, C and D referring to the designation in Figure 2.1. The reflection and transmission factors appearing in the following discussions are defined in this figure.

Although the ladder reactance network has been assumed lossless in previous sections, the effects of network loss on the noise figure will be formulated here using τ_N as the temperature of the network. As shown in the introduction an effective temperature $-\tau_T$ will be used for the tunnel diode. The noise figure is written with respect to a source temperature τ_s rather than the standard $290^{\circ}K$, and any amplified noise arising from the load conductance is also considered when important. The noise which the load would contribute to the output of an ideal matched unilateral amplifier is subtracted from this contribution since it should not be considered as a detrimental factor.

2.31 Type A Reflection Amplifier with Circulator. The presence of the ideal matched circulator in configuration A makes the power gain P_{GA} of the circuit equal to the reflection gain $\rho_N \rho_N^*$. For

a lossless ladder $\rho_1\rho_1^* = \rho_N\rho_N^*$ and the integral limitations on the reflection coefficient given in equation 2.21 are directly the limitations on the bandwidth of this amplifier.

$$\int_0^\infty \ell n\ P_{GA}\ d\omega = 2\pi \frac{G_T}{C_T} \tag{2.31}$$

The Butterworth or Tchebysheff responses therefore represent optimum choices. Figures 2.7 and 2.8 can be used directly to find $\omega_B C_T/G_T$ or $\omega_T C_T/G_T\big|_{\epsilon=1}$ as a function of N, and ρ_{Bo} or $\bar{\rho}_T$.

The circulator reflection amplifier differs from the other configurations which will be analyzed in that its noise figure is fixed by the configuration. We calculate this noise figure by assuming first an ideal matched circulator and then adding the effects of attenuation or mismatch. Using the reciprocity theorem, one may say that the ratio of noise power transmitted to the circulator $P_{out\ T}$ to noise power available from $-G_T$ equals the ratio of power transmitted to $-G_T$ to power available from the circulator.

$$\frac{P_{out\ T}}{-K\tau_T\ df} = -\ |T|^2 \tag{2.32}$$

Similarly reciprocity can be applied to calculate $P_{out\ N}$, the noise out due to losses in the network.

$$\frac{P_{out\ N}}{K\tau_N\ df} = \left|1 + |T|^2 - |\rho_N|^2\right| \tag{2.33}$$

The noise figure of the amplifier relative to a source at temperature τ_s is

$$F_A = 1 + \frac{P_{out\ N} + P_{out\ T}}{K\tau_s\ df\ |\rho_N|^2}$$

$$= 1 + \frac{\tau_T\ |T|^2}{\tau_s\ \rho_N^2} + \frac{\tau_N}{\tau_s} \frac{\left|1 + |T^2| - |\rho_N|^2\right|}{|\rho_N|^2} \qquad (2.34)$$

The contribution to F_A of attenuations A_1 and A_2 in the circulator at temperature τ_c can now be added by application of the noise figure formula for cascade amplifiers

$$F_{12} = F_1 + \frac{F_2 - 1}{P_{G_1}} \qquad (2.35)$$

using

$$F_1 = 1 + \frac{\tau_c}{\tau_s} \left(\frac{1}{A_1} - 1\right) \qquad (2.36)$$

The result is

$$1 + \frac{\tau_c}{\tau_s} \frac{1 - A_1}{A_1} + \frac{\tau_T}{\tau_s} \frac{|T|^2}{A_1|\rho_N|^2}$$

$$+ \frac{\tau_N}{\tau_s} \frac{\left|1 + |T|^2 - |\rho_N|^2\right|}{|\rho_N|^2\ A_1} + \frac{\tau_c}{\tau_s} \frac{1 - A_1}{A_1 A_2 |\rho_N|^2} \qquad (2.37)$$

τ_c should be considered zero if A_1 and A_2 are mismatch losses rather than matched attenuations. Some further attention to the quantity $1 + |T|^2 - |\rho_1|^2$ will be given in section 2.5 .

In closing discussion of the Type A Amplifier, it is well to point out that because of the circulator it is completely stable to changes in the source and load impedance and may be cascaded at will.

Equations 2.26 or 2.27 give the maximum tolerable reactance of the low-pass equivalent circulator or the slope of the reactance about the center frequency, ω_o, of a bandpass circulator in terms of ρ_{Bo} and N or ρ_{To}, N and ϵ.

2.32 Type B Bilateral Reflection Amplifier. The amplifier configuration of type B does not give exact maximally flat or equal ripple response when synthesized in terms of section 2.2. The required reflection poles and zeros to achieve this effect are not known in general and can be calculated only with some difficulty. Sard (16) has done this for $N = 2$ and $N = 3$ maximally flat response. In terms of ρ_N the power gain of configuration B is

$$P_{GB} = \frac{G_s G_L}{(G_s + G_L)^2} (1 + \rho_N)(1 + \rho_N^*) \tag{2.38}$$

Having poles and zeros in opposite half planes, ρ_N will in general exhibit a rapid phase change with frequency. Assuming this phase change roughly uncorrelated with the amplitude changes in ρ_N, the average power gain over the band may be related to the average value of $|\rho_N|^2$, $\overline{\rho_N \rho_N}^*$ by

$$\overline{P}_{GB} \cong \frac{G_s G_L}{(G_s + G_L)^2} (1 + \overline{\rho_N \rho_N}^*) \tag{2.39}$$

and the extra induced ripple or ratio of maximum to minimum gain is on the order of

$$\frac{\overline{\rho_N \rho_N}^* + 1 + 2\sqrt{\overline{\rho_N \rho_N}^*}}{\overline{\rho_N \rho_N}^* + 1 - 2\sqrt{\overline{\rho_N \rho_N}^*}} = \frac{2\sqrt{\overline{P}_G \frac{(G_s + G_L)^2}{G_s G_L}} + 1}{2\sqrt{\overline{P}_G \frac{(G_s + G_L)^2}{G_s G_L}} - 1} \tag{2.40}$$

For a given ρ_N , $\overline{P}_G$ in equation 2.39 has a maximum for $G_s = G_L$

$$\overline{P}_{GB_{max}} = \frac{1}{4}(1 + \rho_N \rho_N^*) \tag{2.41}$$

The fundamental bandwidth limitation on bilateral amplifiers with flat gain has been found by Youla and Smilen (5) to be

$$P_G \leq \left[\frac{e^{\pi G_T/\omega_c C_T} + 1}{2} \right] \tag{2.42}$$

giving only very slightly higher bandwidth than would be predicted using equations 2.41 and 2.21.

The quantity $G_s G_L/(G_s + G_L)^2$ will, however, be chosen on noise consideration and may be considerably less than 1/4 for practical amplifiers. We therefore calculate noise figure before bandwidth. Following the reciprocity technique used before,

$$\frac{P_{out\ T}}{K\ \tau_T\ d\omega} = \frac{G_L}{G_L + G_s} |T|^2 \tag{2.43}$$

$$\frac{P_{out\ N}}{K\ \tau_N\ d\omega} = \frac{G_L}{G_L + G_s} \left| 1 + |T|^2 - |\rho_N|^2 \right|$$

A third source of output noise, namely the amplified noise of the load conductance must be taken into account. The power dissipated in G_L due to its own noise current generator, $I_{N_L}^2 = 4K\tau_L G_L\ df$, is

$$P_{out\ L} = K\tau_L\ df \frac{G_L^2}{(G_s + G_L)^2} (1 + \rho_N)(1 + \rho_N^*) \tag{2.44}$$

$K\tau_L$ df is generally subtracted from this as present in the load of any ideal matched unilateral amplifier. The noise figure is

$$F_B = 1 + \frac{\tau_T}{\tau_s} \frac{|T|^2}{(1+\rho_N)(1+\rho_N^*)} \left(\frac{G_s + G_L}{G_s}\right)$$

$$+ \frac{\tau_N}{\tau_s} \frac{\left|1 + |T|^2 - |\rho_N|^2\right|}{(1+\rho_N)(1+\rho_N^*)} \frac{G_s + G_L}{G_s}$$

$$+ \frac{\tau_L}{\tau_s}\left(\frac{G_L}{G_s} - \frac{(G_s + G_L)^2}{(G_s G_L)(1+\rho_N)(1+\rho_N^*)}\right) \qquad (2.45)$$

For a lossless ladder F_B may be written as

$$1 + \frac{\tau_T}{\tau_s} \frac{\rho_N^2 - 1}{(1+\rho_N)(1+\rho_N^*)} \frac{G_s + G_L}{G_s} + \frac{\tau_L}{\tau_s}\left(\frac{G_L}{G_s} - \frac{1}{P_{GB}}\right) \cong$$

$$1 + \frac{\tau_T}{\tau_s}\frac{G_T}{G_s} + \frac{\tau_L}{\tau_s}\left(\frac{G_L}{G_s} - \frac{1}{P_{GB}}\right) \qquad (2.46)$$

The last additive factor of the noise figure may be very important since τ_L is frequently high. It may be reduced to zero, however, or even negative, by choosing G_L/G_s to be on the order of the reciprocal of the average power gain.,

The required ρ_{Bo} or $\bar{\rho}_T$ for a given average power gain can be calculated from equation 2.39 once G_L/G_s is chosen on noise figure considerations. The normalized bandwidth can then be found from Figures 2.7 or 2.8, or equations 2.24 or 2.25. For $G_L/G_s = 1/\bar{P}_G$, the Butterworth derived bandwidth is

$$\omega_B = \frac{G_T}{C_T} \frac{2 \sin \frac{\pi}{2N}}{(\bar{P}_G^2 + 2\bar{P}_G)^{1/2N} - 1} \tag{2.47}$$

approaching a limit for infinite N

$$\omega_B = \frac{G_T}{C_T} \frac{2\pi}{\ell n(\bar{P}_G^2 + 2\bar{P}_G)} \quad .$$

Figure 2.9 shows the Butterworth bandwidth for $\bar{P}_G = 40$ as a function of the load noise contribution factor $\alpha = \frac{G_L}{G_s} - 1/P_G$ with N as a parameter.

The results of computing the normalized bandwidth on this basis which gives maximally flat response only in the high gain limit agree very well with Sard's (16) results* down to $\bar{P}_G = 10$. It is implicit in this derivation that the reactances associated with the physical source and load generators can be accommodated by the configuration as per equations 2.26 and 2.27.

2.33 Type C Transmission with Load in Parallel with Active Element. With configuration C minimum phase power gain can be achieved, and the Butterworth and Tchebysheff responses, insofar as they are desired for band shaping, are optimum for utilization of the bandwidth capabilities of the C_T, G_T, G_L combination. The bandwidth limitations on ρ_1 are now normalized to $\frac{G_T - G_L}{C_T}$ but the power gain is greater than the transmission gain.

*Figure 7 of Sard's paper showing Bandwidth vs. Gain for Bilateral Reflection Type Negative Conductance Amplifiers for

$$\rho = \frac{4G_L G_s}{(G_L + G_s)^2} = \frac{5}{9}$$

actually represents his calculations for $\rho = 1$.

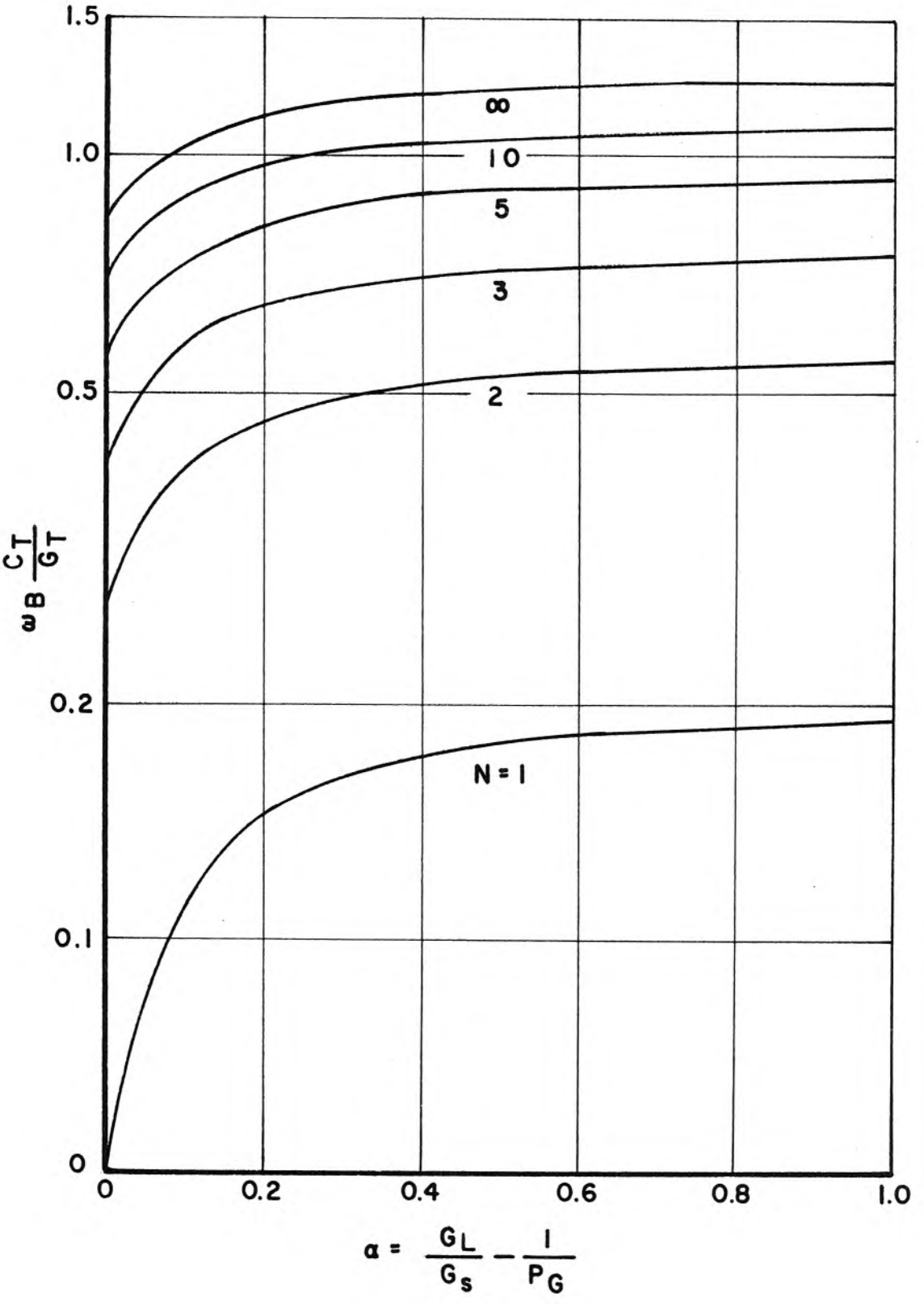

Figure 2.9 Normalized Bandwidth of Butterworth type B reflection amplifier for $\bar{P}_G = 40$ versus $\alpha = G_L/G_s - 1/\bar{P}_G$

$$P_{GC} = \frac{G_L}{G_T - G_L} |T|^2 \tag{2.48}$$

The possibility that G_L is greater than G_T will not be considered here since it gives rise to a very high noise figure and very small bandwidth corresponding to a low noise situation in configuration D . The noise figure may be calculated as before

$$\begin{aligned}
P_{out\ T} &= K\, \tau_T\, df\, \frac{G_T\, G_L}{(G_T - G_L)^2} (1 + \rho_1)(1 + \rho_1^*) \\
P_{out\ N} &= K\, \tau_N\, df\, \frac{G_L}{G_T - G_L} \left| 1 + |T|^2 - |\rho_1|^2 \right| \\
P_{out\ L} &= K\, \tau_L\, df\, \frac{G_L^2}{(G_T - G_L)^2} (1 + \rho_1)(1 + \rho_1^*)
\end{aligned} \tag{2.49}$$

$$\begin{aligned}
F_c = 1 &+ \frac{\tau_T}{\tau_s} \left(\frac{G_T}{G_T - G_L}\right)\left(\frac{(1+\rho_1)(1+\rho_1^*)}{|T|^2}\right) \\
&+ \frac{\tau_N}{\tau_s} \left| \frac{1 + |T|^2 - |\rho_1|^2}{|T|^2} \right| \\
&+ \frac{\tau_L}{\tau_s} \left[\left(\frac{G_L}{G_T - G_L}\right)\left(\frac{(1+\rho_1)(1+\rho_1^*)}{|T|^2}\right) - \frac{1}{P_{GC}} \right]
\end{aligned} \tag{2.50}$$

Since the zeros and poles of ρ_1 lie in the same half plane, its net phase shift may be small over most of the frequency range. It will be shown in a later section that designs in which the maximum phase change exceeds 180° are impractical. For purposes of approximating F_c we assume here that $\arg \rho_1$ is close to π over the bandwidth of the amplifier. It will usually be correct if ρ_1 is

small and will make little difference if ρ_1 is large. In this approximation F_c for lossless networks can be written

$$F_c = 1 + \frac{\tau_T}{\tau_s}\frac{G_T}{G_s} + \frac{\tau_L}{\tau_s}\left(\frac{G_L}{G_s} - \frac{1}{\bar{P}_G}\right) \tag{2.51}$$

which is the same as equation 2.46, the noise figure of the type B amplifier.

For the lossless case the zero frequency power gain can be written as

$$P_{GC}\Big|_{\omega=0} = \frac{4G_L G_s}{(G_s + G_L - G_T)^2} \tag{2.52}$$

Using this equation and equation 2.48, $\rho_{Bo} = \sqrt{|T_{Bo}|^2 - 1}$ or $\bar{\rho}_T = \sqrt{|\bar{T}_T|^2 - 1}$ can be calculated as functions of P_G and G_L/G_s. The normalized bandwidths may then be found from the equations or figures of section 2.2. Figure 2.10 shows the Butterworth transmission bandwidth for $P_G = 40$ as a function of $\alpha = \frac{G_L}{G_s} - \frac{1}{P_G}$. The bandwidth of the type C amplifier generally shows a maximum for G_L/G_s less than unity, but is in all cases slightly lower than for type B amplifiers for equal gain, noise figure, and number of components. These calculations for the bandwidth of the type C transmission amplifier have also been done by Sard (16) for the maximally flat case and the results for this case are identical.

The above calculations assume that the actual tunnel diode can accommodate a load impedance directly in parallel with its internal conductance and that the load impedance does not contribute any additional capacitance to C_T. As we shall see in section 2.8 some

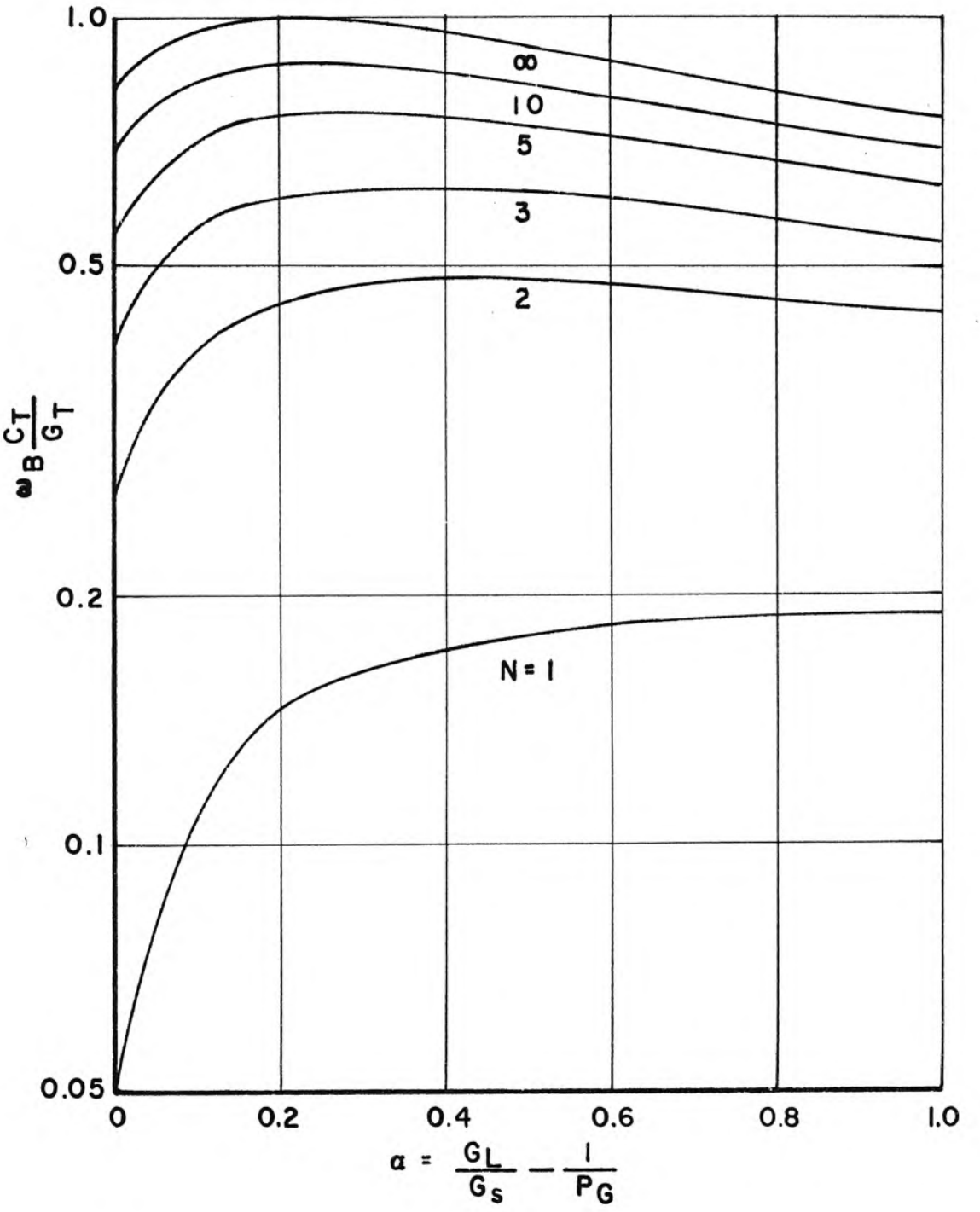

Figure 2.10 Normalized bandwidth of Butterworth type C transmission amplifier for

$$P_G = 40 \quad \text{versus} \quad \alpha = \frac{G_L}{G_S} - \frac{1}{P_G}$$

band pass configurations of the tunnel diode and load or source impedance will be analyzable on these terms without this direct but physically impossible connection being required. In low-pass circuits, however, or in extremely wide band amplifiers, the series inductance of the tunnel diode may limit the practical accuracy of this analysis of type C and D configurations. The effects of inductance intervening between G_T and G_L or G_T and G_s may be considered with results from section 2.6, but compensation for this element must be considered on an individual case basis.

2.34 Type D Transmission Amplifier with Source in Parallel with Active Element. The power gain in the type D amplifier is

$$P_{GD} = \left| \frac{G_s}{G_T - G_s} \right| |T|^2 \tag{2.53}$$

The noise figure may again be evaluated from the components of the output noise power.

$$\begin{aligned} P_{out\ T} &= K \tau_T\ df\ |T|^2 \left| \frac{G_T}{G_T - G_s} \right| \\ P_{out\ L} &= K \tau_L\ df\ (1 + \rho_N)(1 + \rho_N^*) \\ P_{out\ N} &= K \tau_N\ df \left| 1 - |\rho_N|^2 + |T|^2 \right| \quad G_T > G_s \\ &\quad\ K \tau_N\ df \left| 1 - |\rho_N|^2 - |T|^2 \right| \quad G_T < G_s \end{aligned} \tag{2.54}$$

$$F_D = 1 + \frac{\tau_T}{\tau_s}\frac{G_T}{G_s} + \frac{\tau_N}{\tau_s}\left|\frac{1 - |\rho_N|^2 \pm |T|^2}{|T|^2}\right|\left|\frac{G_T - G_s}{G_s}\right|$$

$$+ \frac{\tau_L}{\tau_s}\left[\frac{(1 + \rho_N)(1 + \rho_N^*)}{|T|^2}\left|\frac{G_T - G_s}{G_s}\right| - \frac{1}{\bar{\bar{P}}_G}\right] \qquad (2.55)$$

The poles and zeros of ρ_N lie in opposite half planes, and the arg ρ_N will vary by as much as $2N\pi$ over the passband. Except for the $N = 1$ case in which types B, C, and D are all the same, we are justified in substituting for $(1 + \rho_N)(1 + \rho_N^*)$ its approximate average value in the lossless ladder case.

$$\int_0^{\omega_c} (1 + \rho_N)(1 + \rho_N^*)d\omega = \omega_c\left[1 + |\bar{\rho}_N|^2\right]$$

ω_c = nominal cutoff frequency or bandwidth.

As before, the required reflection coefficient for a given power gain can be calculated with equations 2.52 and 2.53. For the G_L/G_s in the configuration equal to $\frac{1}{G_L/G_s}$ in the type C configuration, the bandwidths are the same. For comparably low noise figure, however, configuration D gives much lower bandwidth. Figure 2.11 shows the Butterworth bandwidth as a function of the load noise factor

$$\alpha \cong \left(\frac{1 + |\rho_N|^2}{|T|^2}\,\frac{G_T - G_s}{G_s}\right) - \frac{1}{\bar{\bar{P}}_G}$$

$$\cong \frac{\bar{\rho}_N^2}{\bar{P}_{GD}}$$

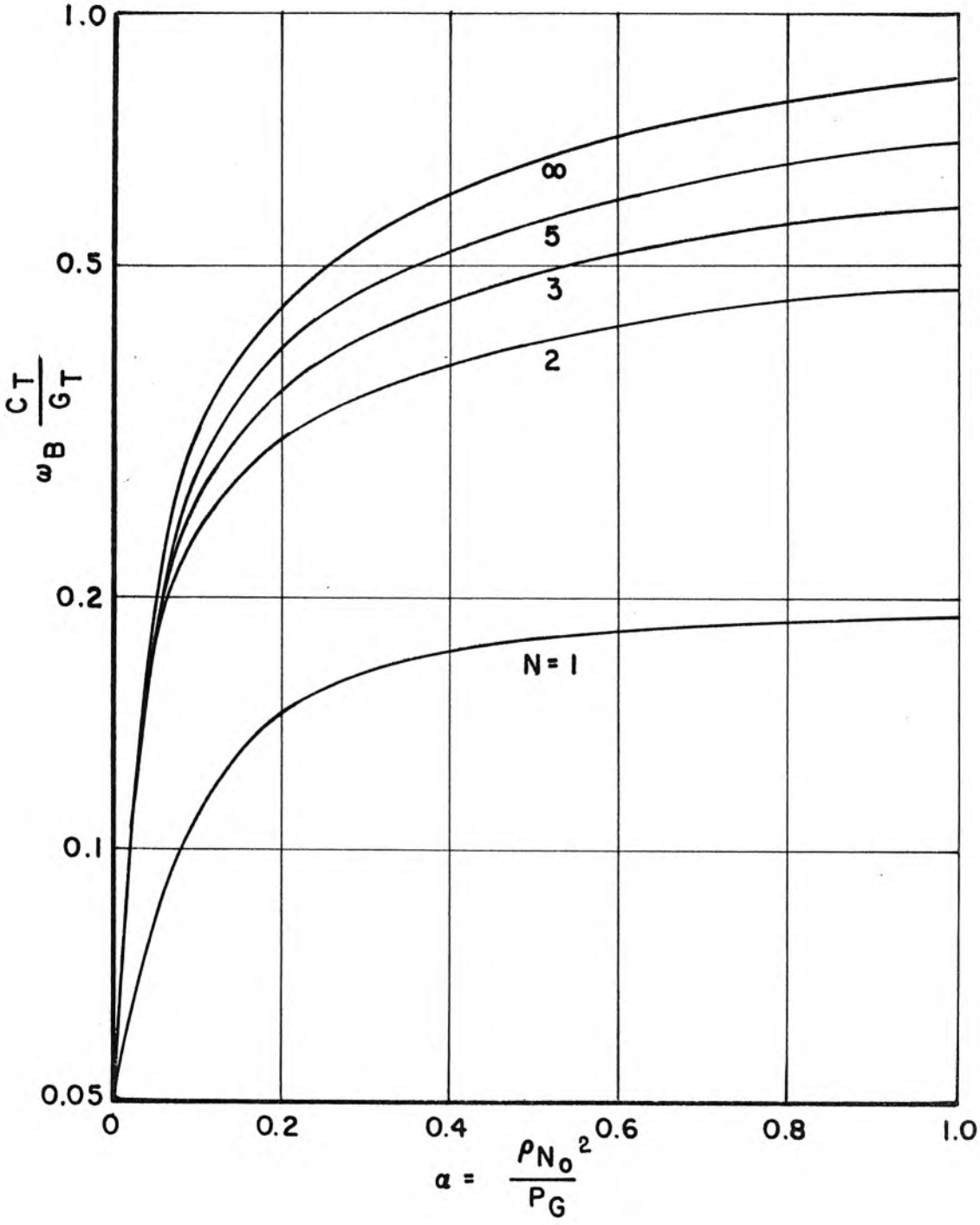

Figure 2.11 Normalized bandwidth of Butterworth type D transmission amplifier versus

$$\alpha = \frac{|\rho_{NO}|^2}{\overline{P}_G} \quad \text{for} \quad P_G = 40$$

While this configuration gives generally lower bandwidth than the others, it may have one advantage. In all other configurations signal power must pass through the ladder network before reaching the negative conductance where amplification can occur. Here, the signal is amplified first and losses in the ladder network would not ostensibly contribute so heavily to the noise figure. This appears as the factor $\frac{G_T - G_S}{G_S}$ in the noise figure term due to τ_N .

2.4 Three Configurations with Tunnel Diodes in Both Terminations

One may calculate the gain bandwidth capability of the ladder network amplifier configurations when the capacitance of a second tunnel diode is used to fill the reactance requirements at the passive termination. Figure 2.12 shows three such configurations which can be called types A', B', and C'. These low-pass configurations are theoretically achievable for odd N only. Some bandpass circuits will be shown in section 2.5, however, which are bandpass approximants of these configurations and yet may contain two tunnel diodes for even N .

In this section the network will be assumed lossless and both tunnel diodes are assumed to have the same time constant C_T/G_T and noise temperature. The required calculations for bandwidth involve the simultaneous application of equations 2.24 and 2.26, or 2.25 and 2.27. The method may be simplified for the A' and B' cases by calculating the increase in gain that may be obtained in these configurations over that of type A amplifiers with the same bandwidth and noise figure. In Figure 2.12A' the admittance level of the circulator is shown raised over that in Figure 2.1A by G_{TN} so that the same network and G_{T1}

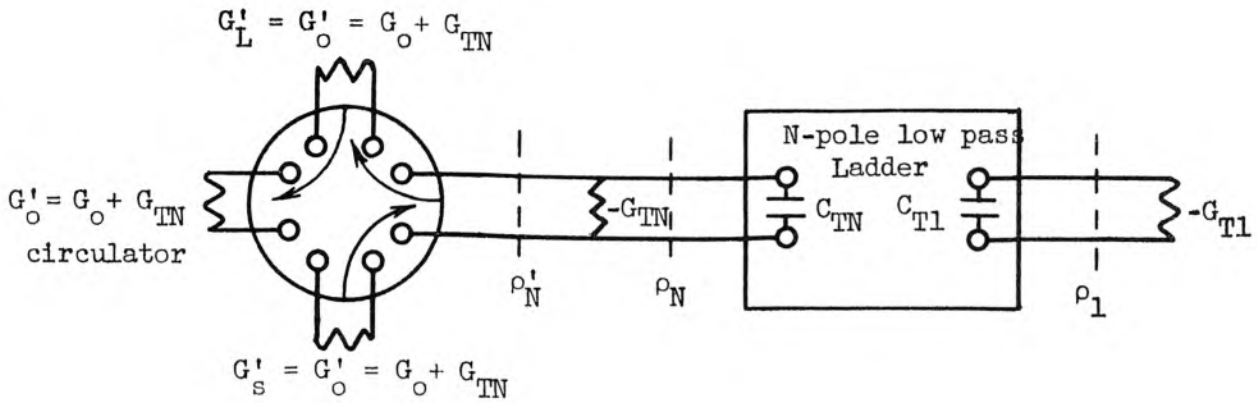

A' Reflection Amplifier with circulator

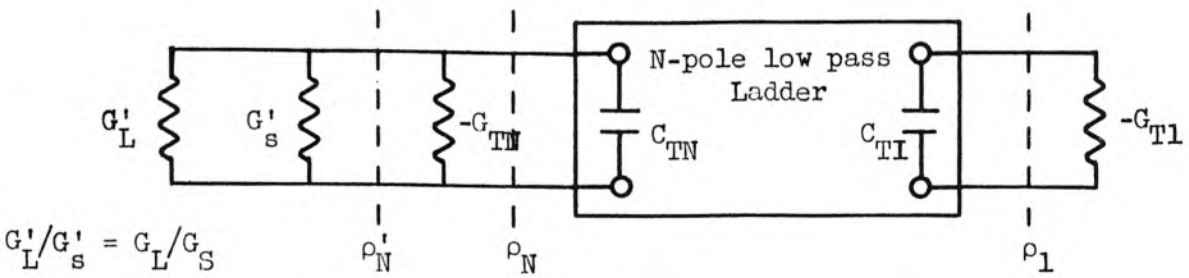

B' Unilateral reflection amplifier

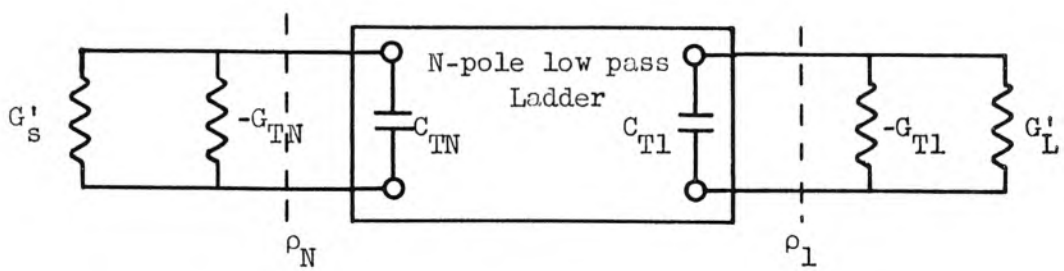

C' Transmission amplifier

Figure 2.12 Three low pass ladder network amplifiers containing tunnel diodes in both terminations

give the same reflection response in both cases. The ideal noise figure will also be essentially $1 + \frac{\tau_T}{\tau_S}$ for both. The increase in gain of A' over A is the ratio $\rho_N' \rho_N'^* / \rho_N \rho_N^*$ as defined in Figure 2.12A'. This may be calculated to be

$$\left| 1 + \frac{G_{TN}}{G_o} \left(1 + \frac{1}{\rho_N}\right) \right|^2$$

or, neglecting $1/\rho_N$

$$\frac{\rho_N' \rho_N'^*}{\rho_N \rho_N^*} \cong \left(1 + \frac{G_{TN}}{G_o}\right)^2 \tag{2.57}$$

in which G_o is the admittance level of the circulator in Figure 2.1A Remembering that $G_{TN}/C_{TN} = G_{T1}/C_{T1}$, G_{TN}/G_o may be computed from section 2.2 as a function ρ_{Bo} or ρ_{To}. The resulting gain increase factor is

$$\frac{\rho_N' \rho_N'^*}{\rho_N \rho_N^*} \cong \left(1 + \frac{\rho_{Bo_N}^{1/N} - 1}{\rho_{Bo_N}^{1/N} + 1} \right)^2 \tag{2.58}$$

for Butterworth response, or

$$\frac{\rho_N' \rho_N'^*}{\rho_N \rho_N^*} \cong \left(1 + \frac{\sinh \frac{1}{N} \sinh^{-1} \frac{\rho_{To_N}}{\epsilon} - \sinh \frac{1}{N} \sinh^{-1} \frac{1}{\epsilon}}{\sinh \frac{1}{N} \sinh^{-1} \frac{\rho_{To_N}}{\epsilon} + \sinh \frac{1}{N} \sinh^{-1} \frac{1}{\epsilon}} \right)^2 \tag{2.59}$$

for Tchebysheff response.

Figure 2.12B' shows the admittance level of the load and signal generator combination raised with respect to Figure 2.1B by G_{TN} but with the ratio of load to generator impedance maintained. For equal noise figures and bandwidths equations 2.58 and 2.59 are again correct for the increase in gain of the B' configuration over configuration B.

The comparison of the type C' circuit to the type C is somewhat more difficult to perform. Their noise performances are essentially equal for equal gains and choices of G_L/G_s . The calculations for $\omega_B C_T/G_T$ have been done for Butterworth response using equations 2.60 through 2.63, below.

$$\frac{C_T\omega_B}{G_T} = \frac{G_s - G_{TN}}{G_{TN}} \frac{2\sin\frac{\pi}{2N}}{\rho_o^{1/N} + 1} = \frac{G_{T1} - G_L}{G_{T1}} \frac{2\sin\frac{\pi}{2N}}{\rho_o^{1/N} - 1} \tag{2.60}$$

$$P_G\Big|_{\omega=0} = \frac{4\, G_L\, G_s}{(G_L + G_s - G_{TN} - G_{T1})^2} \tag{2.61}$$

$$\rho_{Bo} = \frac{G_s - G_{TN} + G_{T1} - G_L}{G_s + G_L - G_{TN} - G_{T1}} \tag{2.62}$$

$$F_{c'} = 1 + \frac{\tau_T}{\tau_s} \frac{G_{T1} + G_{TN}}{G_s} + \frac{\tau_L}{\tau_s}\left(\frac{G_L}{G_s} - \frac{1}{P_G}\right) \tag{2.63}$$

The increase in bandwidth capability was not significantly large in any case, as one might expect. Figure 2.13 shows the normalized bandwidth versus $\alpha = \frac{G_L'}{G_s'} - \frac{1}{P_G}$ for $P_G = 40$.

The power gain increase of these configurations with two tunnel diodes over the comparable single diode configurations cannot exceed four. Considering that the bandwidth in the single diode configurations varies at least as slowly as $P_G^{-1/4}$, this does not represent a very large increase in gain bandwidth capability. The effort required to fit the second diode into a practical circuit may therefore not always be worth while. On the other hand, the second diode acts as a preamplifier of the signal before it enters the network and should reduce the

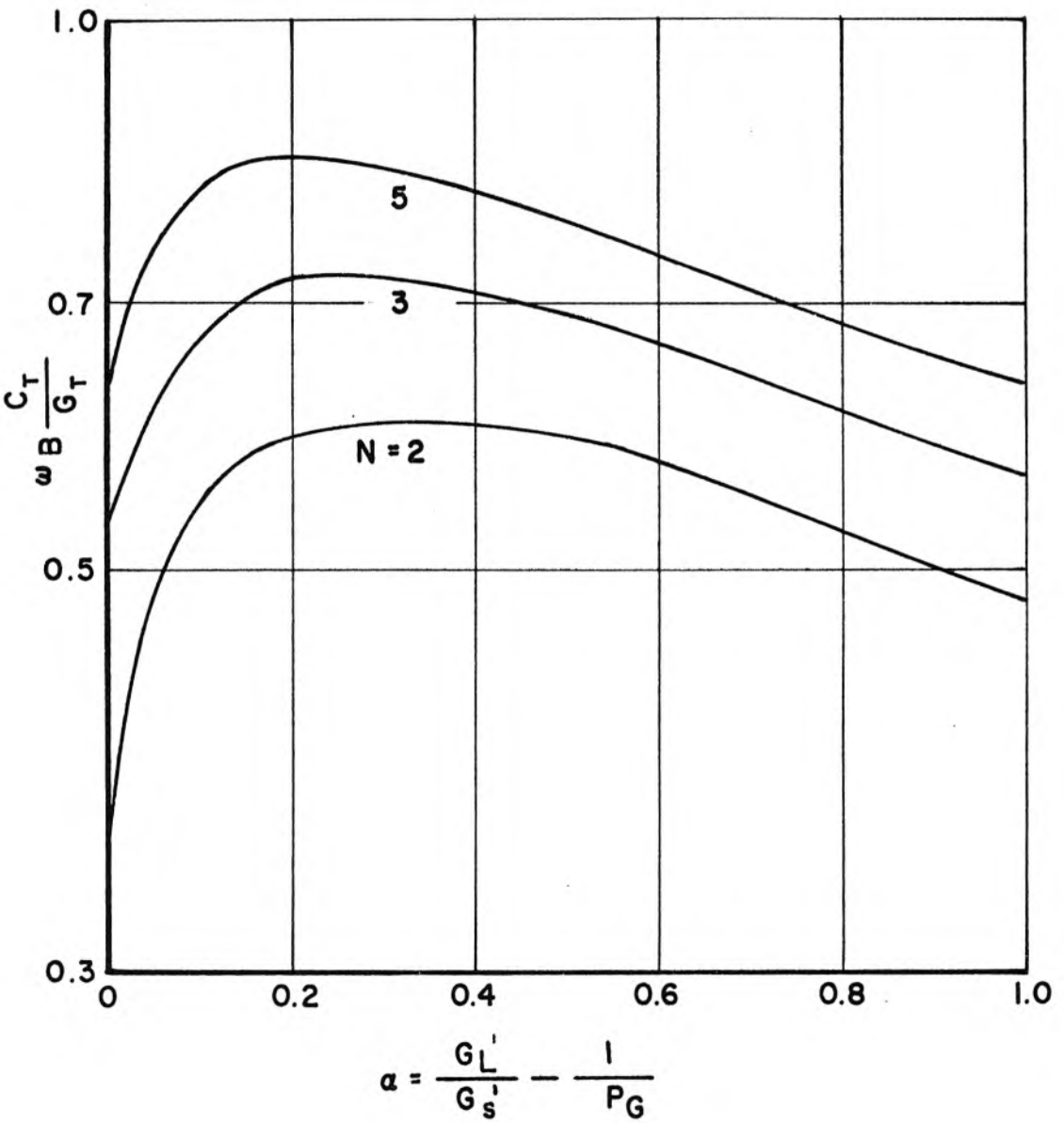

Figure 2.13 Normalized Butterworth bandwidth of type C' transmission amplifier versus

$$\alpha = \frac{G_L'}{G_s'} - \frac{1}{P_G} \quad \text{for} \quad P_G = 40$$

effect of network losses on noise figure by something on the order of the square roots of the factors given in equations 2.58 and 2.59.

2.5 Band Pass Equivalents

The basic low pass characteristics of the ladder circuit may be translated to realizable band pass characteristics by the transformation

$$s = \Omega_o \left(\frac{s'}{\Omega_o} + \frac{\Omega_o}{s'}\right) \tag{2.64}$$

where s' is the new band pass variable and Ω_o is the band center. The new circuits are derived from those in Figures 2.1 and 2.2 by placing a capacitor in series with every inductance L_i and an inductance in parallel with every capacitor C_j such that each branch is resonant at Ω_o. The band pass equivalent of a low pass ladder is shown in Figure 2.14. This is sometimes called the band pass "constant K" configuration. The response has geometric symmetry about the band center so that

$$\omega_1\omega_2 = \Omega_o^2 \tag{2.65}$$

where $\omega_2 - \omega_1$ is equal to the characteristic bandwidth $\omega_c = \omega_B$ or ω_T of the low pass network. No contraction of the bandwidth occurs in the transformation. The ratio of series to shunt inductance is on the order of $(\Omega_o/\omega_c)^2$ which makes the circuits as shown in Figure 2.14 sometimes physically difficult to achieve.

To transform the circuit in Figure 2.14 into one of many coupled resonator configurations, we first add an ideal impedance inverter on both sides of each series or shunt resonant branch and convert these

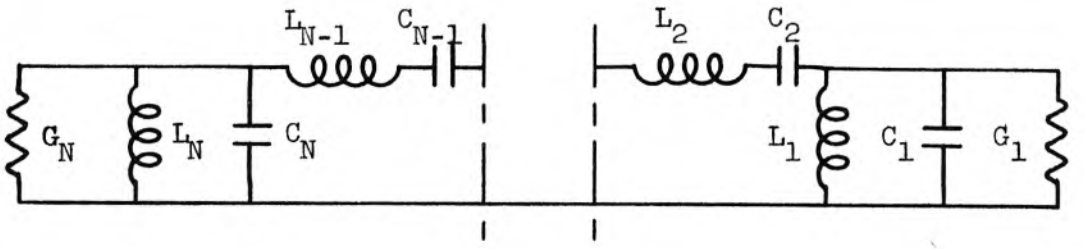

Figure 2.14 "Constant k" bandpass equivalent of low pass ladder in Figure 2.2

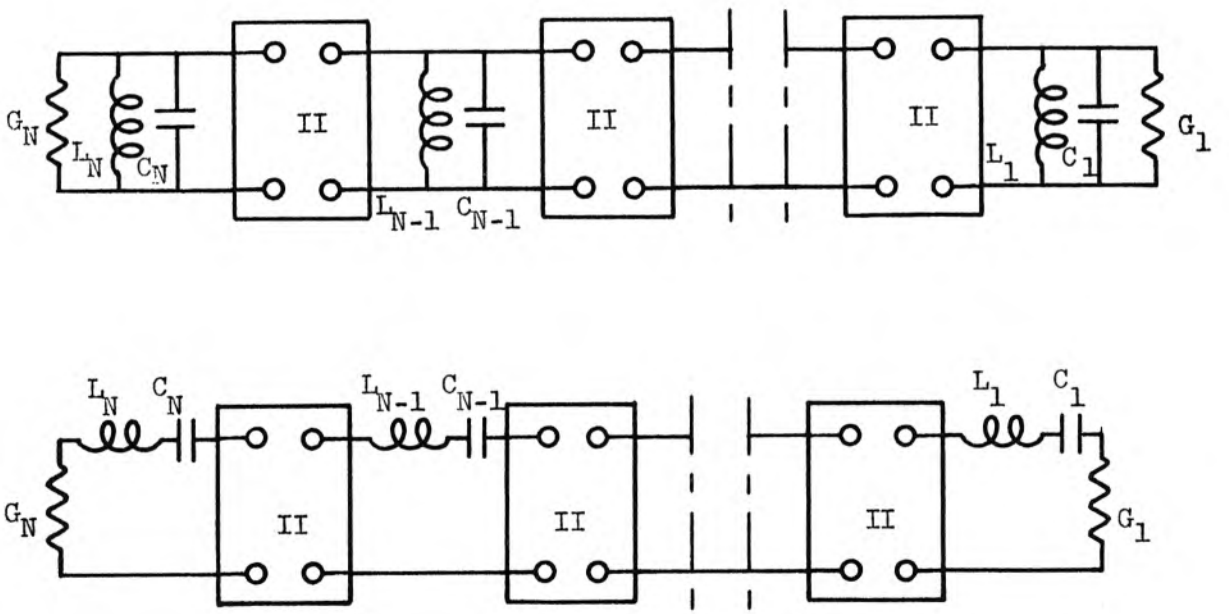

Figure 2.15 Equivalents of Figure 2.14 using ideal impedance inverters

branches to their duals. Two examples are shown in Figure 2.15. An ideal impedance inverter is described in image parameter theory as a four-terminal network with characteristic or image impedance Z_o and a constant phase shift $\theta = \pm \frac{\pi}{2}$. Terminated by Z_1, such an element exhibits an input impedance Z_o^2/Z_1. $1/Z_1$ is physically realizable as the dual network of Z_1. The four impedance inverters shown in Figure 2.16 have constant phase shift $\theta = + \frac{\pi}{2}$, but their image impedance is only approximately constant in narrow band operation. Z_o in each case equals the reactance of the positive arm. Flux coupling may also be used to achieve impedance inversion.

When a proper choice is made the impedance inverters of Figure 2.16 for insertion into the configurations in Figure 2.15, the negative elements are absorbed into larger positive elements giving a realizable circuit. Figure 2.17a and b shows two coupled resonator configurations which are achievable transformations of the basic low pass ladder.

For equal numbers of resonant branches the "constant k" and coupled resonator configurations have the same number of reflection poles and zeros. The transmission response $T(s)T(-s)$ of the "constant k" configuration has two zeros at $s = \infty$ and $s = 0$ for each branch. This is achievable in the coupled resonator only for an odd number of resonators and when the resultant even number of coupling elements is split evenly between inductances and capacitances.

The elements of Figures 2.17a and b may be specified directly in terms of a low pass ladder such as in Figure 2.2 (17) to make their responses equivalent in the narrow band limit. For Figure 2.17a the requirements are:

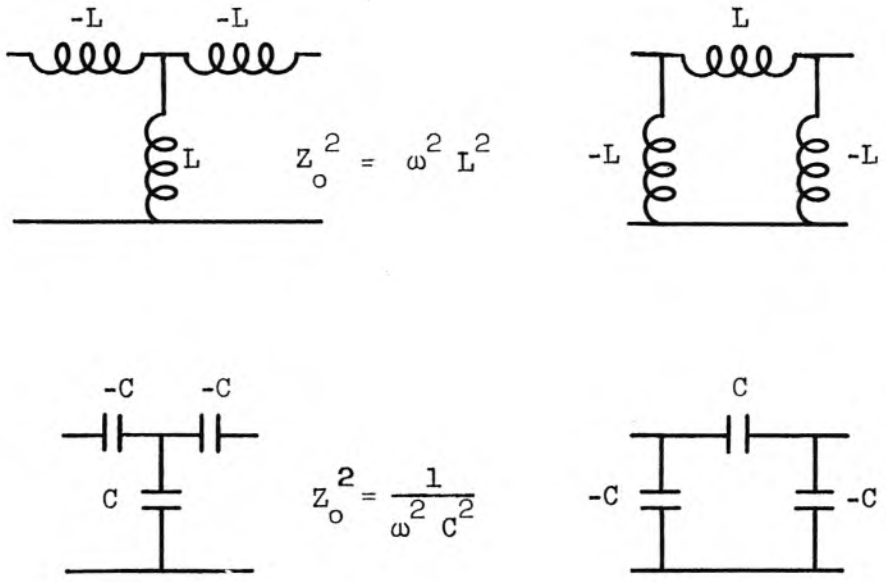

Figure 2.16 Some Non-Ideal impedance inverters

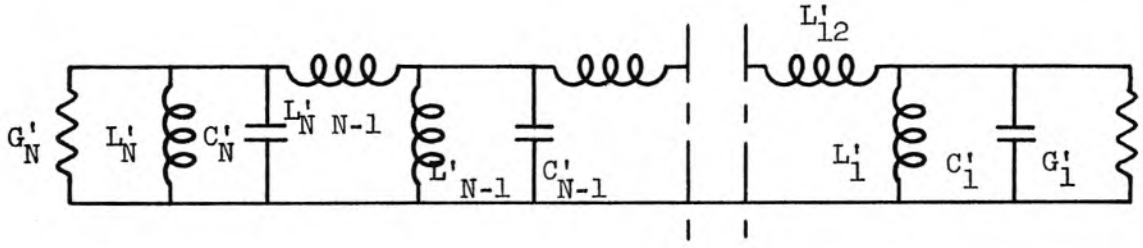

(a) Series inductance coupling

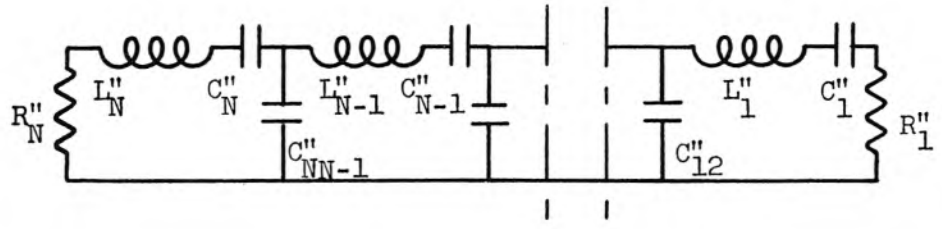

(b) Shunt capacitance coupling

Figure 2.17 Two coupled resonator bandpass approximants to the networks in Figures 2.2 and 2.14

Each node resonates at Ω_o when the other nodes are shorted.

$$\frac{L_1' L_2'}{L_{12}'} = \frac{1}{\Omega_o^2 L_1 C_2} \quad , \text{etc.}$$

$$\frac{G_1'}{C_1'} = \frac{G_1}{C_1} \quad ; \quad \frac{G_N'}{C_N'} = \frac{R_N}{L_N} \text{ or } \frac{G_N}{C_N} \tag{2.66}$$

For Figure 2.17b the requirements are:

Each loop resonates at Ω_o with the other loops open circuited.

$$\frac{C_1'' C_2''}{C_{12}''} = \frac{1}{\Omega_o^2 L_1 C_2} \quad , \text{etc.}$$

$$\frac{R_1''}{L_1''} = \frac{G_1}{C_1} \qquad \frac{R_N'}{L_N'} = \frac{G_N}{C_N} \text{ or } \frac{R_N}{L_N} \tag{2.67}$$

The ratio of series to shunt elements in these configurations usually comes out on the order of ω_c/Ω_o or Ω_o/ω_c rather than these factors squared.

These relations do not completely specify the network elements. Further specification may be obtained by demanding that the new network transform impedance levels; that is, $G_N'/G_1' = n^2 G_N/G_1$. Further specification is undoubtedly also obtained in removing the approximation made in the impedance inverter insertion and synthesizing the network more accurately and directly from the poles and zeros of the desired reflection response. Cohn (18) has shown that Butterworth and Tchebysheff coupled resonator designs with bandwidths greater than 20% are achievable with lumped, waveguide, or coax elements.

Exact low pass to multiple bandpass transformations similar to equation 2.64 can be used to synthesize multiple bandpass negative resistance amplifiers. Coupled resonator approximants for these networks can also usually be found. In Chapter III some double pass band networks are derived for use in wide-banding time varying reactance amplifiers. These allow rather independent specification of the network characteristics in the two bands and provide isolation. They also allow the use of separate terminations for the two bands. Direct transformations on s do not give these capabilities. As will be seen in Section 2.8, double band operation is required in order to obtain stable gain from a tunnel diode at frequencies above its self-resonant frequency, $1/\sqrt{C_T L_p}$. Such networks may also be useful for tunnel diode mixers with gain at two frequencies.

In general, exact low pass to multiple pass transformations distribute the gain and bandwidth but preserve the integral limitations of the active element. Reasonable approximants also have these properties. Thus the basic bandwidth limitations found for the low-pass structure of Figure 2.2 in terms of G_1/C_1 and ρ_o apply equally well to bandpass circuits with the same G_1/C_1 termination. The actual mechanism used to achieve the transformation will depend on the type of elements available in the desired frequency range.

2.6 Sensitivity to Element Variation and Approximate Loss Calculations

It will be of interest in amplifier design to know the approximate limits through which network elements can be varied without causing instability and oscillation. We calculate here approximately these limits for non-simultaneous errors in the ladder terminations.

Let us suppose that a network is designed to give a reflection coefficient ρ_1 and transmission T_1 when terminated in an impedance G_o. The transmission for the same network terminated in $G_o + \Delta Y_o(s)$ gives us a measure of the sensitivity to the error ΔY_o. This response is found to be (9)

$$T_{12}(s) = \frac{T_1(s)\, T_2(s)}{1 - \rho_1(s)\, \rho_2(s)} \tag{2.68}$$

in which $$\rho_2(s) = \frac{\Delta Y_o(s)}{2G_o + \Delta Y_o(s)}$$

and $$T_2(s) = \frac{4G_o\, \mathrm{Re}(G_o + \Delta Y_o(s))}{2G_o + \Delta Y_o(s)}$$

Except when $\rho_2(s) = 0$, the poles of T_{12} are the zeros of $1 - \rho_1(s)\, \rho_2(s)$. For very small $\rho_2(s)$, these zeros must be in the

left half plane since there must exist some small but finite $\Delta Y_o(s)$ which does not lead to instability. These zeros may move toward the $s = i\omega$ axis as $\rho_2(s)$ is increased, and instability sets in when one of the zeros hits this axis. The critical value of $\Delta Y_o(s)$ for this is when

$$\rho_1(s)\,\rho_2(s)\Big|_{i\omega} = 1 \quad \text{for some} \quad \omega \,. \tag{2.69}$$

The magnitude of $\rho_{1(i\omega)}$ is nearly constant and large in a passband and generally decreases rapidly at the band edge. $\rho_{2(i\omega)}$ is presumably a slowly varying function everywhere. If within the passband $|\rho_{2_{i\omega}}| < \frac{1}{|\rho_{1(i\omega)}|_{max}}$, no instability can occur. This sets an approximate limit on the critical magnitude of the error ΔY_o which cannot cause instability

$$\frac{|\Delta Y_o|_{max}}{G_o} \leq \frac{2}{|\rho_1|_{max}} \quad \text{in passband.} \tag{2.70}$$

This formula or its series equivalent may be applied at either termination. To a greater approximation the result is also correct for any other branches of a low pass ladder circuit for which the terminations are approximately G_o, and to "constant k" bandpass equivalents. It must be applied with care in coupled resonator configurations in which impedance transformation occurs.

Using equation 2.68 as a guide, the engineer can set up rough limits on the tolerable element errors in terms of system performance degradation.

It is difficult to obtain useful results from a complete

consideration of simultaneous element variations. One may guess, however, that if the sum of the magnitudes of the fractional immittance errors is within the limits prescribed for any single error, no instability will result. It can be shown that the introduction of uniform loss in all the ladder branches; that is, placing a resistance R_i in series with each L_i and conductance G_i in parallel with each C_i in a low pass circuit so that all R_i/L_i and G_i/C_i are equal, cannot lead to instability. The introduction of this loss is mathematically identical to evaluating real frequency performance at $s = i\omega + \frac{R_i}{L_i}$ rather than at $s = i\omega$. The real frequency axis is thus moved away from left half plane poles and zeros of the lossless system and no instability can ensue.

The effects of this uniform loss on the response can sometimes be removed by "predistorting" the lossless poles to the right. We may make some evaluation of the effects of uniform loss when this predistortion is not carried out, but must base the discussion on results of Chapter IV. Figure 2.18 shows typical poles and zeros of Butterworth transmission and reflections and the distorted $s = \frac{i\omega}{\omega_B} + q_o$ axis.

In low pass circuits q_o represents the inverse quality factor of the network elements at the normalization or cutoff frequency ω_c.

$$q_{oLP} = \frac{1}{Q_c} = \frac{R_i}{\omega_c L_i} = \frac{G_i}{\omega_c C_i} \tag{2.71}$$

For bandpass circuits q_o is associated with the inverse quality factor of the resonant pairs or resonators.

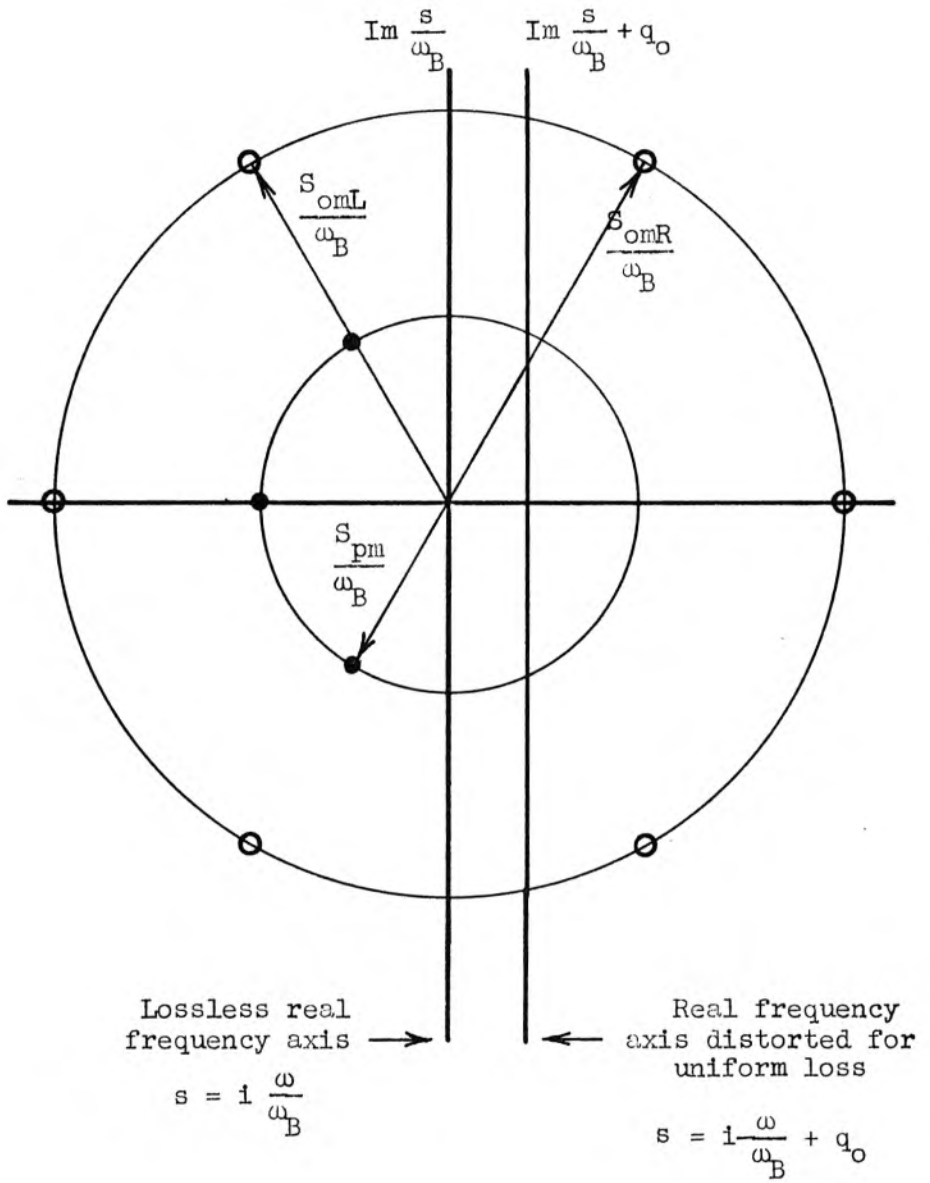

Figure 2.18 Sketch showing poles and zeros of lossless Butterworth response and axis for evaluating response in presence of uniform loss

$$q_{oBP} = \frac{1}{Q_{\Omega_o}} \frac{\Omega_o}{\omega_c} \tag{2.72}$$

Results in Chapter IV give us that for small q_o and Butterworth response

$$\ell n \frac{|T|^2_{q_o}}{|T_B|^2_o} = \ell n \left| \frac{\pi_m(-\frac{s_{pB_m}}{\omega_B})}{\pi_m(q_o - \frac{s_{pB_m}}{\omega_B})} \right|^2 \cong -\frac{4}{\pi} N q_o \tag{2.73}$$

$$\ell n \left| \frac{\pi_m(q_o - \frac{s_{oB_m}}{\omega_B} LHP_m)}{\pi_m(\frac{s_{oB_m}}{\omega_B})_{LHP_m}} \right|^2 \cong \frac{4}{\pi} N \frac{q_o}{\rho_{Bo}^{1/N}} \tag{2.74}$$

$$\ell n \left| \frac{\pi_m(q_o - \frac{s_{oB_m}}{\omega_B})_{RHP_m}}{\pi_m(\frac{s_{oB_m}}{\omega_B})_{RHP_m}} \right|^2 \cong -\frac{4}{\pi} N \frac{q_o}{\rho_{Bo}^{1/N}} \tag{2.75}$$

The effect of the loss on zero frequency transmission is

$$\frac{|T|^2_{q_o}}{|T_B|^2_o} = e^{-\frac{4Nq_o}{\pi}} \tag{2.76}$$

For the active termination reflection

$$\frac{|\rho_1|^2_{q_o}}{|\rho_{1B}|^2_o} = e^{-\frac{4Nq_o}{\pi}} e^{+\frac{4Nq_o}{\pi\rho_{Bo}^{1/N}}} \tag{2.77}$$

and for the passive termination reflection

$$\frac{\left|\rho_N\right|^2_{q_o}}{\left|\rho_{NB}\right|^2_o} = e^{-\frac{4Nq_o}{\pi}} \quad e^{-\frac{4Nq_o}{\pi\rho_{Bo}^{1/N}}} \tag{2.78}$$

The quantities $1 + \left|T\right|^2 - \left|\rho_1\right|^2$ and $1 + \left|T\right|^2 - \left|\rho_N\right|^2$ which appear in noise figure calculations may thus be evaluated at midband frequencies $\omega = 0$ or $\omega = \Omega_o$

$$1 + \left|T\right|^2_{q_o} - \left|\rho_1\right|^2_{q_o} =$$

$$1 + \left|T_B\right|^2_o e^{-\frac{4Nq_o}{\pi}} - \left|\rho_{NB}\right|^2_o e^{-\frac{4Nq_o}{\pi}} e^{\frac{4Nq_o}{\pi\rho_{Bo}^{1/N}}} \tag{2.79}$$

Using the small q_o approximation and $1 + \left|T\right|^2_o = \left|\rho_1\right|^2_o$, we have

$$\left| 1 + \left|T\right|^2_{q_o} - \left|\rho_1\right|^2_{q_o} \right| = \frac{4Nq_o}{\pi}\left(\rho_{Bo}^{2-\frac{1}{N}} - 1\right) \tag{2.80}$$

$$\left| 1 + \left|T\right|^2_{q_o} - \left|\rho_N\right|^2_{q_o} \right| = \frac{4Nq_o}{\pi}\left(\rho_{Bo}^{2-\frac{1}{N}} + 1\right) \tag{2.81}$$

It is not known to what extent these formulas will be correct after predistortion is used.

Equations 2.73 through 2.75 have Tchebysheff complements. The change in the transmission is computed with Tchebysheff poles in Chapter IV.

$$\ell n \frac{|T|^2_{q_o}}{|T_T|^2_o} = \ell n \left| \frac{\pi_m (\frac{s_{pT_m}}{\omega_T})}{\pi_m q_o - \frac{s_{pT_m}}{\omega_T}} \right|^2 = -.6\pi N q_o \qquad (2.82)$$

The Tchebysheff reflection zeros have nearly the same angular spacing as the Butterworth and an average radius

$$\frac{\cosh \frac{1}{N} \sinh^{-1} \frac{\rho_{To}}{\epsilon} + \sinh \frac{1}{N} \sinh^{-1} \frac{\rho_{To}}{\epsilon}}{2} = \frac{1}{2} \left(\frac{2\rho_{To}}{\epsilon}\right)^{1/N} .$$

Thus

$$\ell n \left| \frac{\pi_m (q_o - \frac{s_{oT_m}}{\omega_T})_{LHP_m}}{\pi_m (\frac{s_{oT_m}}{\omega_T})_{LHP_m}} \right|^2 \cong \frac{8}{\pi} N \frac{q_o}{(\frac{2\rho_{To}}{\epsilon})^{1/N}} \qquad (2.83)$$

$$\ell n \left| \frac{\pi_m (q_o - \frac{s_{oT_m}}{\omega_T})_{RHP_m}}{\pi_m (\frac{s_{oT_m}}{\omega_T})_{RHP_m}} \right|^2 = -\frac{8}{\pi} N \frac{q_o}{(\frac{2\rho_{To}}{\epsilon})^{1/N}} \qquad (2.84)$$

2.7 Warm Up Stability

To make a useful amplifier containing a tunnel diode and based on Figure 2.2, one must demand that $-G_1$ be variable from zero to its operating value without causing instability. Otherwise the quiescent operating point may be difficult to reach. This restriction is beyond the scope of the previous analysis and must be considered separately.

The poles and zeros of the reflection coefficient at the active

termination fall in the same half plane. For near unity reflection the zeros approach the poles and ρ_1 has little phase shift. For high reflection, the phase of $-\rho_1$ may change from zero at the origin to a peak of $N\pi/2$ at some value of ω even though it again decreases to zero at infinity. The meaning of this in terms of $Y_{1\ in}$, the admittance seen by $-G_1$, is clarified by Figure 2.19. These diagrams are in a sense Nyquist stability diagrams in which the locus of positive G_1 is the positive real axis. The stability for $G_1 = G_{10}$ has been guaranteed by the synthesis technique. Should G_1 cross the contour instability occurs. An unstable range of G_1 is exhibited in Figure 2.19c. It is of use to calculate the critical value of ρ_o at a given N which gives the tangency of $Y_{in\ 1}(\omega)$ to the real axis shown in Figure 2.19b.

The straightforward analytic approach is to form the imaginary part of $Y_{1\ in}(\omega)$ and demand that its numerator polynomial be zero for some real value of ω. The numerator is of order $N - 1$ in ω^2 and the condition that it has a real ω root implies at least that the discriminant ($b^2 - 4ac$ for a quadratic) vanish. This condition yields an equation of order $2N$ in $\rho_{Bo}^{1/N}$ for Butterworth response. The method is untenable in practice and a less difficult method has been found which gives exact results for the Butterworth cases and limits for the Tchebysheff cases. We consider the new reflection coefficient $\rho_1(\omega)'$ obtained with a termination $- aG_{10}$ in terms of the quiescent state value $\rho_1(\omega)$.

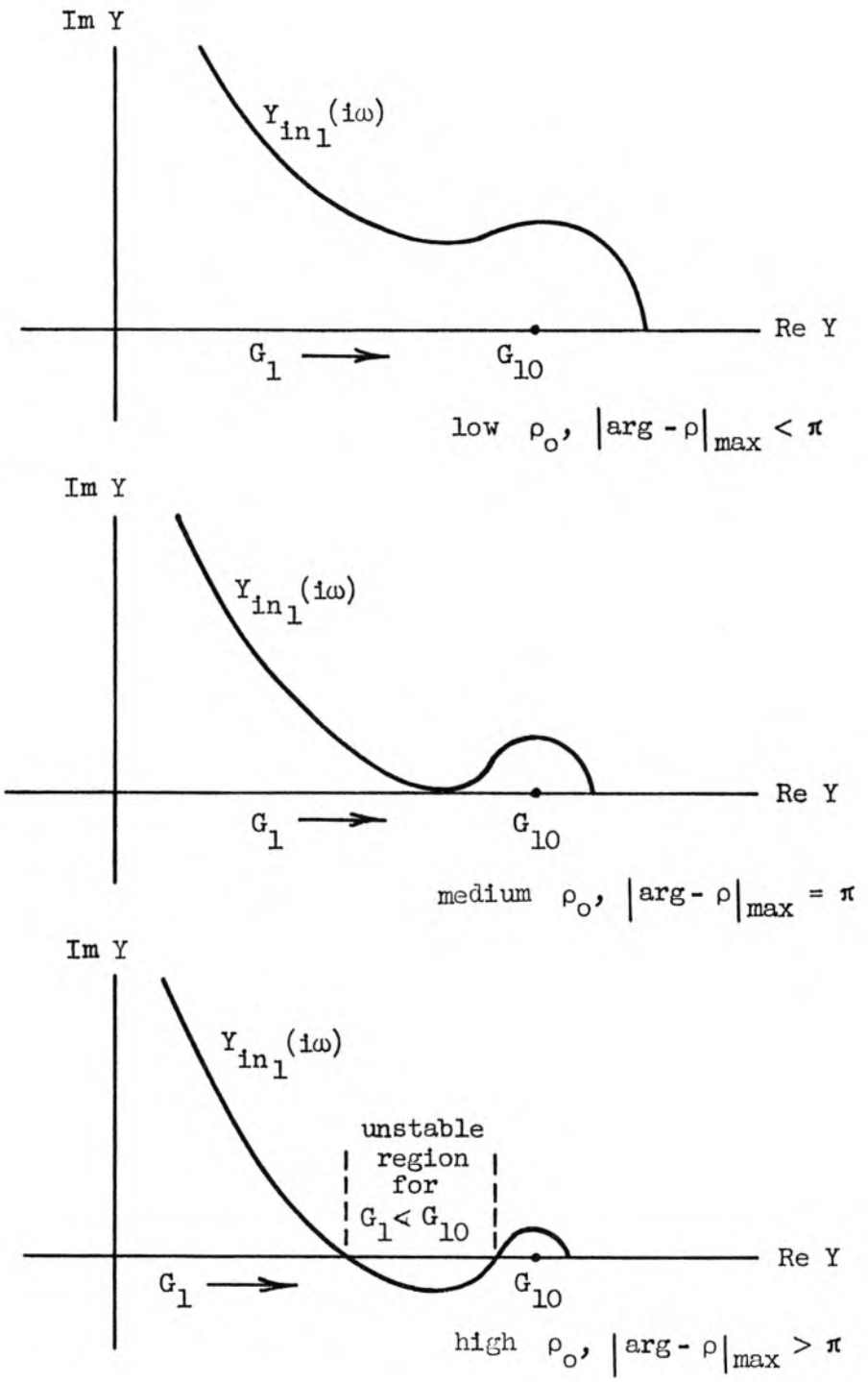

Figure 2.19 Sketches of possible loci of the admittance $Y_{in_1}(i\omega)$ seen by $-G_1$ in Figure 2.2

$$\rho_1(s) = -\frac{G_{10} - Y_{in_1}(s)}{G_{10} + Y_{in_1}(s)}$$

$$Y_{in_1}(s) = \frac{\rho_1(s) - 1}{\rho_1(s) + 1} \qquad (2.85)$$

$$\rho_1'(s) = -\frac{aG_{10} - G_{10}\,\dfrac{\rho_1(s) + 1}{\rho_1(s) + 1}}{aG_{10} + G_{10}\,\dfrac{\rho_1(s) - 1}{\rho_1(s) + 1}}$$

The poles of ρ_1' are the zeros of

$$(\frac{1 - a}{1 + a})(-\rho_1(s)) + 1 \qquad (2.86)$$

As a varies from 1 to -1 the roots of equation 2.85 move from the poles of $\rho_1(s)$ to the zeros of $\rho_1(s)$. The condition that Y_{in_ω} has a point of tangency to the real axis as in Figure 2.19b now results in the condition that the contour, formed by the roots of equation 2.86, has a point of tangency to the $s = j\omega$ axis as shown in Figure 2.20a. At this point, as well as everywhere on the contour, arg $-\rho_1$ equals π. The analytic method of locating this point on the $j\omega$ axis and finding the value or values of ρ_c for which it exists involves as much algebra as the previously suggested analytic method. However, the problem may now be associated with more general techniques in complex variables and, in particular, conformal transformations may be used on both the pole zero configuration and the root contour. The electrostatic analogy is helpful, and using it we associate the desired

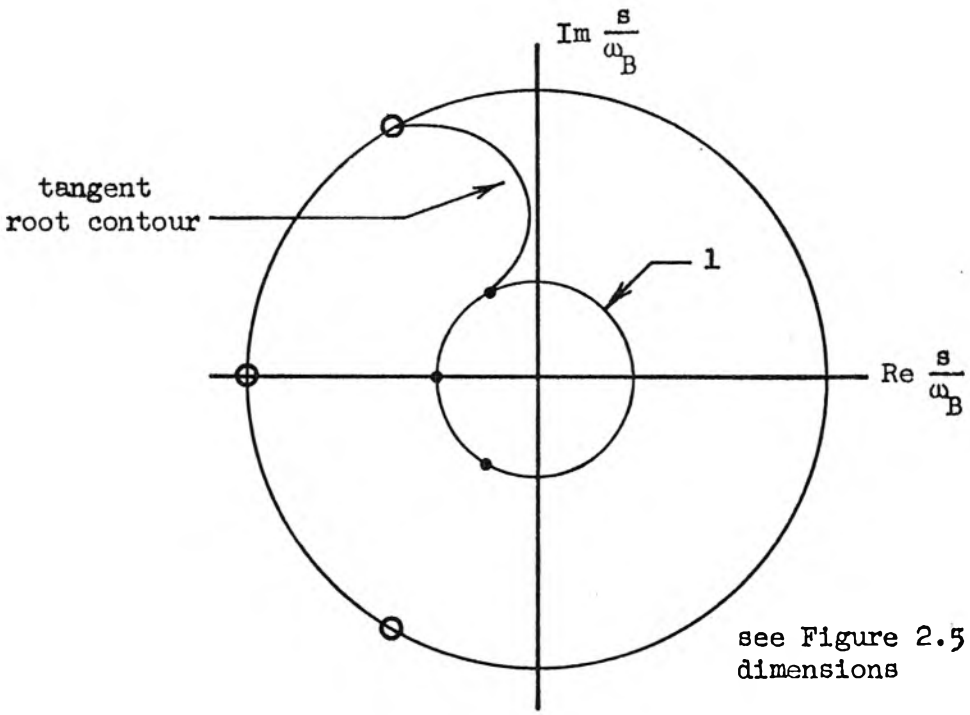

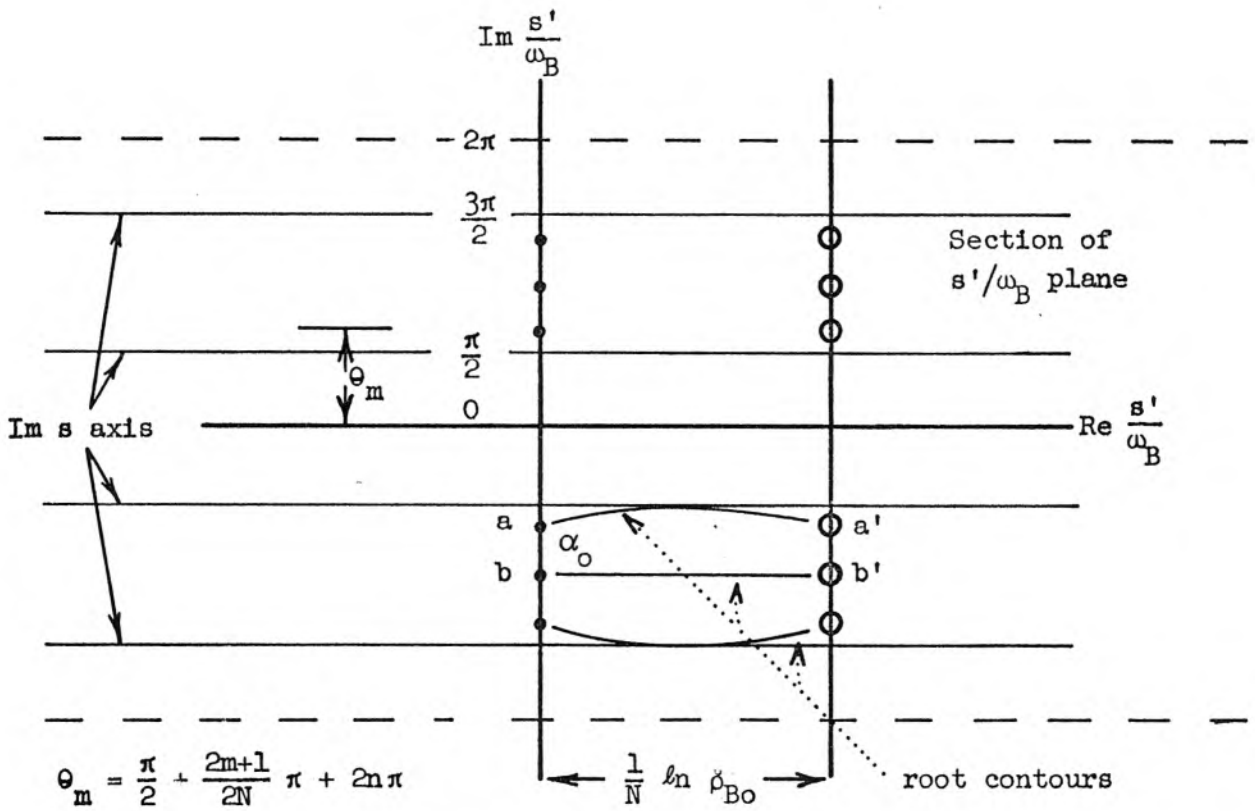

Figure 2.20 Showing the s plane root contour for Butterworth reflection and illustrating the transformation $s'/\omega_B = \ell n\ s/\omega_B$ applied to a Butterworth pole zero configuration

root contours with specific electrostatic flux lines between equal positive and negative line charges corresponding to poles and zeros. Figure 2.20 demonstrates the application of the transformation $\frac{s'}{\omega_B} = \ell n \frac{s}{\omega_B}$ to the Butterworth problem. The infinity of poles and zeros in the s' plane transforms into the Butterworth poles and zeros in the s plane. The root contour cannot be conveniently drawn in the s' plane but from symmetry it is evident that any point of tangency to the $i\frac{\pi}{2} \pm 2\pi i$ line must be at $\text{Re}\frac{s'}{\omega_B} = \frac{1}{2N} \ell n\, \rho_{Bo}$. In the s plane this is $\frac{s}{\omega_B} = \pm i\rho_{Bo}^{1/2N}$. The condition that $\arg -\rho_1 = \pi$ at $\frac{s}{\omega_B} = + i\rho_{Bo}^{1/2N}$ can be written analytically and the resulting transcendental simplified sufficiently to yield a solution for the critical values of ρ_{Bo}. These are shown in Table 2.1

Table 2.1

Critical Values of ρ_{Bo} for Warm Up Stability with Butterworth Response

N	ρ_{Bo} Critical
1	∞
2	∞
3	320
4	92
5	50

The transformation $\frac{s}{\omega_T} = \sinh \frac{s'}{\omega_T}$ is shown in Figure 2.21 applied to a Tchebysheff pole zero system. The similarity of the transformed Tchebysheff system to the transformed Butterworth may be used to establish some limits on the Tchebysheff critical reflection constants. We compare the initial angle of the field line leaving point a at an

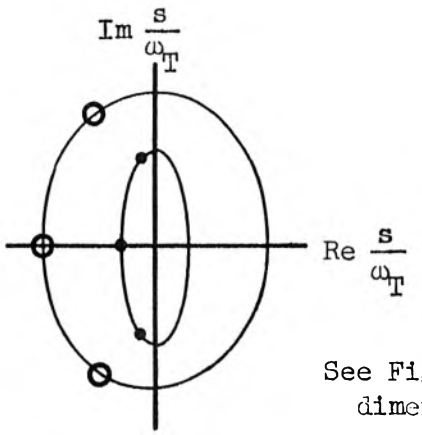

See Figure 2.4 for dimensions

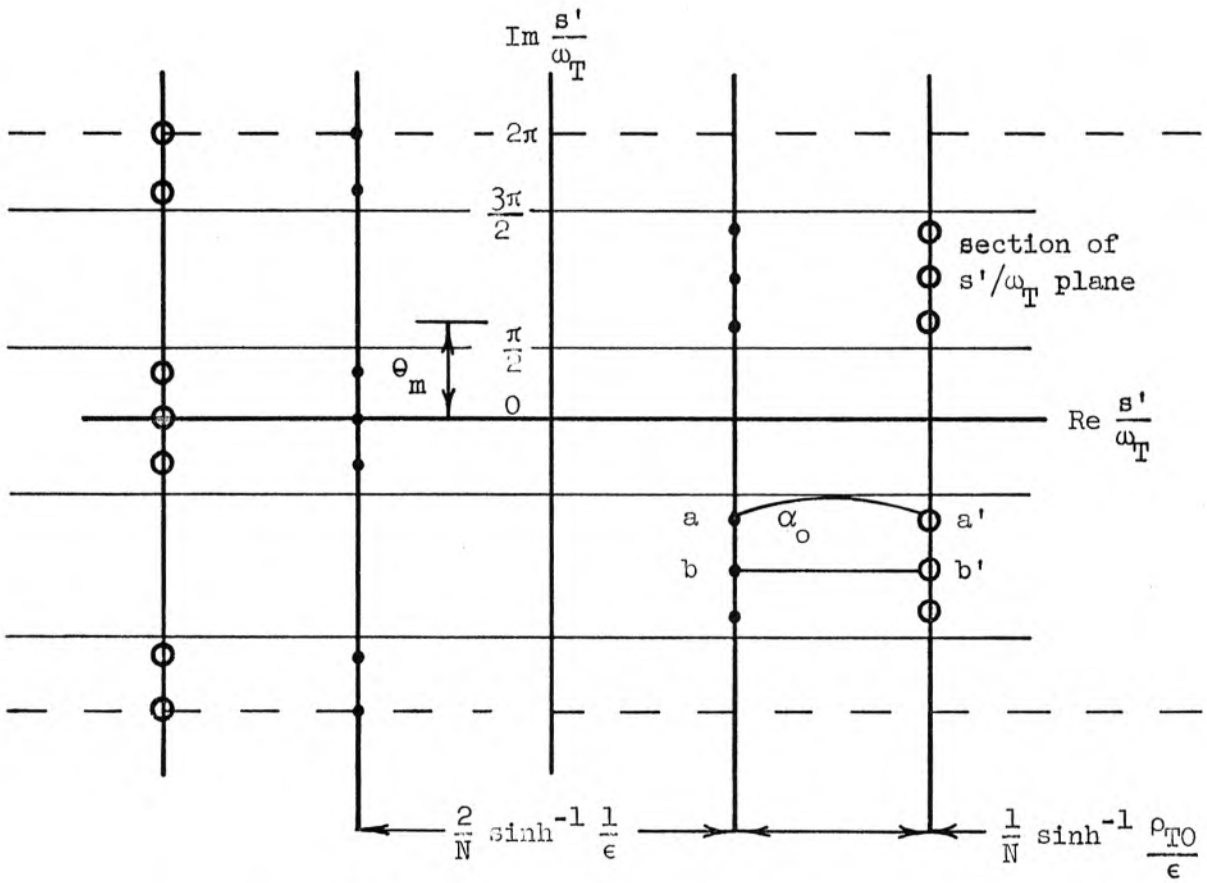

$$\theta_m = \frac{\pi}{2} + \frac{2m+1}{2N}\pi + 2n\pi$$

Figure 2.21 Illustrating the transformation $s/\omega_T = \sinh\ s'/\omega_T$ applied to a Tchebysheff pole zero configuration

angle α_o for point a' which satisfies the conditions $\alpha_o + \sum_i \left[\arg(s_a - s_{pi}) - \arg(s_a - s_{oi})\right] = (2m+1)\pi$, remembering that the known root contour b - b' also satisfies this condition. For spacing $\frac{1}{N}\sinh^{-1}\frac{\rho_{To}}{\epsilon} - \frac{1}{N}\sinh^{-1}\frac{1}{\epsilon}$ equal to $\frac{1}{N}\ln \rho_{Bo}$, the effect of the left side poles and zeros in the Tchebysheff case is to decrease α_o . The Tchebysheff root contour will therefore fall inside the Butterworth contour for equal pole zero spacings. We now have an upper critical limit on ρ_{To} and ϵ .

$$\sinh^{-1}\frac{\rho_{To}}{\epsilon} - \sinh^{-1}\frac{1}{\epsilon}\Bigg|_{critical} \geq \ln \rho_{Bo\ critical}$$

$$\ln\frac{\rho_{To}}{\epsilon} + \sqrt{\left(\frac{\rho_{To}}{\epsilon}\right)^2 + 1} - \ln\frac{1}{\epsilon} + \sqrt{\frac{1}{\epsilon^2} + 1} \geq \ln \rho_{Bo\ critical}$$

$$\left.\frac{\frac{\rho_{To}}{\epsilon} + \sqrt{1 + \left(\frac{\rho_{To}}{\epsilon}\right)^2}}{\frac{1}{\epsilon} + \sqrt{1 + \frac{1}{\epsilon^2}}}\right|_{critical} \geq \rho_{Bo\ critical} \qquad (2.87)$$

$$\therefore \rho_{To\ critical} \geq \rho_{Bo\ critical} .$$

In the limit of small ϵ , for which Tchebysheff and Butterworth characteristics are identical, expression 2.87 gives the predictable result $\rho_{To\ critical} = \rho_{Bo\ critical}$.

2.8 Compatibility of Tunnel Diode Packaging Elements with Basic Configurations

The basic integral limitation on the reflection coefficient of a parallel negative conductance and capacitance

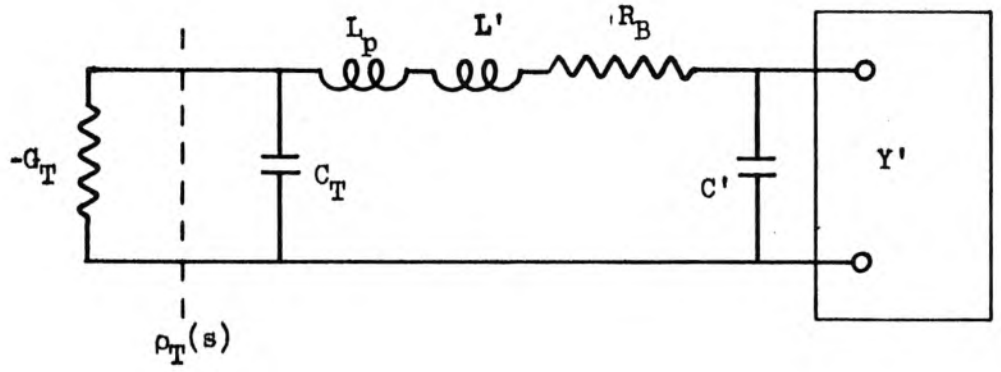

$$-\rho_T(s) = \frac{G_T + sC + \dfrac{1}{s(L_p+L') + R_B + \dfrac{1}{sC'+Y'}}}{-G_T + sC + \dfrac{1}{s(L_p+L') + R_B + \dfrac{1}{sC'+Y'}}} \qquad (2.88)$$

Figure 2.22 Illustrating the circuit for definition of $\rho_T(s)$ and discussion of limitations due to inductance L_p

$$\int_0^\infty \ln \left|\rho_\omega\right| d\omega = \frac{\pi G_T}{C_T}$$

can be generalized to include other reactance effects in a manner similar to that used by Fano (9) on passive reflections. We consider $\oint s^2 \ln(-\rho_T(s))ds$ in which $\rho_T(s)$ is defined in Figure 2.22 and equation 2.88 and the contour is the $s = i\omega$ axis and the infinite half circle enclosing the RHP.

$$\lim_{s \to \infty} -\rho_T(s) = \frac{1 + \frac{G_T}{sC_T} + \frac{1}{s^2(L_p + L')C_T}}{1 - \frac{G_T}{sC_T} + \frac{1}{s^2(L_p + L')C_T}}$$

$$\lim_{s \to \infty} \ln -\rho_T(s) = 2\left(\frac{G_T}{sC_T} - \frac{G_T}{s^3(L_p + L')C_T^3} + \frac{G_T^3}{3s^3C_T^3}\right) \qquad (2.89)$$

Integrating around the circle at infinity with $s = \frac{1}{\epsilon} e^{i\theta}$, $ds = \frac{i}{\epsilon} e^{i\theta} d\theta$ we have $\oint 2s^2 \frac{G_T}{sc} ds = 0$ and

$$\int_0^\infty \omega^2 \ln \left|\rho_\omega\right| d\omega = \pi \frac{G_T}{C_T}\left[\frac{1}{(L_p + L')C_T} - \frac{1}{3}\left(\frac{G_T}{C_T}\right)^2\right] + \frac{\pi}{3} \sum_{RHP_m} \left(s_{pm}^3 - s_{om}^3\right) \qquad (2.90)$$

Integration of $s^2 \ln(-\rho)ds$ around the LHP gives

$$-\int_0^\infty \omega^2 \ln\left|\rho_\omega\right| d\omega = \frac{\pi G_T}{C_T}\left[\frac{1}{(L_p + L')C_T} - \frac{1}{3}\left(\frac{G_T}{C_T}\right)^2\right] + \frac{\pi}{3} \sum_{LHP_m} \left(s_{pm}^3 - s_{om}^3\right) \qquad (2.91)$$

Just as G_T/C_T was determined in Section 2.2 from the pole and zero locations of the desired response, here we may further determine $(L_p + L')C_T$. Equation 2.90 sets an upper limit on L_p which cannot be exceeded if the desired low pass response is to be achieved. The minimum value of the left hand integral for reasonably flat low pass response over a bandwidth ω_c is $\frac{\omega_c^2}{3} \pi \frac{G_T}{C_T}$.

$$\omega_c^2 \frac{\pi}{3} \frac{G_T}{C_T} < \pi\left(\frac{G_T}{C_T} \frac{1}{(L_p + L')C_T} - \frac{1}{3}\left(\frac{G_T}{C_T}\right)^3\right) \tag{2.92}$$

$$\frac{1}{L_{p\,max} C_T} = \Omega_T^2 \geq \frac{\omega_c^2}{3} + \frac{1}{3}\left(\frac{G_T}{C_T}\right)^2 \quad \text{or} \quad \frac{\omega_c^2}{3}\left(1 + \left(\frac{\ell n\, \rho_o}{\pi}\right)^2\right) \tag{2.93}$$

Green's (15) closed form Butterworth and Tchebysheff formulas yield

$$\frac{1}{L_p C_T \omega_B^2} \leq \frac{(1 - \rho_{Bo}^{1/N})^2 + 4\rho_{Bo}^{1/N} \sin^2 \frac{\pi}{2N}}{4 \sin \frac{\pi}{2N} \sin \frac{3\pi}{2N}} \tag{2.94}$$

$$\frac{1}{L_p C_T \omega_T^2} \leq \frac{\sin \frac{\pi}{2N}}{\sin \frac{3\pi}{2N}} \left(\cos^2 \frac{\pi}{2N} + \left(\sinh \frac{1}{N} \sinh^{-1} \frac{\rho_{To}}{\epsilon}\right)\right.$$

$$\left. \times \left(\sinh \frac{1}{N} \sinh^{-1} \frac{1}{\epsilon}\right)\right) + \frac{\left(\sinh \frac{1}{N} \sinh^{-1} \frac{\rho_{To}}{\epsilon} - \sinh \frac{1}{N} \sinh^{-1} \frac{1}{\epsilon}\right)^2}{4 \sin \frac{\pi}{2N} \sin \frac{3\pi}{2N}} \tag{2.95}$$

For stable bandpass response about center frequency Ω_o

$$\int_0^\infty \omega^2 \ell n \left|\rho_\omega\right| d\omega \cong \int_0^\infty \Omega_o^2 \ell n \left|\rho_\omega\right| d\omega \cong \Omega_o^2 \pi \frac{G_T}{C_T} \tag{2.96}$$

and equation 2.90 becomes

$$\Omega_o^2 \frac{\pi G_T}{C_T} = \frac{\pi G_T}{C_T}\left(\frac{1}{(L_p + L')C_T} - \frac{1}{3}\left(\frac{G_T}{C_T}\right)^2\right) \tag{2.97}$$

This may be interpreted as meaning that for stable operation, the self resonant frequency of the tunnel diode $\Omega_T = \left(\frac{1}{L_p C_T}\right)^{1/2}$ must be at least as high as the center frequency of the amplifier. The impossibility of bandpass operation above Ω_T does not extend to multiple bandpass operation. Consider an amplifier design which divides $\rho(\omega)$ into passbands centered at Ω_1 and Ω_2 such that

$$\ell n\ \rho(\omega_1)\ \Delta\omega_1 = (1 - X)\frac{\pi G_T}{C_T}$$

and (2.98)

$$\ell n\ \rho(\omega_2)\ \Delta\omega_2 = X\frac{\pi G_T}{C_T}$$

Equation 2.90 is then written as

$$\left[(1 - X)\Omega_1^2 + X\Omega_2^2\right]\frac{\pi G_T}{C_T} = \frac{\pi G_T}{C_T}\left[\frac{1}{(L_p + L')C_T} - \frac{1}{3}\left(\frac{G_T}{C_T}\right)^2\right] \tag{2.99}$$

The greatest gain and bandwidth at Ω_2 is obtained when Ω_1 is zero and equation 2.99 gives X, the reduction factor of the gain bandwidth integral relation which must be taken to get stable amplification above the self-resonant frequency of the tunnel diode.

Equation 2.90 also sets an upper limit on L_p above which no stable operation of a tunnel diode in an otherwise passive circuit is possible. Since $\int_0^\infty \omega^2\ \ell n|\rho|\, d\omega$ must be positive, either

$\frac{1}{(L_p + L')C_T} - \frac{1}{3}\left(\frac{G_T}{C_T}\right)^2$ is positive or $\sum_{RHP_m} s_{pm}^3 - s_{om}^3$ is positive, or both. We have seen that no $\sum_{RHP_m} s_{om}$ can exist. Therefore, when $(L_p + L') > 3C_T/G_T^2$, the tunnel diode circuit of Figure 2.22 is unstable independent of the nature of passive $Y'(s)$.

These arguments about L_p are based on the assumption that it is a truly lumped inductance. The integrals are not correct for the distributed inductance of transmission lines and must be applied with care in this case. It is likely that when the packaging structure of a tunnel diode need not be specifically analyzed as a transmission line in the design of an amplifier, then these limitations will apply.

In the low pass amplifier models which do not require the load or generator conductance to parallel G_T equations 2.94 and 2.95 indicate the extent to which series inductance may be accommodated for Butterworth and Tchebysheff response. When the load or generator conductance must appear in parallel with G_T, the approximate stability analysis given in Section 2.5 will indicate the stability tolerance on L_p. When L_p is one-tenth this value it is not likely to depreciate the performance badly. The magnitude of the effect of series resistance R_B may be determined in the same way.

For bandpass circuits the normal low pass to bandpass transformation requires an inductance $L = 1/\Omega_o^2 C_T$ to shunt G_T and C_T as in Figure 2.23a. An equivalence between this circuit and that of Figure 2.23b is found, however, which tolerates L_p to about $1/\Omega_o^2 C_T$ and does not change G_T/C_T. This transformation is exact and leads to an element ratio L_2'/L_1' not much different than the original L_2/L_1. It has

already been suggested that this ratio becomes too large in narrow band amplifiers with "constant k" configurations.

For narrow bandpass operation it is possible to represent the parallel conductance and capacitance of the tunnel diode by an approximate series resistance and capacitance as shown in Figure 2.24. The representation can be made exact at the band center, $s = i\Omega_o$, and is good for $s \cong i\Omega_o$. The series resistance R_B, as well as any generator or load resistance, can be accommodated directly in previously discussed amplifier configurations when this representation is used. When amplifiers are synthesized on this basis, however, it will in general be necessary to check the second order terms of the series representation approximation to guarantee that they do not severely affect the actual response. The approximation will not, in general, be useful for high fractional bandwidth amplifiers, and the use of the equivalence shown in Figure 2.23 is preferable for that case.

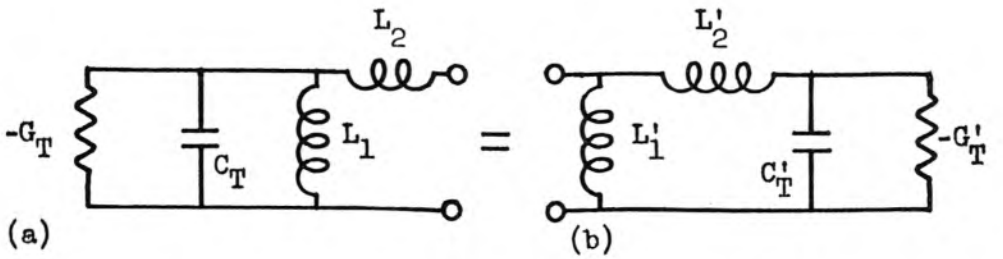

$$G'_T = \frac{L_1}{2L_2 + L_1 + L_2^2/L_1} G_T \qquad C'_T/G'_T = C_T/G_T \tag{2.100}$$

$$L'_1 = L_1 + L_2 \qquad L'_2 = L_2 + L_2^2/L_1$$

Figure 2.23 Two equivalent networks which evidence the compatibility of tunnel diode lead inductance with the "constant k" bandpass configuration.

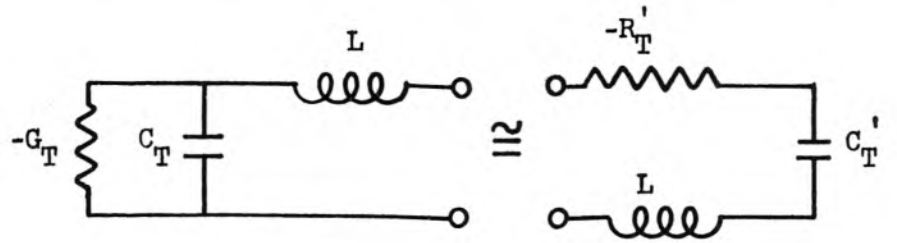

$$R'_T = \frac{G_T}{G_T^2 - s^2 C_T^2} \cong \frac{G_T}{G_T^2 + \Omega_o^2 C_T^2} \quad \text{for } s \cong i\Omega_o$$

$$C'_T = C_T\left(1 - \frac{G_T^2}{s^2 C_T^2}\right) \cong C_T\left(1 + \frac{G_T^2}{\Omega_o^2 C_T^2}\right) \quad \text{for } s \cong i\Omega_o \tag{2.101}$$

$$\text{for } LC'_T = 1/\Omega_o^2 \quad , \quad R'_T/L = G_T/C_T$$

Figure 2.24 An illustration of a narrow band equivalent representation of a tunnel diode

CHAPTER III

GAIN AND BANDWIDTH IN NONLINEAR REACTANCE AMPLIFIERS

3.0 Introduction

That the bandwidth of nonlinear reactance amplifiers depends on the number of tuning elements in the amplifier circuit was recognized by Seidel and Herrmann (19). They postulated that maximally flat reflection response would be obtained in degenerate parametric amplifiers, and that with N control factors or independent reactance slopes at their disposal, the first $2N-2$ coefficients of a Taylor series expansion of the power gain could be set to zero at the band center. They found $\omega_B \rho_o^{1/N}$ to be an invariant for constant N and felt that this indicated finite bandwidths could be obtained at unlimited gain by choosing sufficiently large N. Their failure to find a logarithmic relation between ρ_o and ω_B was due to the inability of their analysis to yield values for the non-zero coefficients in this Taylor expansion.

Matthei (20) has attempted a design of wide band multiply tuned parametric amplifiers by using the D.C. reactance of the nonlinear reactor as an element of a filter circuit whose input admittance, including this reactance, is nearly constant in a desired band. He has chosen to synthesize these filters as matched Tchebysheff bandpass networks whose transmission response with the correct passive termination is

$$|T|^2 = \frac{1}{1 + \epsilon^2 T_N^2 \frac{\omega}{\omega_T}} \quad .$$

These filters he finds, when inserted into parametric amplifier circuits,

do not give adequately smooth gain response, and it is necessary to insert further reactances to shape the gain. Matthei's procedure is basically a "cut and try" method which does not attempt to approach an optimum synthesis based on a recognition of a fundamental bandwidth limitation and in terms of the circuit complexity.

In this chapter we will make essentially the same assumptions as Herrmann and Seidel and Matthei have made in their works. Somewhat greater space will be expended with fundamental and background material to remove from the complete equations of nonlinear reactance amplifiers all factors except those essential to the synthesis of parametric amplifiers and upconverters in their simplest form. Many of these factors can be later reinstated as perturbations.

The resulting first order theory, plus assumptions which are necessary for an analytic treatment of a two-frequency problem, do lead to a definite bandwidth limitation for the parametric amplifier. A consideration of some physical requirements of an amplifier operating at two frequencies further delineates this limitation. The low pass ladder network is again chosen as a configuration for synthesis.

3.1 Basic Equations of Nonlinear Reactance Amplifiers

Let us consider a nonlinear capacitance

$$\frac{dq}{dV} = C(V) \tag{3.1}$$

in the presence of a large "pump" voltage $V_p(t)$ and a vanishingly small signal voltage $dV(t)$. As long as $q(t)$ is analytic, it may be expanded in a Taylor series about $V_p(t)$ as

$$q_p(t) + dq(t) = q_o + \int_{}^{V_p(t)} C(V)dV + C[V_p(t)]$$

$$+ \frac{1}{2!}\frac{d}{dV} C(V)\Big|_{V_p(t)} [dV(t)]^2 + \cdots \qquad (3.2)$$

For $dV(t)$ small, it is correct to write

$$q_p(t) = q_o + \int_{}^{V_p(t)} C(V)dV$$

$$dq(t) = C[V_p(t)]\, dV(t) \qquad (3.3)$$

effectively separating the pump excitation equations from the small signal equations. The quantity $C[V_p(t)]$ is called a time varying capacitance and in this work will be given explicit time dependence,

$$C[V_p(t)] = C(t) = C_o(1 + \eta \cos \Omega_p t) \quad , \quad \eta < 1 \qquad (3.4)$$

In a similar manner the large and small signal equations of a nonlinear elastance $\frac{dV}{dq} = S(q)$ can be separated to give

$$V_p(t) = V_o + \int_{}^{q_p(t)} S(q)\, dq$$

$$dV(t) = S[q_p(t)] \qquad (3.5)$$

and we will consider only the case

$$S[q_p(t)] = S(t) = S_o(1 + \eta \cos \Omega_p t) \qquad (3.6)$$

The small signal voltage, charge, and current can now be written as a summation of cisoidal functions with complex coefficients:

$$dV(t) = \sum_{n=-\infty}^{\infty} V_n e^{i(\omega_o + n\Omega_p)t} + V_n^* e^{-i(\omega_o + n\omega_p)t}$$

$$dq(t) = \sum_{n=-\infty}^{\infty} q_n e^{i(\omega_o + n\Omega_p)t} + q_n^* e^{-i(\omega_o + n\Omega_p)t}$$

$$di(t) = \sum_{n=-\infty}^{\infty} i_n e^{i(\omega_o + n\omega_p)t} + i_n^* e^{-i(\omega_o + n\omega_p)t} \qquad (3.7)$$

in which one of the frequencies $\omega_n = \omega_o + n\Omega_p$, usually ω_o, is associated with a single small signal source in the system. In this work both ω_o and Ω_p are taken as positive and $\omega_o < \Omega_p$. There is, however, some significance to negative frequencies in time varying reactance amplifier equations and the general formulation methods of circuit analysis with complex variables can be used only when negative frequencies are allowed.

The circuit equations for a time varying capacitance $C_o(1 + \eta \cos \Omega_p t)$ in parallel with an admittance $Y'(\omega)$ and a current generator $2I_m \cos(\omega_o + n\omega_p)t$ as shown in Figure 3.1 can now be separated by harmonic components. The time dependence is then removed giving the set of equations 3.8 and their complex conjugates.

$$\frac{I_n}{i\omega_n} = (C_o + \frac{Y_n'}{i\omega_n})V_n + \frac{\eta}{2} C_o(V_{n+1} + V_{n-1})$$

$$Y_n' = Y'(i\omega)\Big|_{\omega_n} \qquad (3.8)$$

Desoer (21) has pointed out that an equivalent network can be drawn for such a system of equations in which the V_n can be associated with node voltages. Such a network is shown in Figure 3.2. It is useful as

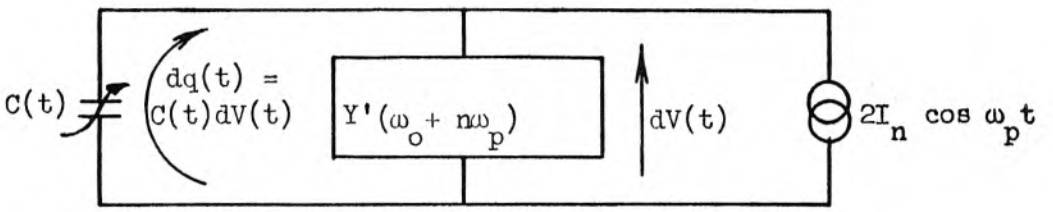

Figure 3.1 An equivalent circuit leading to equations 3.8

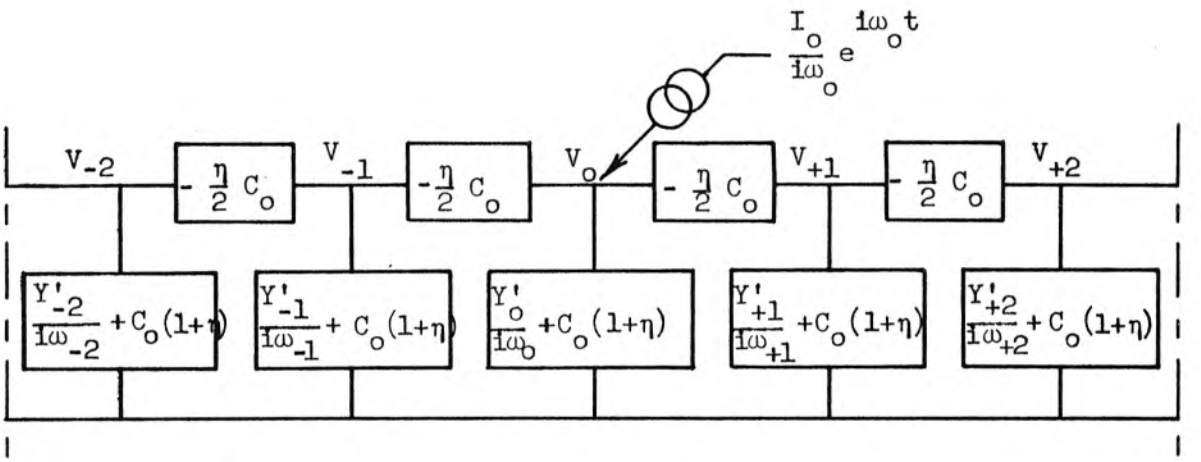

Figure 3.2 A section of a network whose loop equations are the same as equations 3.8

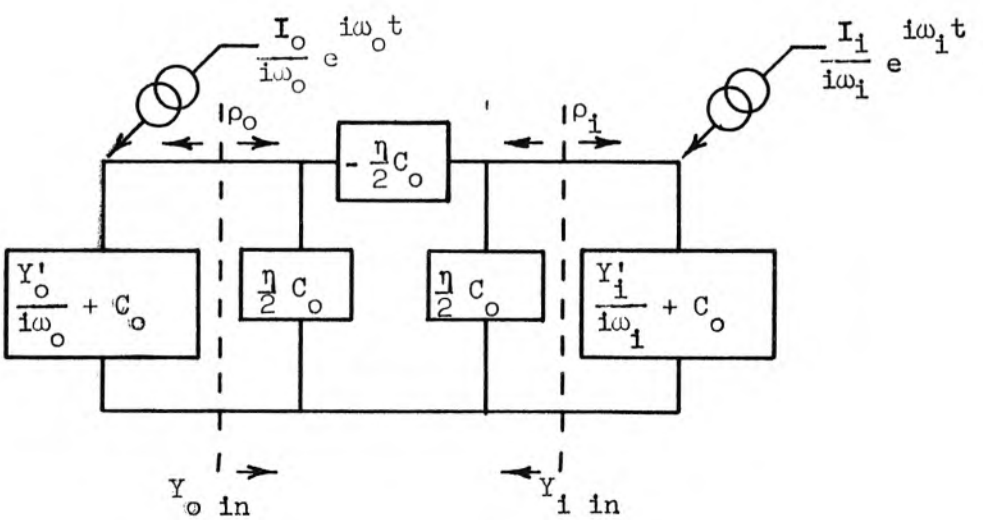

Figure 3.3 First order network extracted from Figure 3.2

an aid in visualizing the effects of eliminating most of the frequencies ω_n from first order consideration in a synthesis technique. It is seen in Figure 3.2 that unless the shunt branches are near resonance, that is, $\frac{Y_n'}{i\omega_n} + C_o(1+\eta) = 0$, the series branches represent much higher impedance levels. For first order synthesis we will make the assumption that those branches whose frequencies are of fundamental interest, ω_o and ω_{+1} for the non-inverting upconverter, or ω_o and ω_{-1} for the parametric amplifier are near resonance and that all other branches are effectively short circuits. These other shunt branches can then be treated as perturbations after the general Y_n are calculated from the resulting first order synthesized network. The equivalent circuit resulting from this approximation is shown in Figure 3.3 in which ω_i may be either ω_{-1} or ω_{+1} . Input admittances $Y_{o\ in}$ and $Y_{i\ in}$ and reflection coefficients ρ_o and ρ_i as shown in this figure may be written out as

$$Y_{o\ in} = \frac{Y_{ci}^2}{Y_i' + i\omega_i C_o} = \frac{Y_{ci}^2}{Y_i}$$

$$Y_{i\ in} = \frac{Y_{ci}^2}{Y_o' + i\omega_o C_o} = \frac{Y_{ci}^2}{Y_o} \qquad (3.9)$$

in which $Y_{ci}^2 = (\frac{\eta}{2} C_o)^2 \omega_i\omega_o$

$$\rho_o = \frac{Y_o^* - \frac{Y_{ci}^2}{Y_i}}{Y_o + \frac{Y_{ci}^2}{Y_i}} \quad , \qquad \rho_i = \frac{Y_i^* - \frac{Y_{ci}^2}{Y_i}}{Y_i + \frac{Y_{ci}^2}{Y_o}} \qquad (3.10)$$

When $\omega_i = \omega_{-1}$ is negative both $Y_{o\ in}$ and $Y_{i\ in}$ have negative real parts and the reflection coefficients are greater than unity. The power flow from Re Y_o to Re Y_i can be shown to obey the Manley Rowe relations, and in all cases $|\rho_o| = |\rho_i|$. Thus we may write

$$|T_{oi}|^2 = \frac{\omega_i}{\omega_o}(1 - |\rho|^2)$$

$$|T_{io}|^2 = \frac{\omega_o}{\omega_i}(1 - |\rho|^2) \qquad (3.11)$$

Analogous equations and equivalent representations exist for the analysis of the time varying elastance $S_o(1 + \eta \cos \omega_p t)$. Postulating such an element in series with an impedance $Z'(\omega)$ and a voltage generator $2V_n \cos(\omega_o + n\omega_p)t$ as shown in Figure 3.4, one finds the harmonic components of the charge through $S(t)$ to obey the equations

$$V_n = (S_o + i\omega_n Z_n')q_n + \frac{1}{2} S_o(q_{n+1} + q_{n-1})$$

$$Z_n' = Z'(i\omega)\Big|_{\omega_n} \qquad (3.12)$$

This results in an equivalent circuit representation in which the q_n are loop charges as shown in Figure 3.5. The assumption of resonance in the ω_o and $\omega_i = \omega_{+1}$ or ω_{-1} branches again justifies the removal of the other frequency effects to first order giving the equivalent circuit of Figure 3.6. As analogues of equations 3.9 and 3.10 we have

$$Z_{o\ in} = \frac{Z_{ci}^2}{Z_i' + \frac{S_o}{i\omega_i}} = \frac{Z_{ci}^2}{Z_i} \qquad (3.13)$$

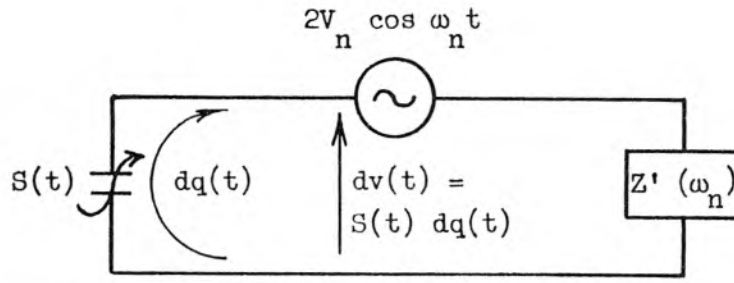

Figure 3.4 An equivalent circuit leading to equations 3.12

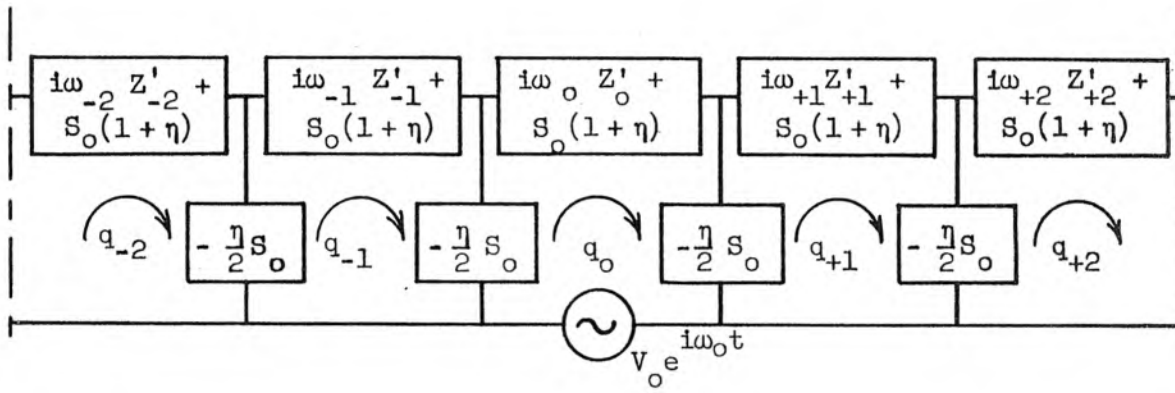

Figure 3.5 A section of a network whose loop equations are the same as equations 3.12

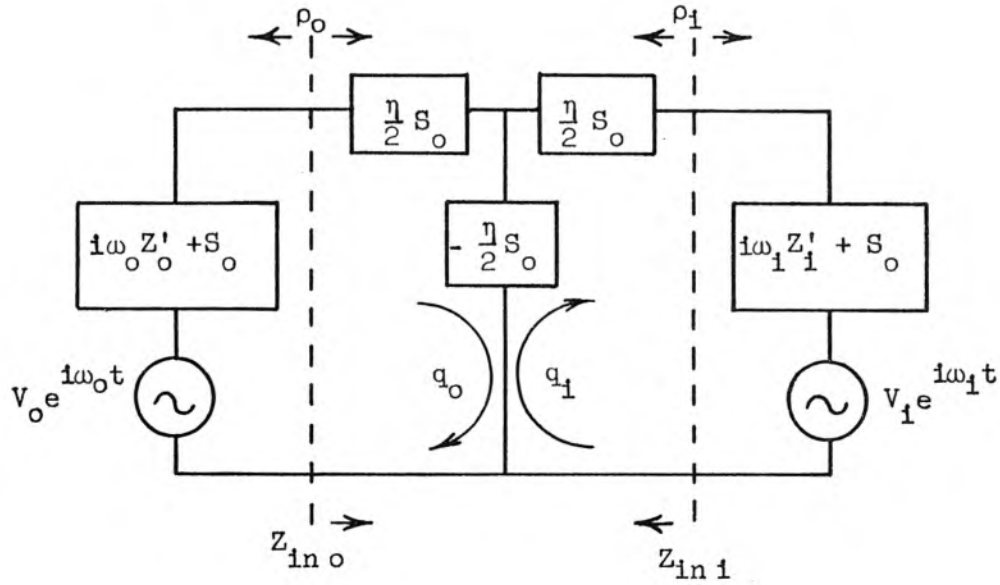

Figure 3.6 First order network extracted from Figure 3.5

$$Z_{i\ in} = \frac{Z_{ci}^2}{Z_o' + \frac{S_o}{i\omega_o}} = \frac{Z_{ci}^2}{Z_o} \tag{3.13}$$

in which $Z_{ci}^2 = \left(\frac{\eta}{2} S_o\right)^2 \frac{1}{\omega_i \omega_o}$

$$\rho_o = \frac{\frac{Z_{ci}^2}{Z_i} - Z_o^*}{\frac{Z_{ci}^2}{Z_i} + Z_o} \quad , \quad \rho_i = \frac{\frac{Z_{ci}^2}{Z_o} - Z_i^*}{\frac{Z_{ci}^2}{Z_o} + Z_i} \tag{3.14}$$

Equations 3.11 are also valid for this circuit.

The essential properties of the sinusoidal capacitance $\eta C_o \cos \Omega_p t$ and elastance $\eta S_o \cos \Omega_p t$ working into admittances at frequencies ω_o and $\omega_i = \omega_o \pm \Omega_p$ are the properties of the center T and π sections in Figures 3.3 and 3.6. These properties may be better delineated by looking at equations 3.9 through 3.14. They are seen to be impedance inversion with or without negation depending on the sign of ω_i, and a unilateral gain mechanism which we may call Manley Rowe amplification. A four-terminal network representation of these mechanisms is shown in Figure 3.7. The Manley-Rowe amplifier does not change impedance levels and may therefore be removed from reflection coefficient synthesis problems.

The assumption that Y_o and Y_i or Z_i are resonant allows us to calculate roughly the perturbations due to neglected frequencies. Let us consider, for example, the degenerate parametric amplifier for which ω_o and $-\omega_{-1}$ are approximately $\Omega_p/2$. The resonance condition demands

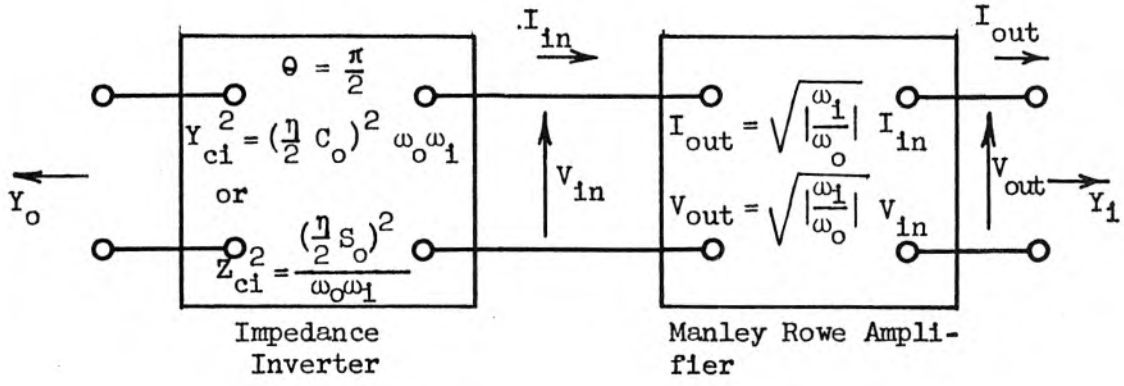

Figure 3.7 A four-terminal equivalent circuit of sinusoidal reactance operating between admittances at ω_o and ω_i

that an inductance $L = 1/C_o\Omega_o^2$ parallel C_o. Inserting the admittances Y_{+1} and Y_{-2} of this parallel combination at $\omega_o + \omega_p$ and $\omega_o - 2\omega_p$ into Figure 3.2, one finds the perturbing admittance at ω_o and ω_{-1} to be approximately $-i\omega_o(\frac{\eta}{2})^2 C_o$ and $-i\omega_{-1}(\frac{\eta}{2})^2 C_o$. Thus the perturbation appears as a negative capacitance and decreases the effective D.C. capacitance C_o by $(\frac{\eta}{2})^2 C_o$. Since η will in practice rarely exceed one-half, this perturbation is likely to give a negligible increase in bandwidth capability. In highly sensitive amplifiers, however. this effect may be important for accurate circuit alignment. A similar calculation may be done on a series basis with S_o assumed in series with an inductance $S_o/(\Omega_p/2)^2$ to make Z_o and Z_{-1} resonant at $\Omega_p/2$. The resulting perturbation impedance to be added to Z_o due to Z_{+1} is approximately $-i\omega_o(\frac{\eta}{2})^2 \frac{S_o}{[(\frac{3}{2})\Omega_p]^2}$. This perturbation appears as a negligible negative inductance which is down by a factor $(\frac{\eta}{6})^2$ from that already in the circuit.

For nondegenerate operation, more must be known about the amplifier circuit but the perturbations are generally on the same order of magnitude. Only in the case where Ω_p/ω_o is very large $(-\omega_{-1} \cong \omega_{+1})$ are the perturbations likely to become so large as to invalidate the synthesis procedure.

Throughout the following sections, admittances Y_o and Y_i will be assumed resonant at frequencies Ω_o and Ω_i. It will also be necessary in most analytic work to take the factor $\omega_o\omega_i$ appearing in Z_{ci}^2 and Y_{ci}^2 as a constant $\Omega_o\Omega_i$ over the amplifier passband. The actual variation of $\omega_o\omega_i$ can probably be incorporated in intensive

synthesis focused on special cases. It is appropriate to evaluate here the conditions when this may be necessary.

For the upconverter ρ may be written from equation 3.10 as

$$\rho_o = \frac{Y_o^* Y_{+1} - (\frac{\eta}{2}C_o)^2 \Omega_o\Omega_{+1} - (\frac{\eta}{2}C_o)^2 (\omega_o\omega_{+1} - \Omega_o\Omega_{+1})}{Y_o Y_{+1} + (\frac{\eta}{2}C_o)^2 \Omega_o\Omega_{+1} + (\frac{\eta}{2}C_o)^2 (\omega_o\omega_{+1} - \Omega_o\Omega_{+1})} \tag{3.15}$$

For a matched amplifier synthesis $Y_o^* Y_{+1} \cong (\frac{\eta}{2}C_o)^2 \Omega_o\Omega_{+1}$ and the reflection $\Delta\rho_o$ due to the variation of $\omega_o\omega_{+1}$ is approximately

$$\Delta\rho_o \cong \frac{1}{2}\left(\frac{\omega_o\omega_{+1} - \Omega_o\Omega_{+1}}{\Omega_o\Omega_{+1}}\right) \tag{3.16}$$

For $\omega_{+1} \gg \omega_o$

$$\Delta\rho_o = \frac{1}{2}\left(1 - \frac{\omega_o}{\Omega_o}\right) = \frac{1}{2}\frac{\Omega_o - \omega_o}{\Omega_o} \tag{3.17}$$

The maximum value of $\Delta\rho_o$ occurs when ω_o is at either band edge and $\Delta\rho_{o\ max}$ is therefore recognizable as one-fourth of the fractional bandwidth of the amplifier

$$\Delta\rho_{o\ max} = \frac{1}{4}\frac{\omega_{co}}{\Omega_o} = \frac{1}{4}\ \text{fractional B.W.} \tag{3.18}$$

Thus even with upconverters whose fractional bandwidth is unity, the effect of this approximation is very small. In a similar fashion the reflection coefficient of the parametric amplifier can be written approximately in terms of the synthesized reflection coefficient ρ_o and the error $\Omega_o\Omega_{-1} - \omega_o\omega_{-1}$ as

$$\rho \cong \frac{1}{\frac{1}{\rho_o} + \frac{\Omega_o\Omega_{-1} - \omega_o\omega_{-1}}{2\Omega_o\Omega_{-1}}} \tag{3.19}$$

For the degenerate ($\Omega_o = \Omega_{-1}$) case, $\Omega_o\Omega_{-1} - \omega_o\omega_{-1}$ is always very small. For the worst case, when $-\Omega_{-1} \gg \Omega_o$, we may arbitrarily stipulate that the effects of the approximation become important when $\frac{\Omega_o\Omega_{-1} - \omega_o\omega_{-1}}{2\Omega_o\Omega_{-1}} = \frac{1}{2\rho_o}$ at the band edges. This defines a gain bandwidth product below which the approximation is reasonably good.

$$\frac{\omega_c}{\Omega_o} = \text{fractional B.W.} < \frac{2}{\rho_o} \tag{3.20}$$

In most amplifier synthesis the fractional bandwidth will be limited to something under $2/\rho_o$ by other factors, and this approximation will cause little trouble.

In the following work Y_{ci}^2 and Z_{ci}^2, unless explicitly written out, will be assumed to have $\omega_o\omega_i$ replaced by $\Omega_o\Omega_i$.

3.2 Required Symmetry and the Ladder Network Representation

The analytic treatment of time varying reactance devices demands that further restrictions be made on the immittance functions $Y_o = Y_o' + i\omega_o C_o$, $Y_i = Y_i' + i\omega_i C_o$, $Z_o = Z_o' + \frac{S_o}{i\omega_o}$, and $Z_i = Z_i' + \frac{S_o}{i\omega_i}$ beyond that already made in section 3.1 concerning resonance properties. The most commonly made assumption is that these functions exhibit exact complex conjugate symmetry about their respective band center frequencies Ω_o and Ω_i , i.e., $Y_o(i\Omega_o + \omega) = [Y_o(i\Omega_o - \omega)]^*$. This assumption not only makes possible mathematical synthesis techniques but also can be realized approximately in the simplest physical circuitry. Although it is not clear to what extent this assumption narrows the possibilities of time varying reactance amplifier synthesis and removes interesting results from our view, we shall nevertheless make it here. This allows us to choose as the complex frequency variable

$$s = i(\omega_o - \Omega_o) \tag{3.21}$$

where Ω_o is the ω_o band center frequency. Using the relationship between ω_o, ω_i, and Ω_p of section 3.1 we have also

$$i(\omega_i - \Omega_i) = i(\omega_o \pm \Omega_p - \Omega_o \mp \Omega_p) = s \tag{3.22}$$

In order to apply to time varying reactance amplifiers the low pass ladder network formalism established in Chapter II we now restrict the form of Y_o and the other immittance functions to that defined below. Over the range of s values with which the synthesis procedure is to be directly concerned, let the immittance functions be written as a

continued fraction expansion of reactance slopes about their resonant center frequencies. This means choosing the immittance functions as bandpass equivalents of input impedances to low pass ladder networks. The forms of these immittance functions are written below.

$$Y_o\Big|_{i\Omega_o+s} = Y_o' + i\omega_o C_o =$$

$$sC_{10} + G_{10} + \cfrac{1}{sL_{20} + R_{20} + \cfrac{1}{\ddots + \cfrac{1}{sC_{NO} + G_{NO}}}} \qquad (3.23)$$

$$Z_o\Big|_{i\Omega_o+s} = Z_o' + \frac{S_o}{i\omega_o} =$$

$$sL_{10} + R_{10} + \cfrac{1}{sC_{20} + G_{20} + \cfrac{1}{\ddots + \cfrac{1}{sL_{NO} + R_{NO}}}} \qquad (3.24)$$

$$Y_i\Big|_{i\Omega_i + s} = Y_i' + i\omega_o C_i =$$

$$sC_{1i} + G_{1i} = \cfrac{1}{sL_{2i} + R_{2i} + \cfrac{1}{\ddots + \cfrac{1}{sC_{Ni} + G_{Ni}}}} \tag{3.25}$$

$$Z_i\Big|_{i\Omega_i + s} = Z_i' + \frac{S_o}{i\omega_i} =$$

$$sL_{1i} + R_{1i} + \cfrac{1}{sC_{2i} + G_{2i} + \cfrac{1}{\ddots + \cfrac{1}{sL_{Ni} + R_{Ni}}}} \tag{3.26}$$

In these formulas the G_N and R_N should be associated with network terminations. The other conductances and resistances represent losses in the network. Except for R_1 and G_1 which represent parasitic losses in the nonlinear reactance element, circuit losses will not be considered in this work. The first reactive terms in each of these expressions, C_{1o} and C_{1i}, or L_{1o} and L_{1i}, must somehow be fixed by the necessity of bringing C_o or S_o to resonance at two frequencies Ω_o and Ω_i.

Low pass ladder networks representing these immittance functions can now be added to the four-terminal network of Figure 3.7 to give an

over-all low pass equivalent of the parametric amplifiers or non-inverting upconverters to be synthesized. Figures 3.8 and 3.9 show such equivalent circuits. The ω_i circuit has been converted by the impedance inverter to its positive or negative dual. The Manley Rowe amplifier is represented by the dotted line M-R across which power gain ω_i/ω_o takes place from left to right or gain ω_o/ω_i from right to left. The properties of these equivalent circuits and syntheses using them will be discussed in later sections. It is pertinent to state now, however, that any fundamental bandwidth limitations which arise in this lossless circuit must be normalized in terms of the fixed elements C_{lo} and C_{li}/Y_{ci}^2 or L_{lo} and L_{li}/Z_{ci}^2. The only possible combinations which have the dimensions of angular frequency are

$$\omega_N = \sqrt{\frac{|Y_{ci}^2|}{C_{lo}\,C_{li}}} = \frac{\eta}{2}\,\frac{C_o}{\sqrt{C_{lo}C_{li}}}\,\sqrt{|\Omega_o\Omega_i|} \tag{3.27}$$

and

$$\omega_N = \sqrt{\frac{|Z_{ci}^2|}{L_{li}\,L_{lo}}} = \frac{\eta}{2}\,\frac{S_o}{\sqrt{L_{lo}\,L_{li}}}\,\frac{\sqrt{|\Omega_o\Omega_i|}}{|\Omega_o\Omega_i|}\,. \tag{3.28}$$

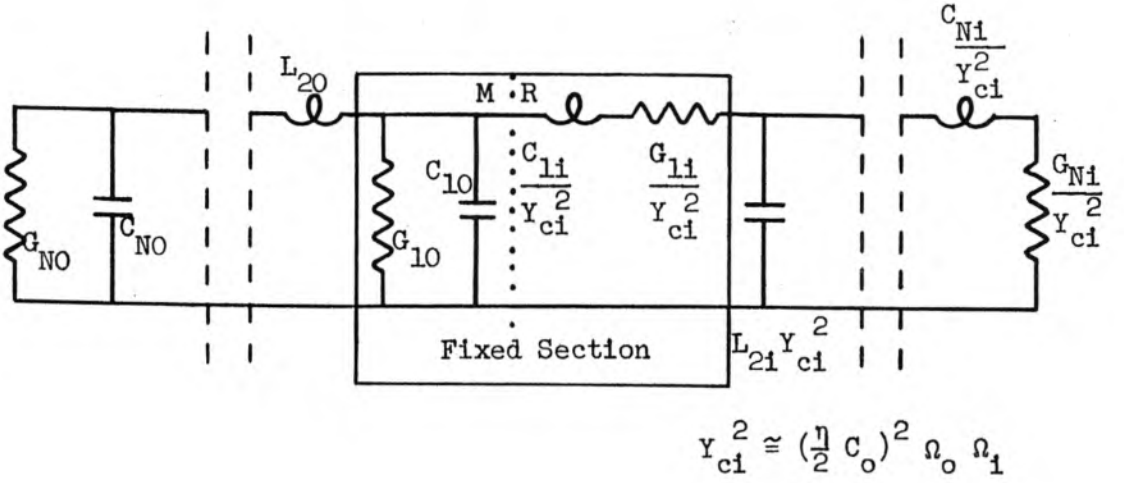

Figure 3.8 Low pass ladder network equivalent of a sinusoidally varying capacitance amplifier working at frequencies ω_o and ω_i

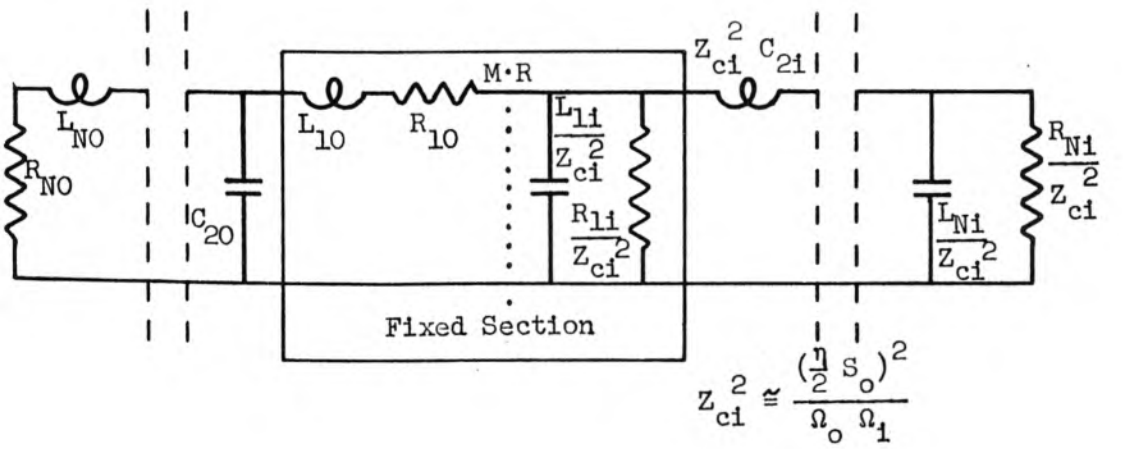

Figure 3.9 Low pass ladder network equivalent of a sinusoidally varying elastance amplifier working at frequencies ω_o and ω_i

3.3 Physical Configurations which Approximate Low Pass Ladder Networks in One or Two Frequency Bands

The aim of this section is to give physically realizable circuit configurations which approximate as closely as possible the conditions laid down in section 3.2. It is hoped that these conditions will appear more reasonable in the light of their physical embodiments. Some relation between C_o and $\sqrt{C_{lo}C_{li}}$ and between S_o and $\sqrt{L_{lo}L_{li}}$ is also sought so as to further our knowledge of bandwidth limitations in time varying reactance amplifiers.

In the so-called "degenerate" parametric amplifier with $\Omega_o = -\Omega_{-1}$ filter networks with only one complex conjugate symmetric passband are required. The "constant k" bandpass configuration or any of the coupled resonator configurations (see Figures 2.14 - 2.17) both fulfill the symmetry conditions exactly in the narrow band limit and reasonably well otherwise. For a "constant k" configuration C_o must be the capacitance of the first shunt resonator or S_o the elastance of the first series resonator. The admittance slope of the first resonator at Ω_o is to be associated with C_{lo} and C_{li} and is given by $2C_o$ for the shunt case;

$$C_{lo} = C_{1\,-1} = 2C_o \tag{3.29}$$

For the series case an inductance $L_o = S_o/\Omega_o^2$ must appear in series with S_o and the reactance slopes about Ω_o are

$$L_{lo} = L_{1\,-1} = \frac{2S_o}{\Omega_o^2} \tag{3.30}$$

Just as the "constant k" bandpass configuration is derived from the low

pass ladder by the transformation $s' \rightarrow \Omega_o(\frac{s}{\Omega_o} + \frac{\Omega_o}{s})$, other transformations may be found which convert low pass ladders into multiple bandpass ladders. The transformation

$$s' \rightarrow \frac{(s^2 + \Omega_o^2)(s^2 + \Omega_i^2)}{s(s^2 + \Omega_r^2)} \tag{3.31}$$

converts a low pass ladder with first element C_o into a double passband ladder with first element C_o . Figure 3.10 illustrates this. This transformation also yields the desired symmetry about Ω_o and Ω_i in the narrow band limit and the admittance slopes C_{lo} and C_{li} are given respectively by

$$C_{lo} = \frac{ds'C_o}{ds}\Big|_{\Omega_o} = 2(\frac{\Omega_i^2 - \Omega_o^2}{\Omega_r^2 - \Omega_o^2})C_o$$

$$C_{li} = \frac{ds'C_o}{ds}\Big|_{\Omega_i} = 2(\frac{\Omega_i^2 - \Omega_o^2}{\Omega_i^2 - \Omega_r^2})C_o \tag{3.32}$$

A fundamental principle of conservation of bandwidth is embodied in this transformation resulting in the relation

$$\frac{1}{C_{lo}} + \frac{1}{C_{li}} = \frac{1}{2C_o} \tag{3.33}$$

The minimum value of $C_{lo}C_{li}$ is obtained when $\Omega_r^2 = \frac{\Omega_o^2 + \Omega_i^2}{2}$ for which C_{lo} and C_{li} are equal.

$$C_{lo}\, C_{li}\Big|_{min} = 16C_o^2 \tag{3.34}$$

A transformation can also be found to change a low pass ladder whose first element is a unit series inductance into a double bandpass filter whose first section contains a series elastance S_o .

$$s' \rightarrow \frac{S_o \Omega_r^2}{\Omega_i^2 \Omega_o^2} \frac{(s^2+\Omega_o^2)(s^2+\Omega_i^2)}{(s^2+\Omega_r^2)s} \tag{3.35}$$

This is illustrated in Figure 3.11. The slope parameters are found to be

$$\frac{L_{lo}|\Omega_i\Omega_o|}{S_o} = \frac{2\Omega_r^2}{|\Omega_i\Omega_o|}\left(\frac{|\Omega_i|^2-\Omega_o^2}{\Omega_r^2-\Omega_o^2}\right)$$

$$\frac{L_{li}|\Omega_i\Omega_o|}{S_o} = \frac{2\Omega_r^2}{|\Omega_i\Omega_o|}\left(\frac{|\Omega_i|^2-\Omega_o^2}{|\Omega_i|^2-\Omega_r^2}\right) \tag{3.36}$$

Writing $$K = \frac{\Omega_o^2 L_{lo}}{|\Omega_i^2|^2 L_{li}} \tag{3.37}$$

one can show that

$$\frac{\Omega_r^2}{\Omega_o^2} = \frac{K+1}{K+\left|\frac{\Omega_o}{\Omega_i}\right|^2} \tag{3.38}$$

and

$$\frac{L_{lo}L_{li}|\Omega_o^2\Omega_i^2|}{S_o^2} = \frac{4(K+1)^2}{K} \tag{3.39}$$

This has a minimum value of 16 at $K = 1$. Figure 3.12 shows the function $\frac{S_o}{|\Omega_o\Omega_i|}\frac{1}{\sqrt{L_{lo}L_{li}}}$, which appears in bandwidth normalization equation 3.28, as a function of $K = \Omega_o^2 L_{lo}/\Omega_i^2 L_{li}$.

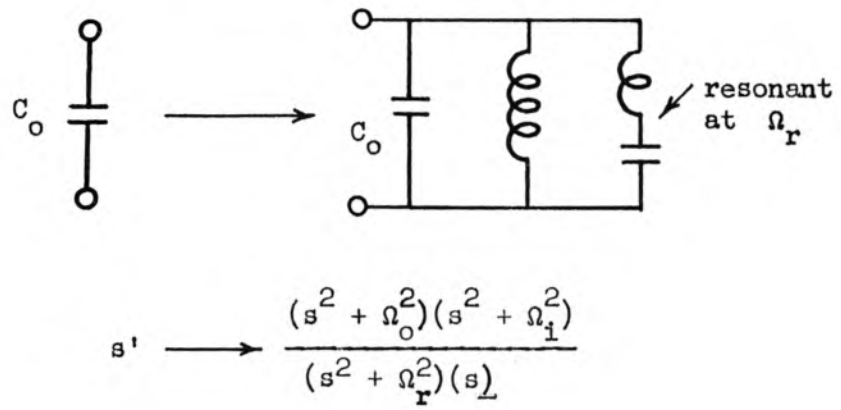

Figure 3.10 Illustrating a low pass to double bandpass transformation which preserves shunt capacitance C_o

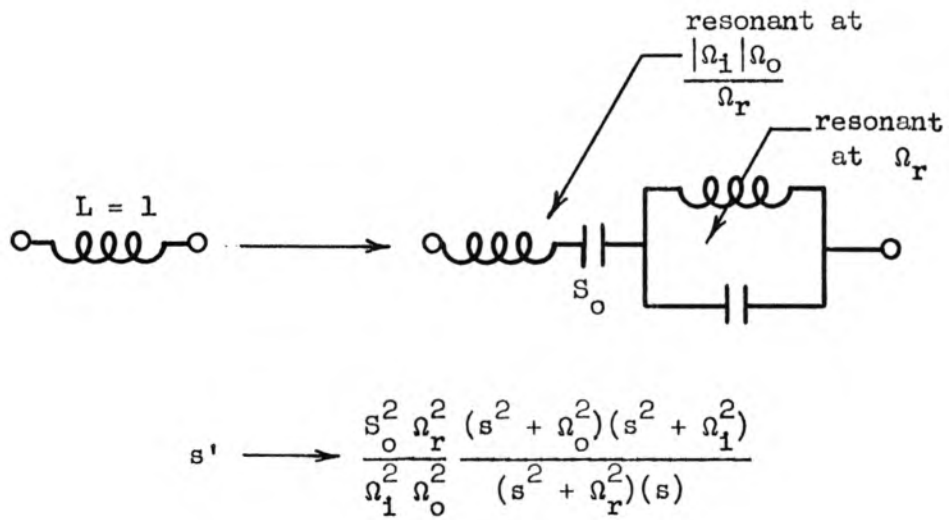

Figure 3.11 Illustrating a low pass to double bandpass transformation which results in a series elastance S_o

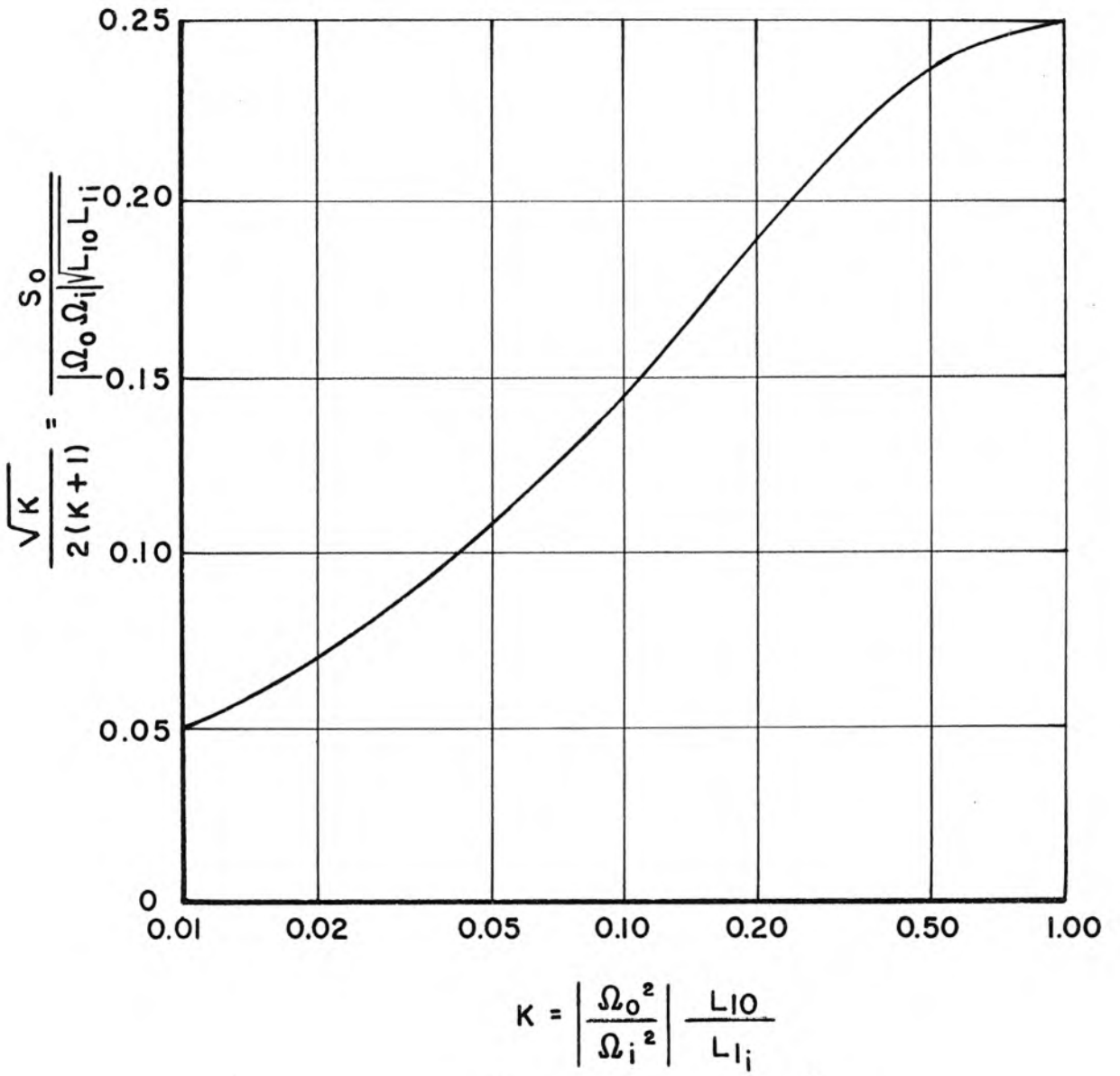

Figure 3.12 A plot of $\frac{S_o}{|\Omega_o \Omega_i| \sqrt{L_{10} L_{1i}}}$ versus $\frac{\Omega_o^2}{\Omega_i^2} \frac{L_{10}}{L_{1i}}$

The limitations on the minimum values of $C_{lo}C_{li}$ and $L_{lo}L_{li}$, while derived here from double bandpass transformations, appear to be much more general. They are, in a sense, fundamental expressions of conservation of bandwidth for resonant elements. The maximum values of the frequency normalization factors given in equations 3.27 and 3.28 can now be found. They have the same maximum for both the shunt and series derived circuit:

$$\omega_{N\,max} = \frac{\eta}{8}\sqrt{\Omega_o\,\Omega_i} \tag{3.40}$$

One other case of interest is that in which the series inductance associated with S_o is greater than the value $S_o\Omega_r^2 / |\Omega_i^2|\Omega_o^2$ demanded by the transformation 3.35. More elastance S_o' must then be added in series with S_o to bring the physical element to double resonance and the effective value of η is reduced by the factor $\Omega_D^2\,\Omega_r^2/\Omega_o^2\,\Omega_i^2$ in which Ω_D^2 is the self-resonant frequency of S_o and its associated series inductance.

$$\eta' = \eta\frac{\Omega_D^2\,\Omega_r^2}{\Omega_o^2\,\Omega_i^2} \qquad \text{for} \qquad \frac{\Omega_D^2\,\Omega_r^2}{\Omega_o^2\,\Omega_i^2} \leq 1 \tag{3.41}$$

ω_N is still maximized by $K = 1$ and its maximum value is

$$\omega_{N\,max}' = \frac{\eta}{8}\frac{\Omega_D^2\,\Omega_r^2}{\Omega_o^2\,\Omega_i^2} = \frac{\eta}{8}\frac{2\Omega_D^2}{\Omega_i^2+\Omega_o^2} \quad \text{for} \quad \Omega_D^2 \leq \frac{\Omega_i^2+\Omega_o^2}{2} \tag{3.42}$$

The double bandpass circuitry leaves something to be desired in terms of flexibility. It restricts discussion to situations in which the idler and signal frequencies have the same number of tuning

elements, and it is not completely compatible with separate terminations for these two frequencies. A more general approach is shown in Figures 3.13 and 3.14 in which a doubly resonant section containing the time varying element is placed between two single passband filters. The elements of the double tuned section must be chosen to resonate near Ω_o with the input immittance of the Ω_i filter and to resonate near Ω_i with the input immittance of the Ω_o filter. The limitations expressed in equations 3.32, 3.33, and 3.34 for C_{lo} and C_{li}, and in equations 3.36, 3.37 and 3.39 for L_{lo} and L_{li} are still approximately correct for these new configurations. To indicate this more clearly for one case we consider the circuit in Figure 3.14b. The formulation of the coupled resonator configuration, as in Chapter II, demands that loop 0 of Figure 3.14b be resonant at Ω_o when loop 1 is open. At this frequency, the input impedance to the Ω_i filter is essentially set at $i\Omega_o L_{cli}$. The application of this same condition at Ω_i demands that loop 0 resonate at Ω_i with loop 2 open. The input impedance of the Ω_o filter at Ω_i is essentially $i\Omega_i L_{clo}$. The simultaneous application of these resonance conditions demands that the double tuned section in series with both L_{clo} and L_{cli} be resonant at both Ω_o and Ω_i. The configuration of these elements, however, is exactly that of Figure 3.11, and the reactance slope limitations found for this figure are therefore applicable directly.

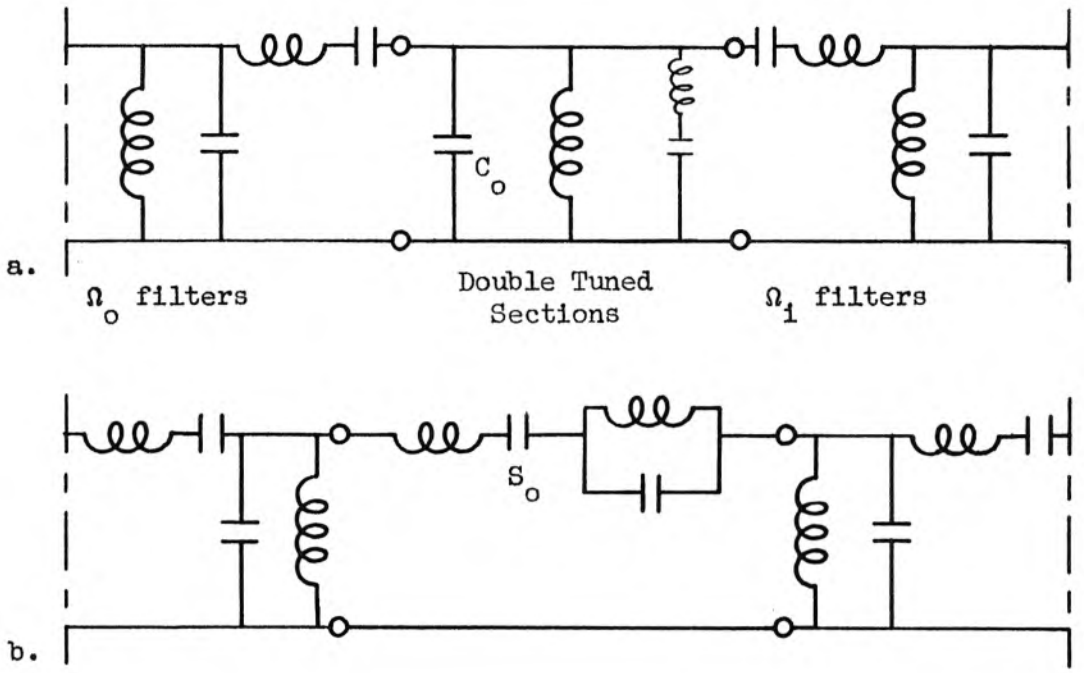

Figure 3.13 "Constant k" filters at Ω_o and Ω_i joined at a double tuned section

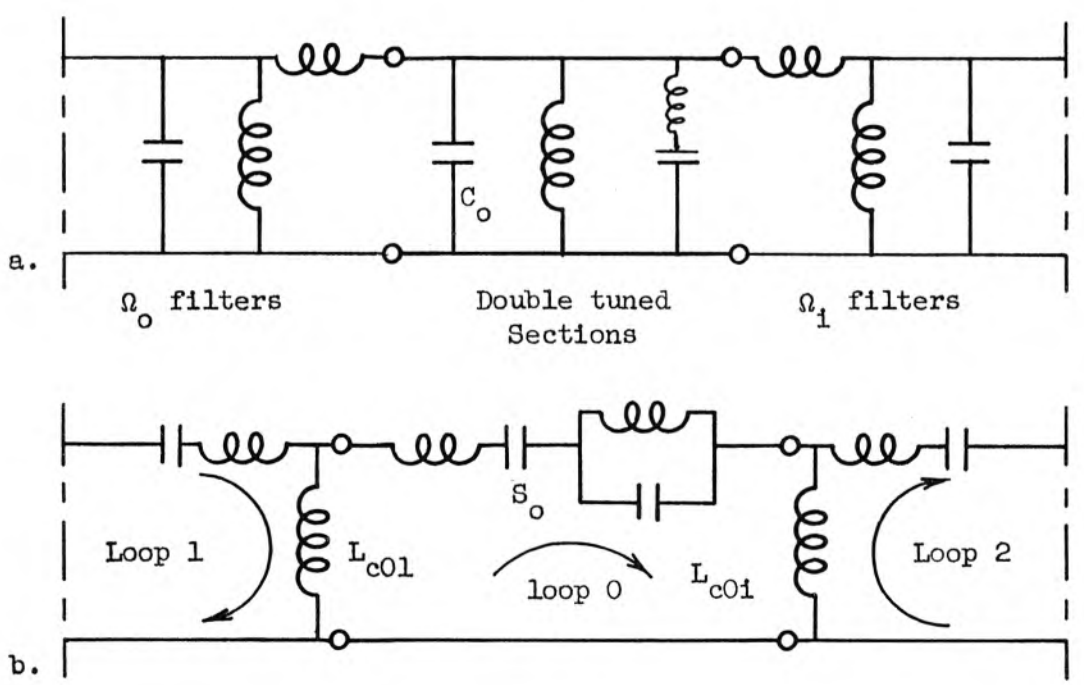

Figure 3.14 Coupled resonator filters at Ω_o and Ω_i joined at a double tuned section

3.4 The Non-inverting Upconverter

A rather complete analysis of the gain and noise figure capabilities of the upconverter including series or shunt losses in the nonlinear reactance has been given by Leenov (22). In this section the bandwidth capability of the device will be explored, neglecting these losses. Figures 3.7, 3.8 and 3.9, in which $\omega_i = \omega_{+1}$ and Y_{c+1}^2 and Z_{c+1}^2 are positive, have been derived as equivalent circuits of the upconverter. No integral limitation on the bandwidth of the upconverter has yet been shown in the literature. A non-rigorous derivation of the bandwidth over which the upconverter equivalent circuit can be perfectly matched is given below. It definitely proves that no limitation in the form of an integral of the logarithm of the reflection coefficient exists.

The basic problem here is to transmit power from an arbitrary network through a fixed L,C segment of a ladder into a second arbitrary network. Let us suppose the arbitrary networks to be infinite iterative chains of shunt capacitances and series inductances very slightly lossy, but otherwise identical to the fixed L,C section. We know from image parameter theory (29) that the frequency range over which power can flow unreflected through the fixed section of this iterative circuit is the frequency range over which the image or characteristic impedance of the network is real. The characteristic impedance of a basic L,C section is

$$\sqrt{\frac{i\omega L}{i\omega C} + \frac{(i\omega)^2 L^2}{4}} \tag{3.43}$$

and is real between angular frequencies $+ 2/\sqrt{LC}$ and $- 2/\sqrt{LC}$. In

terms of this, characteristic bandwidth limits may be written for the fixed sections of Figures 3.8 and 3.9

$$\omega_c = 4 \frac{\frac{\eta}{2} C_o \sqrt{\Omega_o \Omega_{+1}}}{\sqrt{C_{1o} C_{1+1}}} \tag{3.44}$$

$$\omega_c = \frac{4(\frac{\eta}{2} S_o)}{\sqrt{\Omega_o \Omega_{+1}} \sqrt{L_{1o} L_{1+1}}} \tag{3.45}$$

How fundamental the above bandwidth limitation is, is open to some question. Even if it is basic, it is not clear how to approach it with the least number of elements. This leaves us with little alternative but to synthesize the networks shown in Figures 3.8 and 3.9 for various transmission responses to see whether any of them approach or exceed the bandwidths expressed in equations 3.44 and 3.45. Table 3.1 shows the results of synthesis based on Tchebysheff transmission $|T|^2 = \frac{1}{1 + \epsilon^2 T_N^2 \frac{\omega}{\omega_T}}$. The actual gain is of course higher than this by the frequency ratio Ω_{+1}/Ω_o. The three decibel down bandwidth is shown normalized to the bandwidth factors in equations 3.44 or 3.45. N represents here the total number of reactances in the equivalent circuits, and r represents the position of the first fixed reactance, C_{1o} or L_{1o}, relative to the Ω_o termination. For $r = N/2$ the bandwidth does indeed approach that calculated on the image impedance argument. The Butterworth bandwidth is 71% of its maximum value at $N = 2$ and jumps to 93% at $N = 4$.

The even ordered ladder network equivalents synthesized on this

TABLE 3.1

$$\omega_{3DB} \frac{\sqrt{C_{1o}C_{1i}}}{2\eta C_o \sqrt{\Omega_o \Omega_{+1}}} \quad \text{or} \quad \omega_{3DB} \frac{\sqrt{L_{1o}L_{1i}}\ \sqrt{\Omega_o \Omega_{+1}}}{2\eta\, S_o}$$

ϵ	Ripple in DB	N	r = 1	r = 2	r = 3	r = 4	r = 5	r = 6
0	0		.707					
.5	1	2	.675					
1	3		.64					
0	0		.707	.707				
.5	1	3	.775	.775				
1	3		.77	.77				
0	0		.595	.925	.595			
.5	1	4	.76	.915	.76			
1	3		.8	.9	.8			
0	0		.50	.9	.9	.50		
.5	1	5	.79	.935	.935	.79		
1	3		.815	.93	.93	.815		
0	0		.4275	.825	.965	.825	.4275	
.5	1	6	.79	.94	.98	.94	.79	
1	3		.82	.86	.955	.86	.82	
0	0		.3475	.75	.945	.945	.75	.3475
.5	1	7	.79	.94	.965	.965	.94	.79
1	3		.825	.945	.965	.965	.945	.825

basis have an interesting symmetry property; one half is the dual of the other half. In terms of an upconverter with equal order of signal and idler tuning, this means $Y_o(s)$ is proportional to $Y_{+1}(s)$. The reflection coefficient as defined in equation 3.10 is

$$\frac{Y_o^* - Y_{c+1}^2 / Y_{+1}}{Y_o + Y_{ci}^2 / Y_{+1}}$$

and is zero when $Y_o^* Y_{+1} = Y_{c+1}^2$. Since for the above mentioned cases Y_o is proportional to Y_{+1}, we have actually synthesized networks for which $|\rho_o|^2$ is approximately constant in the passband.

Green's (15) closed form expressions for Tchebysheff and Butterworth ladder network elements can be used to calculate the bandwidth capabilities of the mismatched upconverter in which the gain is always less than Ω_{+1}/Ω_o. The bandwidth is found to increase very slowly as a function of reflection coefficient for certain values of r, but the results are not inportant enough to include here.

For lossless upconverters two types of bandwidth limitation have thus been found. One is the physical limitation on the product of the first reactance slopes at Ω_o and Ω_{+1}. The second is the mathematical limitation on the bandwidth of power transmission through an L,C section. Neither of these limitations is actually a consequence of choosing the low pass ladder network formalism, but both depend on the requirement of complex conjugate symmetry on Y_o and Y_{+1} or Z_o and Z_{+1}.

The technique of synthesizing upconverters when the loss

conductances associated with the time varying reactance are not negligible must deviate from the line established here. Maximum gain and minimum noise considerations and compromises will usually predetermine the impedance levels of the ω_o and ω_{+1} terminations. This removes from the bandwidth optimization problem the flexibility of choosing L_{1o} and L_{1i} or C_{1o} and C_{1i} so as to minimize their product without delineating any other properties of the equivalent circuit. It appears likely that a four reactance equivalent circuit will still be sufficient to approach the ultimate bandwidth capability of the lossy upconverter, and it is quite possible that a "cut and try" technique will give the fastest results for this case.

3.5 Fundamental Parametric Bandwidth Limitations

The essential difference between the parametric amplifier and the non-inverting upconverter is that the impedance inverter shown in Figure 3.7 is also a negator. This leads to effective negative terminations and reactances in the equivalent circuits of Figures 3.8 and 3.9, in which Y_{c-1}^2 and Z_{c-1}^2 are negative. The negative termination leads to a larger than unity reflection coefficient in the circuit. The negative reactances prevent the zeros of the reflection coefficient from being in one plane only. To show this, let us consider the experiment shown in Figure 3.15 in which a network N_1 with a single negative reactance (here taken as series inductance) is joined to an arbitrary but physically realizable and linear passive network, N_2. The reflection coefficients at both ends of each network, and the transmission coefficients are measured with the networks terminated in arbitrary resistances R_o. No generality is lost here since N_2 may contain ideal transformers. The transmission T_{12} of the composite network with terminations R_o is then calculable in terms of the characteristics of the separate networks (9).

$$T_{12}(s) = \frac{T_1(s)\, T_2(s)}{1 - \rho_1(s)\, \rho_2(s)} \tag{3.47}$$

The magnitude of ρ_1 is always less than unity when evaluated on the $s = i\omega$ axis. It has a single pole which must lie in the RHP. ρ_2 has poles only in the LHP because it is physically realizable; its magnitude is also less than one on the $s = j\omega$ axis. The response poles of the composite network are seen from equation 3.47 to be the zeros of

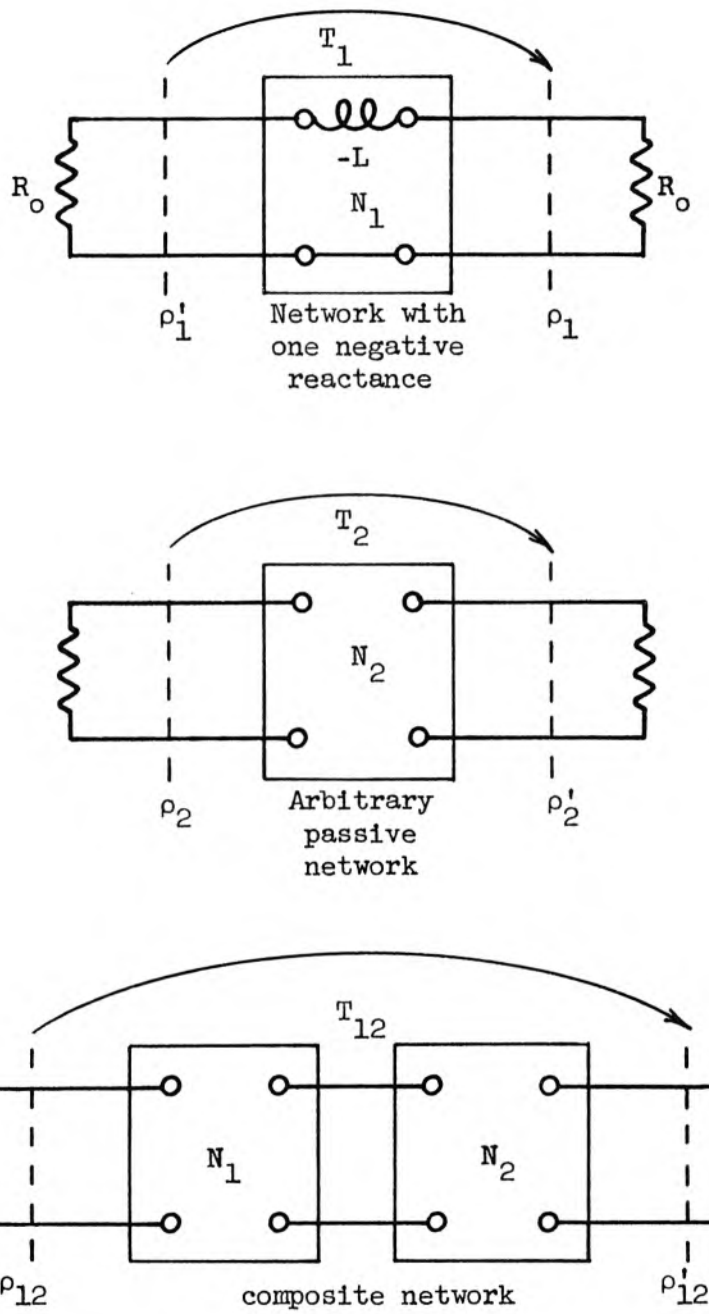

3.15 Illustrating the definitions of the response functions of the partial sections of a composite network

$1 - \rho_1(s)\,\rho_2(s)$. We apply the Nyquist (23) criterion to this function. The number of clockwise encirclements which the complex plane plot of $\rho_1(s)\rho_2(s)$ evaluated for the closed contour $s = i\omega$ and the infinite circle enclosing the RHP, makes about the point +1 is equal to the difference between the number of RHP poles and RHP zeros of $1 - \rho_1(s)\,\rho_2(s)$. The function $\rho_1(i\omega)\,\rho_2(i\omega)$ is physically restricted to be less than unity. The asymptotic value of $\rho_1(s)\,\rho_2(s)$ for infinite s can equal +1 if the asymptotic behavior of $\rho_1(s)$ and $\rho_2(s)$ is the same. This corresponds to having the input reactances of both N_1 and N_2 approach the same value (both inductive or capacitive), and the number of poles of T_{12} is one less than that of $\rho_1\,\rho_2$. For our purposes in dealing with ladder networks the asymptotic input reactances are not of the same kind, and $\rho_1(s)\,\rho_2(s)$ is asymptotic to -1. The Nyquist contour cannot encircle +1; therefore, the number of RHP poles of T_{12}, ρ_{12}, or ρ'_{12} is equal to the number of RHP poles of $\rho_1(s)$, namely one for the simple N_1 taken.

This theory may be applied to successively larger segments N_1 of a ladder network until N_1 represents the whole network. The result is that the number of RHP response poles of a passively terminated ladder network is equal to the number of negative reactive elements in it. In Chapter II we have seen that the poles and zeros of a reflection coefficient defined at a termination invert when the sign of the termination is reversed. Thus the number of RHP zeros in the reflection coefficient at a negative termination of a ladder network is equal to the number of negative reactances in the ladder network.

In Chapter II formulas such as equation 2.23 were developed to give the inverse time constants

$$\frac{1}{\tau} = \left(\frac{R}{L} \text{ or } \frac{G}{C}\right)$$

of the end sections of lossless ladder networks in terms of the positions of the poles and zeros of the reflection coefficient. In that chapter τ was negative at one end of the ladder and positive at the other. In the lossless equivalent circuits of the parametric amplifier, Figures 3.8 and 3.9, both of the terminating time constants are positive even though some of the elements are negative. In terms of the zeros and poles of the reflection at the negative termination in these figures, we may write

$$\begin{aligned} \frac{2}{\tau_{-1}} &= \frac{2G_{N-1}}{C_{N-1}} \text{ or } \frac{2R_{N-1}}{2L_{N-1}} = \sum_m \left(-s_{pm} + s_{om}\right) \\ \frac{2}{\tau_o} &= \frac{2G_{No}}{C_{No}} \text{ or } \frac{2R_{No}}{L_{No}} = \sum_m \left(-s_{pm} - s_{om}\right) \end{aligned} \tag{3.48}$$

The poles must all be in the left half plane from stability considerations.

$$\sum_m -s_{pm} > 0 \tag{3.49}$$

Equation 3.48 places an upper limit directly on $\sum s_{om}$ if both τ_{-1} and τ_o are to be positive.

$$\left|\sum_m s_{om}\right| < \sum_m -s_{pm} \tag{3.50}$$

Equations similar to 3.50 can be found to relate the time constants of any adjacent pairs of elements to summations of the pole and zero positions and summations of odd powers of the pole and zero positions (9). These equations would further delineate the pole zero restrictions in terms of the positive and negative element positions in the equivalent circuit. These restrictions are all in a sense nonholonomic boundary conditions and are difficult to apply in a synthesis procedure. Considerable difficulty is experienced if one tries to write down the general relations, and they will not be given here. One interesting case should be mentioned, however. If it be required that a reflection response function have equal but unspecified numbers of RHP and LHP zeros, the choice of these zeros in positive and negative pairs will make all the $\sum_m s_{om}$ and $\sum_m s_{om}^{2N+1}$ equal to zero. This choice of zeros makes equations 3.50 and the like compatible with a configuration in which all the elements to one side of center are positive and all to the other side are negative. This choice is otherwise somewhat restrictive, however. It demands that one half be the negative dual of the other half. It is suspected that for an infinite network with equal numbers of negative and positive elements grouped by sign to be stable, the choice of real conjugate zeros is not only sufficient but also necessary.

It is the essential presence of these RHP reflection zeros in parametric amplifiers which makes difficult the production of a fundamental bandwidth theorem in integral form. The reflection coefficient ρ_o may, however, be factored into a part ρ_{1o} which contains all the zeros and a part ρ_{2o} which is more in the form of the reflection

coefficient from a pure negative conductance and does not have RHP singularities.

$$\rho_o = \left. \frac{Y_o^*(s)\, Y_{-1}(s) + (\frac{\eta}{2} C_o)^2 \, |\omega_o \omega_{-1}|}{Y_o(s)\, Y_{-1}(s) - (\frac{\eta}{2} C_o)^2 \, |\omega_o \omega_{-1}|} \right|_{i\omega} =$$

$$\frac{Y_o^*(s)\, Y_{-1}(s) + (\frac{\eta}{2} C_o)^2 \, |\omega_o \omega_{-1}|}{\left(\sqrt[+]{Y_o(s)}\, \sqrt[+]{Y_{-1}(s)} + (\frac{\eta}{2} C_o) \sqrt{|\omega_o \omega_{-1}|}\right)^2} \quad \frac{\sqrt{Y_o(s)}\, \sqrt{Y_{-1}(s)} + (\frac{\eta}{2} C_o) \sqrt{|\omega_o \omega_{-1}|}}{\sqrt{Y_o(s)}\, \sqrt{Y_{-1}(s)} - (\frac{\eta}{2} C_o) \sqrt{|\omega_o \omega_{-1}|}}$$

$$\rho_{10} \qquad\qquad \rho_{20} \qquad\qquad (3.51)$$

We can show that ρ_{10} is not highly dependent on the form of $Y_o(i\omega)$ and $Y_{-1}(i\omega)$ when ρ_{20} is large and that the frequency range over which $\ell n\, \rho_{20}$ is large is limited.

For reasonably high ρ_{20}, $\sqrt{Y_o}\, \sqrt{Y_{-1}}$ must be approximately $(\frac{\eta}{2} C_o) \sqrt{|\omega_o \omega_{-1}|}$ and ρ_{10} can be written as

$$\rho_{10} \cong \frac{(1 + 2 \frac{\rho_{10}}{\rho_o})^2 \, e^{i\alpha} + 1}{(2 + \frac{2\rho_{10}}{\rho_o} e^{i\beta})^2} \qquad (3.52)$$

in which $\alpha = \arg Y_o^* Y_{-1}$ and $\beta = \arg \rho_{20}$. The factor ρ_{10} is thus seen to be maximized at a value near $1/2$ for $\alpha = \arg Y_o^*(i\omega) Y_{-1}(i\omega) = 0$

$$\rho_{10_{max}} \cong \frac{1}{2} \text{ for } \arg Y_o = \arg Y_{-1} \; .$$

This relation holds only in the region where ρ_o is high. The error at midband where Y_o and Y_{-1} are expected to be real is about $\pm 1/2\rho_o^2$.

The error is always less than $\pm \frac{1}{2} \frac{1}{(\rho_o - 1)}$ in the passband if arg $Y_o(i\omega)$ = arg $Y_{-1}(i\omega)$. Thus the factor ρ_{10} contributes a factor of 1/2 to ρ_o if the optimum choice arg Y_o = arg Y_{-1} is made. For other choices ρ_{10} is less but can be expected to vary slowly.

The factor ρ_{20} then contributes the large amplitude factor and shaping to ρ_o . ρ_{20} has been written so that all its singularities are poles of ρ_o . It therefore has no RHP singularities. ρ_{20} is in almost the same form as the reflection coefficient from a tunnel diode. The asymptotic dependence of $\sqrt{Y_o(s)}\ \sqrt{Y_{-1}(s)}$ is $s\sqrt{C_{10}\ C_{1-1}}$. $\sqrt{|\omega_o \omega_{-1}|}$, however, is neither constant nor analytic in the s plane. When $\sqrt{Y_o(s)\ Y_{-1}(s)}$ approaches reasonably close to its asymptotic value at frequencies $\Omega_o \pm \omega_a$ and $\Omega_{-1} \pm \omega_a$ which are not very different from Ω_o and Ω_{-1} , we are justified in taking $\sqrt{|\omega_o \omega_{-1}|}$ = $\sqrt{|\Omega_o \Omega_{-1}|}$ over the frequency range $\Omega_o \pm \omega_a$. Then by analogy with equations 2.20 and 2.21

$$\int_{\Omega_o - \omega_a}^{\Omega_o + \omega_a} \ell n |\rho_{20}| d\omega_o \cong \frac{2\pi \frac{\eta}{2} C_o \sqrt{|\Omega_o \Omega_{-1}|}}{\sqrt{C_{10}\ C_{1-1}}} \tag{3.53}$$

Presumably by proper choice of $Y_o(s)$ and $Y_1(s)$, $\ell n|\rho_{20}|$ can be made constant over a bandwidth ω_c and zero elsewhere giving rise to the bandwidth limitation for flat gain.

$$\omega_{c\ \text{parametric}} \cong \frac{\pi \eta C_o \sqrt{|\Omega_o \Omega_{-1}|}}{\sqrt{C_{10} C_{1-1}}\ \ell n\ 2\rho_o} \tag{3.54}$$

A similar result based on the series circuit with $S_o(1 + \eta \cos \Omega_p t)$ gives

$$\omega_c = \frac{\pi \eta S_o}{\sqrt{L_{10}L_{1-1}}\sqrt{|\Omega_o\Omega_{-1}|}\ \ell n\ 2\rho_o} \tag{3.55}$$

Inserting the minimum values of $C_{10}\ C_{1-1}$ and $L_{10}\ L_{1-1}$ for the nondegenerate case, one finds

$$\omega_c = \frac{\pi \eta}{4}\ \frac{\sqrt{|\Omega_o\Omega_{-1}|}}{\ell n\ 2\rho_o} \tag{3.56}$$

For the degenerate case, the bandwidth is twice as large.

3.6 Degenerate and Pseudo-Degenerate Cases

There are four reasons one can find for assuming that the choice $Y_{-1}(s) = B\, Y_o(s)$ will lead to an ultimate bandwidth synthesis of a parametric amplifier. First of all, Y_o and Y_{-1} share completely equal value in the reflection coefficient. It is most frequent in physical problems that the maximum of a quantity with respect to two variables of equal value occurs when these variables are set equal. This very weak argument is bolstered by the fact that it is preferable to have $\arg Y_o(i\omega) = \arg Y_1(i\omega)$ as shown in the previous section. The choice $Y_{-1}(s) = B\, Y_o(s)$ gives the equivalent circuit of Figure 3.8 negative dual symmetry about the middle and gives ρ_o positive and negative pairs of zeros. To show this directly, it is necessary to restore the analytic properties of ρ_o as written in equation 3.51 by writing $Y_o(i\omega) = P_o(i\omega) / Q_o(i\omega)$

$$\rho_o = \frac{B\, P_o^*(i\omega)\, P_o(i\omega) + Q_o(i\omega)\, Q_o^*(i\omega) |Y_{c-1}|^2}{B\, P_o(i\omega)\, P_o(i\omega) - Q_o(i\omega)\, Q_o(i\omega) |Y_{c-1}|^2} \frac{Q_o(i\omega)}{Q_o^*(i\omega)} \tag{3.57}$$

The removal of the phase rotation factor $Q_o(i\omega)/Q_o^*(i\omega)$ puts ρ_o in proper form for the association of s with $i\omega$ and $-s$ with $(i\omega)^*$. Then it is seen that ρ_o has real conjugate zeros. Thus, as has been mentioned in the previous section, there is no incompatibility between an equivalent circuit with equal numbers of positive and negative reactances and the choice $Y_{-1}(s) = B\, Y_o(s)$. None of these arguments, however, can be used to prove that the choice $Y_{-1} = B\, Y_o$ will give a synthesis which approaches the ultimate bandwidth most rapidly as a

function of circuit complexity. The fourth argument in favor of this choice is that it is the only basis on which we can presently synthesize the admittance function $\sqrt{Y_o(s)}\ \sqrt{Y_{-1}(s)}$ from the reflection factor

$$\rho_{20} = \frac{\sqrt{Y_o(s)}\ \sqrt{Y_{-1}(s)} + \frac{\eta}{2} C_o \sqrt{|\Omega_o \Omega_{-1}|}}{\sqrt{Y_o(s)}\ \sqrt{Y_{-1}(s)} - \frac{\eta}{2} C_o \sqrt{|\Omega_o \Omega_{-1}|}} .$$

In this section, therefore, we consider lossless ladder equivalent networks for which $Y_{-1}(s) = B\, Y_o(s)$ or $Z_{-1}(s) = B\, Z_o(s)$. We call this the pseudo-degenerate case unless $\Omega_o = -\Omega_{-1}$. Then $B = 1$ and we have the degenerate case.

When $Y_{-1} = B\, Y_o$, the Ω_o reflection coefficient

$$\rho_o = \frac{Y_o^*(s)\, Y_{-1}(s) + |Y_{c-1}|^2}{Y_o(s)\, Y_{-1}(s) - |Y_{c-1}|^2}$$ may be equivalently written as

$$\rho_o = \frac{\rho_{o-} + \rho_{o+}}{2} = \frac{1}{2}\left(\frac{Y_o^* + \frac{1}{\sqrt{B}} |Y_{c-1}|}{Y_o - \frac{1}{\sqrt{B}} |Y_{c-1}|} + \frac{Y_o^* - \frac{1}{\sqrt{B}} |Y_{c-1}|}{Y_o + \frac{1}{\sqrt{B}} |Y_{c-1}|} \right) \qquad (3.58)$$

The two quantities ρ_{o-} and ρ_{o+} represent respectively the reflection coefficients between Y_o and negative or positive conductance $\mp |Y_{c-1}| / \sqrt{B}$. The minus sign is used here to indicate gain. It is clear that ρ_{o+} will contribute very little to the gain of the amplifier and may be neglected in the synthesis. Then since $Y_o(s)$ is in ladder network form with first element sC_{10}, the synthesis of $Y_o(s)$ from ρ_{o-} may be carried out in a manner identical to that used in Chapter II. In order that $Y_{-1}(s) = B\, Y_o(s)$, $C_{1\,-1}$ must equal BC_{10}. ρ_{o-} can be treated as the reflection from a termination with

$$-\frac{G}{C}\Big|_{\text{effective}} = -\frac{\frac{\eta}{2} C_o \sqrt{|\Omega_o \Omega_{-1}|}}{\sqrt{C_{10}\, C_{1\,-1}}} \tag{3.59}$$

Similarly for the series derived circuit

$$-\frac{R}{L}\Big|_{\text{effective}} = -\frac{\frac{\eta}{2} S_o}{\sqrt{|\Omega_o \Omega_{-1}|}\sqrt{L_{10} L_{1\,-1}}} \tag{3.60}$$

We have also the relation $\rho_o = \frac{1}{2}\rho$. Equations 2.24 and 2.25, or Figures 2.7 and 2.8 may be used to calculate the Butterworth and Tchebysheff reflection bandwidths with the substitutions

$$\frac{G_1}{C_1} = \frac{\eta C_o \sqrt{|\Omega_o \Omega_{-1}|}}{\sqrt{C_{10}\, C_{1\,-1}}} \quad \text{or} \quad \frac{\eta S_o}{\sqrt{L_{10} L_{1\,-1}\,|\Omega_o \Omega_{-1}|}} \tag{3.61}$$

and

$$\rho_{\text{parametric}} = \frac{1}{2}\rho_{\text{tunnel diode}} \tag{3.62}$$

The Butterworth bandwidth

$$\omega_B = \frac{\eta C_o \sqrt{|\Omega_o \Omega_{-1}|}}{\sqrt{C_{10}\, C_{1\,-1}}} \; \frac{2 \sin \frac{\pi}{2N}}{(2\rho_{Bo})^{1/N} - 1} \tag{3.63}$$

is asymptotic to the ultimate bandwidths calculated in the previous section.

Having synthesized the parametric amplifier on this approximate basis, one may well inquire as to the exact response functions to be expected. Where are the RHP zeros of ρ_o caused by the negative

reactances in the equivalent circuit? From equation 3.58 we can see that the synthesis of ρ_o establishes all of the poles of ρ_o. Half of these poles are zeros of ρ_{o-} and half are the poles of ρ_{o-}. It has already been demonstrated that the zeros of ρ_o must be in real conjugate pairs. This condition implies that the numerator of the exact response function $\rho_o(s)\ \rho_o(-s)\big|_{i\omega}$ is a perfect square. Let us suppose we have synthesized $|\rho_{o-}|^2$ to have Butterworth response

$$\frac{\rho_{o-B}^2 + \left(\frac{\omega}{\omega_B}\right)^{2N}}{1 + \left(\frac{\omega}{\omega_B}\right)^{2N}}$$ in which N is the number of elements in the equivalent ladder for Y_o or one-half the total number of reactances in the total equivalent circuit. Then the actual transmission response must be

$$\frac{-\left|T_{oB}'\right|^2}{\left(1+\left(\frac{\omega}{\omega_B}\right)^{2N}\right)\left(1+\frac{1}{\rho_{o-B}^2}\left(\frac{\omega}{\omega_B}\right)^{2N}\right)} \tag{3.64}$$

with $|T_{oB}'|$ not yet known. From the conservation of energy formula $\rho(s)\ \rho(-s) + T(s)\ T(-s) = 1$, we have

$$\rho_o(s)\ \rho_o(-s)\Big|_{i\omega} = \frac{\left|T_{oB}'\right|^2 + \left(1+\left(\frac{\omega}{\omega_B}\right)^{2N}\right)\left(1+\frac{1}{\rho_{o-B}^2}\left(\frac{\omega}{\omega_B}\right)^{2N}\right)}{\left(1+\left(\frac{\omega}{\omega_B}\right)^{2N}\right)\left(1+\frac{1}{\rho_{o-B}^2}\left(\frac{\omega}{\omega_B}\right)^{2N}\right)} \tag{3.65}$$

The demand that the numerator is a perfect square determines

$$\left|T_{oB}'\right|^2 + 1 = \left(\frac{\rho_{o-B} + \frac{1}{\rho_{o-B}}}{2}\right)^2 \tag{3.66}$$

and the true response is found to be

$$\rho_o(s)\,\rho_o(-s)\Big|_{i\omega} = \frac{\left(\frac{\rho_{o-B} + (1/\rho_{o-B})}{2} + \frac{1}{\rho_{o-B}}\left(\frac{\omega}{\omega_B}\right)^{2N}\right)^2}{\left(1 + \left(\frac{\omega}{\omega_B}\right)^{2N}\right)\left(1 + \frac{1}{\rho_{o-B}^2}\left(\frac{\omega}{\omega_B}\right)^{2N}\right)} \tag{3.67}$$

A similar form can be established if ρ_{o-} is synthesized to have Tchebysheff response.

$$\rho_o(s)\,\rho_o(-s)\Big|_{i\omega} = \frac{\left(\frac{\rho_{o-T} + (1/\rho_{o-T})}{2} + \frac{\epsilon_-^2}{\rho_{o-T}}\,T_N^2\,\frac{\omega}{\omega_T}\right)^2}{\left(1 + \epsilon_-^2\,T_N^2\left(\frac{\omega}{\omega_T}\right)\right)\left(1 + \frac{\epsilon_-^2}{\rho_{o-T}^2}\,T_N^2\,\frac{\omega}{\omega_T}\right)} \tag{3.68}$$

Some physical significance can be attached to the writing of ρ_o as $\frac{\rho_{o-} + \rho_{o+}}{2}$ and to the factor of two in general which has crept into bandwidth relations for the parametric amplifier. The Manley-Rowe relations demand that the ratio of power into or out of the time varying reactance at Ω_o to power in or out at Ω_{-1} is $\left|\Omega_o/\Omega_{-1}\right|$. The Manley-Rowe relation does not predict the direction of power flow and one might suspect that there should be two normal modes in every circuit, each characterized by the Manley-Rowe power relations but differing in the direction of power flow. Two modes have already been found; reflection of a signal from a generator at Ω_o, and reflection of a signal from a generator at Ω_{-1}. The two new modes we seek must be a linear combination of these two or vice versa. The two new normal modes, therefore,

require generators at both Ω_o and Ω_{-1}. It is instructive to find these modes for the degenerate case and the results will also be useful in Chapter IV.

We consider the time varying capacitance $(C_o \eta \cos \omega_p t + \Theta_p)$ in the presence of two voltages $V_o e^{i\omega_o t + \Theta_o}$ and $V_{-1} e^{+i\omega_{-1} t - \Theta_{-1}}$ and calculate the current $I(t) = \frac{d}{dt} C(t) V(t)$ neglecting all frequencies but ω_o and ω_{-1}.

$$I(t) = I_o e^{i\omega_o t} + I_{-1} e^{+i\omega_{-1} t} =$$

$$\frac{\eta}{2} i\omega_o C_o V_{-1} e^{i\omega_o t} e^{i(\Theta_p - \Theta_{-1})} +$$

$$\frac{\eta}{2} i\omega_{-1} C_o V_o e^{i\omega_{-1} t} e^{-i(\Theta_p - \Theta_o)} \qquad (3.69)$$

We define admittances $\Delta Y_o = I_o/V_o = i\omega_o C_o \frac{\eta}{2} \frac{V_{-1}}{V_o} e^{i(\Theta_p - \Theta_{-1} - \Theta_o)}$ and $\Delta Y_{-1} = I_{-1}/V_{-1} = i\omega_{-1} C_o \frac{\eta}{2} \frac{V_o}{V_{-1}} e^{-i(\Theta_p - \Theta_{-1} - \Theta_o)}$. In the parametric amplifier these admittances ΔY_o and ΔY_{-1} essentially terminate the ω_o and ω_{-1} networks as shown in Figure 3.16. The power flows out of ΔY_o and ΔY_{-1} always satisfy the Manley-Rowe relation directly. We are therefore free to choose V_{-1} and V_o and search for the corresponding values of E_o and E_{-1}. For this pseudo-degenerate case in which $Y_o = B\, Y_{-1}$ we first choose V_{-1}/V_o such that ΔY_o and ΔY_{-1} are negative real and in the ratio $\Delta Y_o / \Delta Y_{-1} = 1/B$. We assume some values E_o^- and E_{-1}^- are found which are compatible with the required $\left.\frac{V_{-1}}{V_o}\right|_-$ and go on to try ΔY_o^+ and ΔY_{-1}^+, positive real and in the same

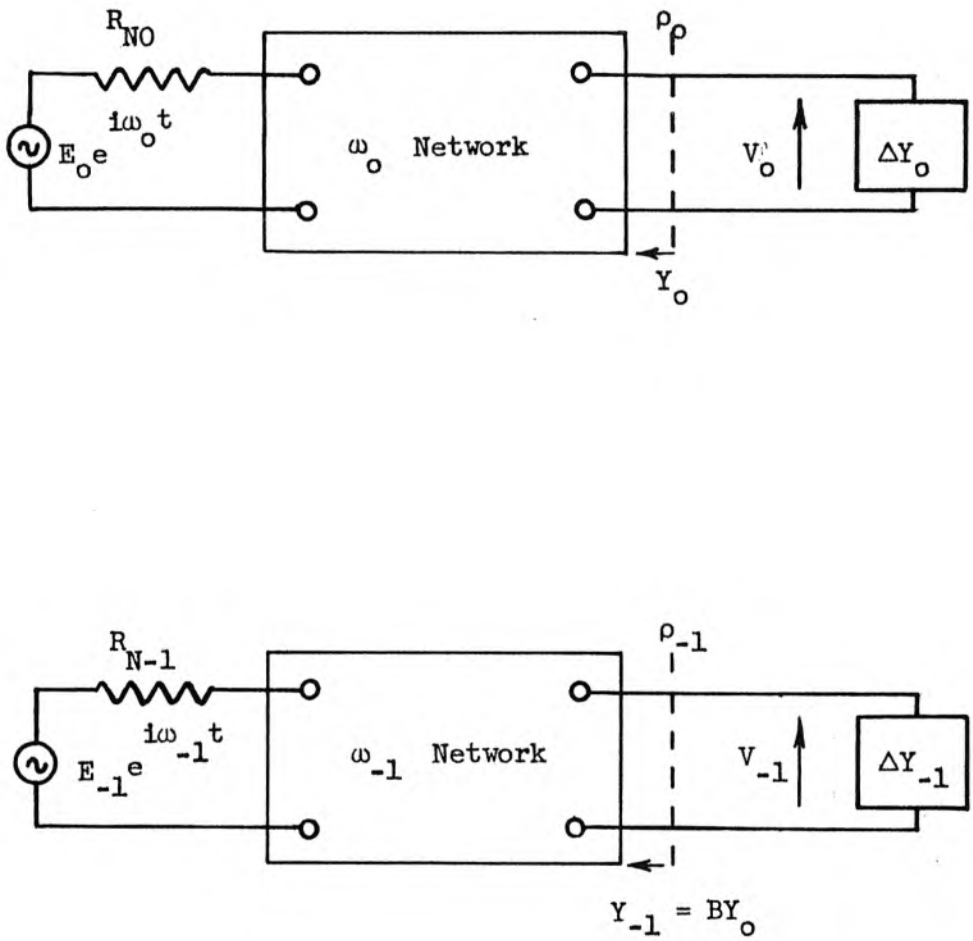

Figure 3.16 Illustrating the isolation of two modes in the degenerate or pseudo-degenerate parametric amplifier.

ratio, 1/B . This requires a 180^{o} phase shift of $\left.\frac{V_{-1}}{V_o}\right|_{+}$ with respect to $\left.\frac{V_{-1}}{V_o}\right|_{-}$. New values E_o^+ and E_{-1}^+ will be found. The ratios of $|E_o|$ to $|E_{-1}|$ in the two experiments must be the same since under conditions of equal reflection coefficient at Ω_o and Ω_{-1} , the available power from the two generators must also satisfy the Manley Rowe relations. The transmission coefficients which relate E_o to V_o and E_{-1} to V_{-1} in the two circuits must be identical in each case because of the circuit degeneracy. In the second experiment V_{-1}/V_o is shifted 180^{o} with respect to its phase in the first experiment and E_{-1}^-/E_o^- must be similarly related to E_{-1}^+/E_o^+ ,

$$\frac{E_{-1}^-}{E_o^-} = -\frac{E_{-1}^+}{E_o^+} \quad .$$

We have thus found two normal modes characterized by a change in sign of E_o/E_{-1} and a change in sign of ΔY_o and ΔY_{-1} . The reflection coefficients in the two modes are reciprocals because of the change in sign of ΔY_o. These appear to be the fundamental normal modes of the degenerate amplifier. A generator $E_o e^{i\omega_o t}$ alone couples to both of these modes equally giving rise to the representation

$$\rho_o = \frac{1}{2}(\rho_{o-} + \rho_{o+}) \quad .$$

When unsymmetrical losses G_{10} and G_{1-1} spoil the degeneracy established by $Y_{-1}(s) = B\, Y_o(s)$, the parametric amplifier reflection coefficient may still be separated approximately into passive and active parts. The reflection gain in the ω_o filter is

$$\rho_o = \frac{(Y_o^* - G_{10})(BY_o + G_{1-1}) + |Y_{c-1}|^2}{(Y_o + G_{10})(BY_o + G_{1-1}) - |Y_{c-1}|^2} =$$

$$\frac{1}{2}\left(\frac{Y_o^* Y_o + \frac{|Y_{c-1}|^2}{B} - \frac{G_{10}G_{1-1}}{B} + \frac{G_{1-1}}{B} Y_o^* - G_{10}Y_o}{Y_o^* Y_o + \frac{|Y_{c-1}|^2}{B} - \frac{G_{10}G_{1-1}}{B} + \frac{Y_o^* - Y_o}{2}\left(G_{10} + \frac{G_{1-1}}{B}\right)}\right)$$

$$\times \left(\frac{Y_o^* - \frac{BG_{10} + G_{1-1}}{2B} + \sqrt{\left(\frac{BG_{10} - G_{1-1}}{2B}\right)^2 + \frac{|Y_{c-1}|^2}{B}}}{Y_o + \frac{BG_{10} + G_{1-1}}{2B} - \sqrt{\left(\frac{BG_{10} - G_{1-1}}{2B}\right)^2 + \frac{|Y_{c-1}|^2}{B}}}\right.$$

$$\left. + \frac{Y_o^* - \frac{BG_{10} + G_{1-1}}{2B} - \sqrt{\left(\frac{BG_{10} - G_{1-1}}{2B}\right)^2 + \frac{|Y_{c-1}|^2}{B}}}{Y_o + \frac{BG_{10} + G_{1-1}}{2B} + \sqrt{\left(\frac{BG_{10} - G_{1-1}}{2B}\right)^2 + \frac{|Y_{c-1}|^2}{B}}}\right)$$

$$= (\rho_{co})(\rho_{o-} + \rho_{o+}) \quad . \tag{3.70}$$

The first factor can again be thought of as a coupling factor dividing the voltage of a generator into two modes, one of which gives active reflection and the other passive. For $G_{1-1} = BG_{10}$, that is when G_{1-1} and G_{10} are in the same ratio as Y_{-1} and Y_{10}, this factor has magnitude one-half. For small G_{1-1} and G_{10} not in this ratio

$$\rho_{co} \cong \frac{1}{2}\left(1 + \sqrt{B}\ \frac{\frac{G_{1\,-1}}{B} - G_{10}}{2\,|Y_{c-1}|}\right) \tag{3.71}$$

in the passband. For the reflection coefficient in the idler or Ω_{-1} network, everything is the same except G_{10} and $G_{1\,-1}$ must be interchanged in ρ_{co} to produce ρ_{ci}. For small $G_{1\,-1}$ and G_{10}

$$\rho_{ci} \cong \frac{1}{2}\left(1 + \sqrt{B}\ \frac{G_{10} - \frac{G_{1\,-1}}{B}}{2|Y_{c-1}|}\right) \tag{3.72}$$

The reflection coefficient at the ideal time varying reactance terminals can also be written simply by changing the sign of G_{10} in the numerator of ρ_{co}. All these equations can be corrected for the series case with $Z_{-1} = BZ_o$ by changing all admittances to their corresponding impedances.

The use of equation 3.70 to synthesize approximate Butterworth or Tchebysheff reflection coefficients is straightforward. One neglects the passive reflection part and synthesizes Y_o from ρ_o as with tunnel diode amplifiers. With Y_o asymptotic to sC_{10} and $B = C_{1\,-1}/C_{10}$, the effective

$$-\frac{G}{C} = \frac{\frac{G_{10}}{C_{10}} + \frac{G_{1\,-1}}{C_{1\,-1}}}{2} - \sqrt{\left(\frac{\frac{G_{10}}{C_{10}} - \frac{G_{1\,-1}}{C_{1\,-1}}}{2}\right)^2 + \frac{\left(\frac{\eta}{2}\,C_o\right)^2 |\Omega_o \Omega_{-1}|}{C_{10}\,C_{1\,-1}}} \tag{3.73}$$

The reflection bandwidth capability as a function of circuit complexity N can be obtained from equations 2.24 and 2.25 or Figures 2.7 and 2.8

by associating $-G_1/C_1$ in these with twice the $-G/C$ given in equation 3.73 and requiring that

$$\rho_{\text{parametric}} = \rho_{co}\,\rho_{\text{tunnel diode}} = \frac{1}{2}\,\rho_{\text{tunnel diode}} .$$

The nondegenerate parametric amplifier can also be used as a transmission amplifier between a signal source at ω_o and a load at ω_{-1}. In the lossless case this transmission gain is given simply by the Manley–Rowe frequency ratio ω_{-1}/ω_o times the transmission gain in the equivalent circuit.

$$|T_{o\,-1}|^2 = (1 - |\rho_o|^2)\frac{\omega_{-1}}{\omega_o} \tag{3.74}$$

In the lossy case the transmission will still be approximately Butterworth or Tchebysheff because the synthesis technique fixes the critical transmission pole positions exactly. The magnitude of this transmission at midband as a function of ρ_o is best evaluated in the lossy case by using Figure 3.8 or 3.9 directly.

3.7 Some Nondegenerate Cases

In the previous section we found a synthesis procedure which yielded gain bandwidth relations which were asymptotic to the apparent ultimate limitation of the parametric amplifier. This synthesis, however, was restricted to situations in which the number of tuning elements in the idler circuit equalled the number of tuning elements in the signal circuit. Moreover, it required that the ratio of signal terminating admittance to idler terminating admittance G_{NO}/G_{N-1} be equal to the ratio of the reactance slope parameters C_{1O}/C_{1-1}, or for the series circuit, $R_{NO}/R_{N-1} = L_{1O}/L_{1-1}$. The noise figure optimization problem for the lossy case usually results in an optimum choice for the G_{NO}/G_{N-1} or R_{NO}/R_{N-1} (see section 3.8). If this does not correspond to an optimum choice of C_{1O}/C_{1-1} or L_{1O}/L_{1-1} with respect to minimizing the products $C_{1O}\,C_{1-1}$ or $L_{1O}\,L_{1-1}$, then some "other" synthesis technique which does not require $G_{NO}/G_{N-1} = C_{1O}/C_{1-1}$ may give a wider bandwidth. It has not been shown that this synthesis gives greatest bandwidth for a given total network complexity. No more general synthesis technique has yet been found, however, and it is possible that no synthesis techniques can be found which will allow the independent specification of C_{1O}/C_{1-1} and G_{NO}/G_{N-1} and approach the ultimate bandwidth limitation at the same time.

Two special case synthesis techniques which result in Butterworth or Tchebysheff response will be given here. Let us consider the general symmetric matched ladder network with N odd and its perturbation as shown in Figure 3.17. In the perturbed network, half the ladder has been shifted in impedance level by the factor A. The reflection coefficients

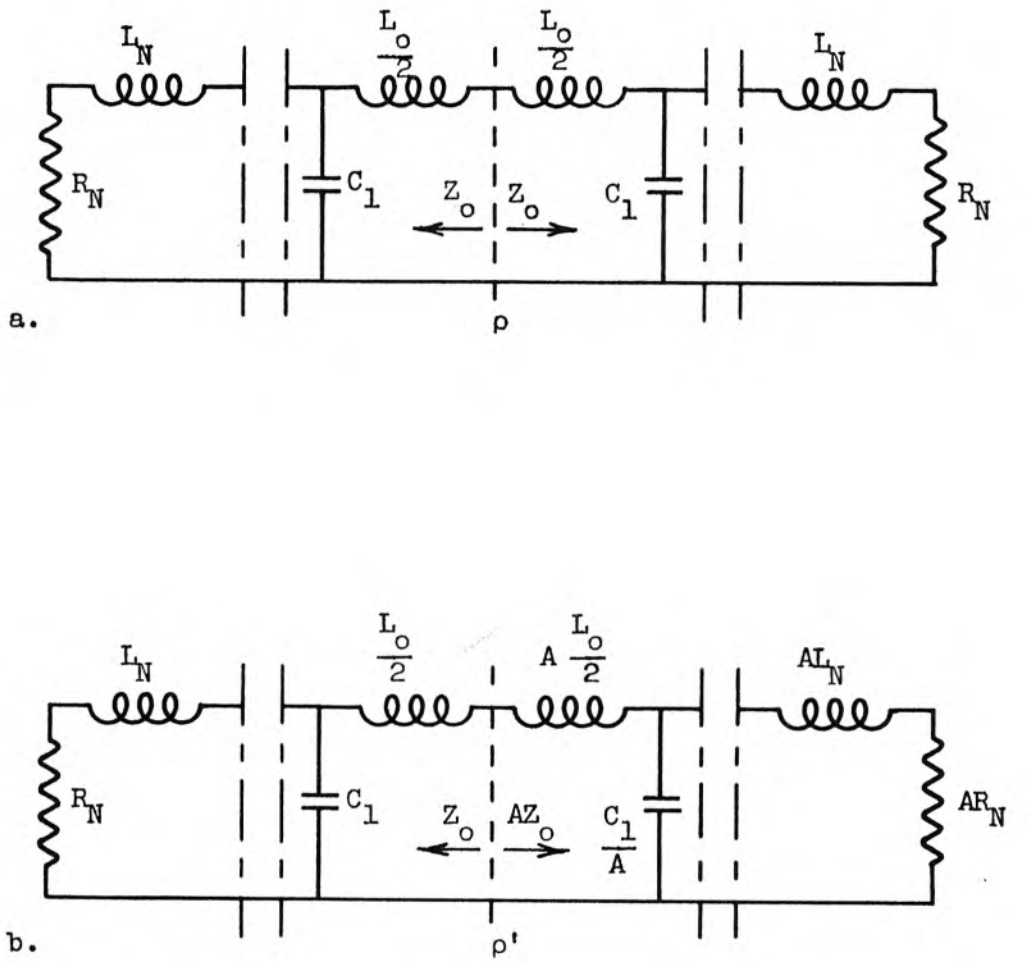

Figure 3.17 A perturbation of a symmetric network leads to a parametric amplifier configuration for negative A

of the two ladders may be written in terms of the input impedance $Z = P(s)/Q(s)$ of the half ladder as

$$\rho = \frac{Z - Z^*}{Z + Z} = \frac{P(s)\,Q(-s) - Q(s)\,P(-s)}{2P(s)\,Q(s)} \frac{Q(i\omega)}{Q^*(i\omega)}$$

$$\rho' = \frac{AZ - Z^*}{(1+A)Z} = \frac{AP(s)\,Q(-s) - Q(s)\,P(-s)}{P(s)\,Q(s)(1+A)} \frac{Q(i\omega)}{Q^*(i\omega)} \qquad (3.75)$$

It is noticed that the poles of ρ' and ρ are the same for any value of A even if it is negative. Therefore, if the transmission response of the symmetric ladder is Butterworth, the response of the new ladder is also Butterworth and stable. Weinberg (24) has shown that the reflection coefficient zeros produced by this method of designing a mismatched filter from a matched symmetrical network always alternate from the left to right half plane in order of the magnitudes of the real parts such that $\sum s_{om} = 0$. Thus equation 3.50 is satisfied for all ρ_o .

The configuration for negative A is that of a parametric amplifier equivalent circuit with one tuning element or reactance more or less in the Ω_o network than in the Ω_{-1} network. The product $L_o C_1 \omega_B^2$ or $L_o C_o \omega_T^2$ can be obtained from Green's (15) formulas for ladder networks, and by associating the elements of Figure 3.17b with Figure 3.8 or 3.9, the bandwidth capability of this synthesis can be evaluated in terms of the reflection coefficient $\rho_o' = \frac{1 - A}{1 + A}$. The results in which N is now the total number of reactances in the equivalent circuit are:

$$\omega_B = \frac{2 \sin^{1/2} \frac{N-2}{N} \frac{\pi}{2}}{\sqrt{1 + |\rho_{Bo}|}} \frac{\eta C_o \sqrt{|\Omega_o \Omega_{-1}|}}{\sqrt{C_{10} C_{1-1}}}$$

or

$$\frac{2 \sin^{1/2} \frac{N-2}{N} \frac{\pi}{2}}{\sqrt{1 + |\rho_{Bo}|}} \frac{\eta S_o}{\sqrt{|\Omega_o \Omega_{-1}|} \sqrt{L_{10} L_{1-1}}} \tag{3.76}$$

$$\omega_T = \frac{\sin^{1/2} \frac{N-2}{2} \frac{\pi}{2}}{\sqrt{1 + |\rho_{To}|}} \frac{\frac{\eta C_o \sqrt{|\Omega_o \Omega_{-1}|}}{\sqrt{C_{10} C_{1-1}}}}{(\sin^2 \frac{N-2\pi}{4N} \cos^2 \frac{N-2\pi}{4N} + \frac{1}{4} \sinh \frac{1}{N} \sinh^{-1} \frac{1}{\epsilon})^{1/2}} \tag{3.77}$$

The quantities $C_{10}/G_{NO})(G_{N-1}/C_{1-1}$ and $(L_{10}/R_{NO})(R_{N-1}/L_{1-1})$ which were required to be unity in the pseudo-degenerate synthesis have been evaluated approximately and are on the order of $\frac{1}{1 + |\rho_o|}$ or $1 + |\rho_o|$ depending on whether the Ω_o network has one less or one more tuning element than the Ω_{-1} network. This ratio is thus again fixed by the configuration but at a different value than for the pseudo-degenerate case.

One last situation which we may consider is that in which either the signal or idler is single tuned and the other frequency has N tuning elements. We attempt a synthesis based on the approximation

$$\frac{1}{G_{-1} + sC_{1-1}} \cong \frac{1}{G_{-1}} \left(1 - \frac{sC_{1-1}}{G_{-1}}\right) \tag{3.78}$$

ρ_o can now be written as

$$\frac{\frac{1}{Z_o^{*'}} - sC_{10} + \frac{|Y_{c-1}|^2}{G_{-1}}\left(1 - \frac{sC_{1\,-1}}{G_{1\,-1}}\right)}{\frac{1}{Z_o'} + sC_{10} - \frac{|Y_{c-1}|^2}{G_{-1}}\left(1 - \frac{sC_{1\,-1}}{G_{1\,-1}}\right)} \tag{3.79}$$

The effective $-G/C$ of this reflection is

$$-\frac{G}{C} = \frac{-|Y_{c-1}|^2}{G_{-1}C_{10} + \frac{C_{1\,-1}}{G_{-1}}|Y_{c-1}|^2} \tag{3.80}$$

which has a broad maximum for

$$G_{-1} = |Y_{c-1}|\sqrt{\frac{C_{1\,-1}}{C_{10}}} \tag{3.81}$$

of

$$-\frac{G}{C} = \frac{-|Y_{c-1}|}{2\sqrt{C_{10}C_{1\,-1}}} = \frac{\frac{\eta}{2}C_o\sqrt{|\Omega_o\Omega_{-1}|}}{2\sqrt{C_{10}C_{1\,-1}}} \tag{3.82}$$

The maximum is wide enough so that except at very high gain with very high N, the approximation in 3.78 does not affect the response. The Butterworth bandwidth based on equation 3.82 is

$$\omega_B = \frac{2\sin\frac{\pi}{2N}}{\rho_{Bo}^{1/N} - 1}\,\frac{\frac{\eta}{2}C_o\sqrt{\Omega_o\Omega_{-1}}}{\sqrt{C_{10}C_{1\,-1}}} \tag{3.83}$$

in which N is one less than the total number of reactive elements in the equivalent circuit. The quantity $(C_{10}/G_{NO})(G_{N-1}/C_{1\,-1})$ or its equivalent for a series derived result is required by this synthesis to be nearly unity except at very low ρ_o.

3.8 Comparison of Nondegenerate and Pseudo-Degenerate Results

Figure 3.18 shows the normalized parametric amplifier Butterworth derived bandwidth plotted against N_T, the total number of reactive elements in the equivalent circuit, for $\rho_{Bo} = 4$, 8, and 16. It can be seen that both of the nondegenerate syntheses yield comparable or higher bandwidths than the pseudo-degenerate for N_T under six. This figure indicates that while the pseudo-degenerate synthesis is the only one found which is asymptotic to the ultimate bandwidth limitation, it is not optimum in the sense of giving the greatest possible bandwidth for a given circuit complexity. Neither are the syntheses in section 3.7.

There seems to be a fundamental difference between the wide banding achieved by the method based on Figure 3.17 and the other procedures. The pseudo-degenerate synthesis and the synthesis based on the approximation in equation 3.78 both place equal emphasis on the bandwidth limitations due to C_{10} and $C_{1\,-1}$. All other elements in the circuit are used to tune out the combined effects of these two elements. The essential difference in the third synthesis technique can be seen from Figure 3.17b. Let us say that $L_o/2\,(1+A)$ represents the effects of $C_{1\,-1}$, and C_1/A the effects of C_{10}. For high gain, $A \cong -1$, $L_o/2\,(1+A)$ is almost negligible. The method of broadbanding is not so much tuning as it is one of direct cancellation. The effects of $C_{1\,-1}$ are minimized with respect to and at the expense of those due to C_{10}. A third reactance is then inserted in an attempt to cancel the effects of C_{10}.

The choice of Butterworth or Tchebysheff response in this cancellation scheme are incidental. It is unlikely that they are optimum. No method of constructing general realizable response polynomials which

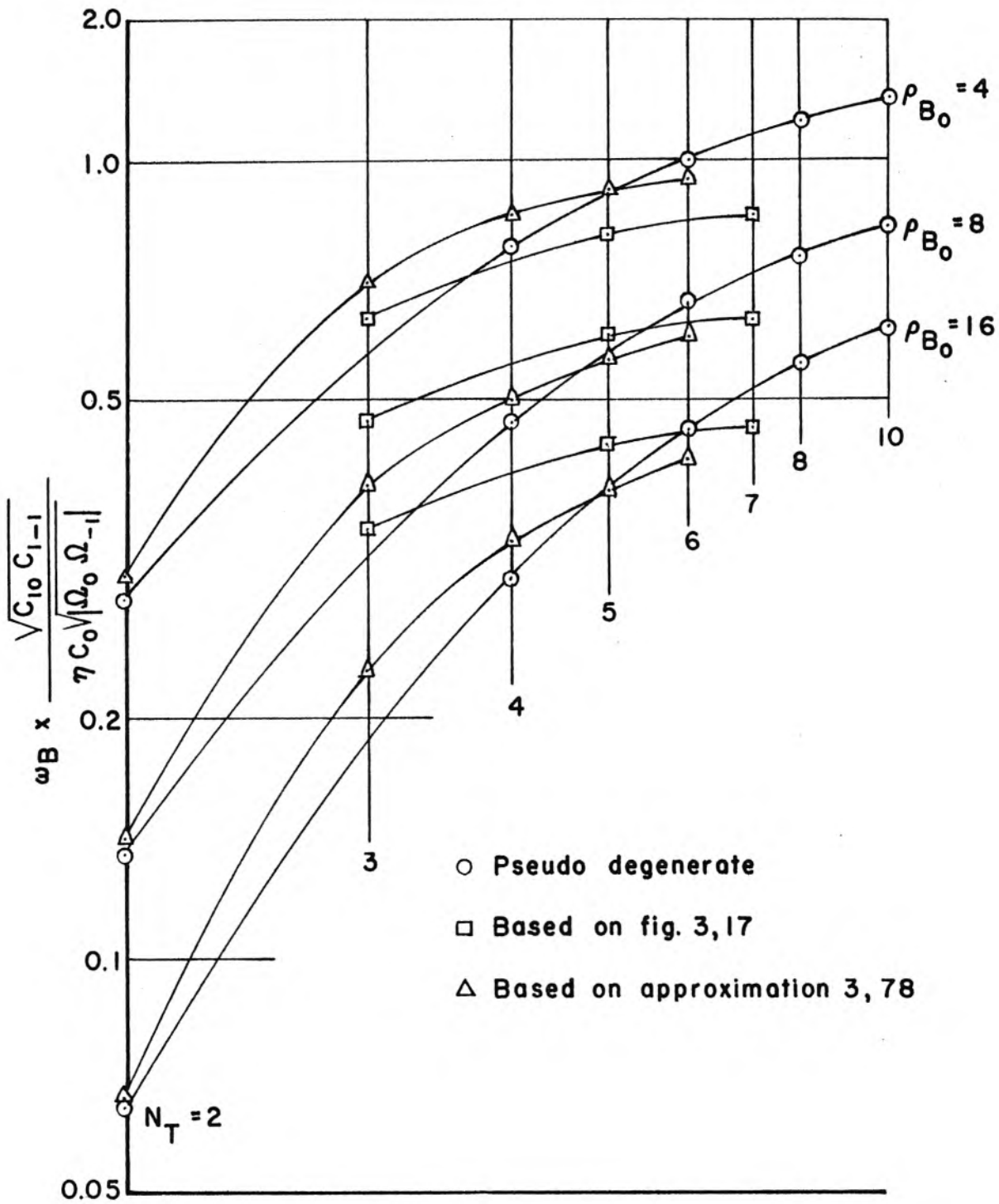

Figure 3.18 Comparison of pseudo-degenerate and non-degenerate bandwidths for $\rho_{Bo} = 4, 8, 16$

result in this cancellation type phenomena for an arbitrary splitting of the number of negative and positive elements has been found. Several other Butterworth zero distributions have been tried. In general they fail to satisfy equations 3.50 and the like and at low gain result in configurations in which the positive and negative elements alternate.

3.9 Configurations and Noise Figure

The nondegenerate parametric amplifier can be used either as a reflection amplifier with or without a circulator or as a transmission amplifier operating between a source generator at Ω_o and a load at Ω_{-1}. The single element reflection amplifier configurations of Figure 2.1 in Chapter II and the subsequent analysis of the relation between actual gain and reflection gain in that chapter, can be applied straightforwardly to the reflection parametric amplifiers. The noise figure equations in Chapter II can also be applied directly if we can write an effective temperature for the effective negative conductance. At midband this can be done by inserting noise generators in Figure 3.8 or 3.9 which results in Figure 3.19. The effective temperature of each element is given the same subscript as the element. The line MR shown in these figures illustrates a hypothetical plane at which Manley Rowe amplification takes place. Power flowing from right to left across this line is multiplied by Ω_o/Ω_{-1} while power flowing in the other direction is multiplied by Ω_{-1}/Ω_o. Thus in evaluating the effective temperature of $-G_{eff_o}$, the temperatures of Ω_{-1} elements will become multiplied by Ω_o/Ω_{-1}. The effective input conductance for Figure 3.19a is

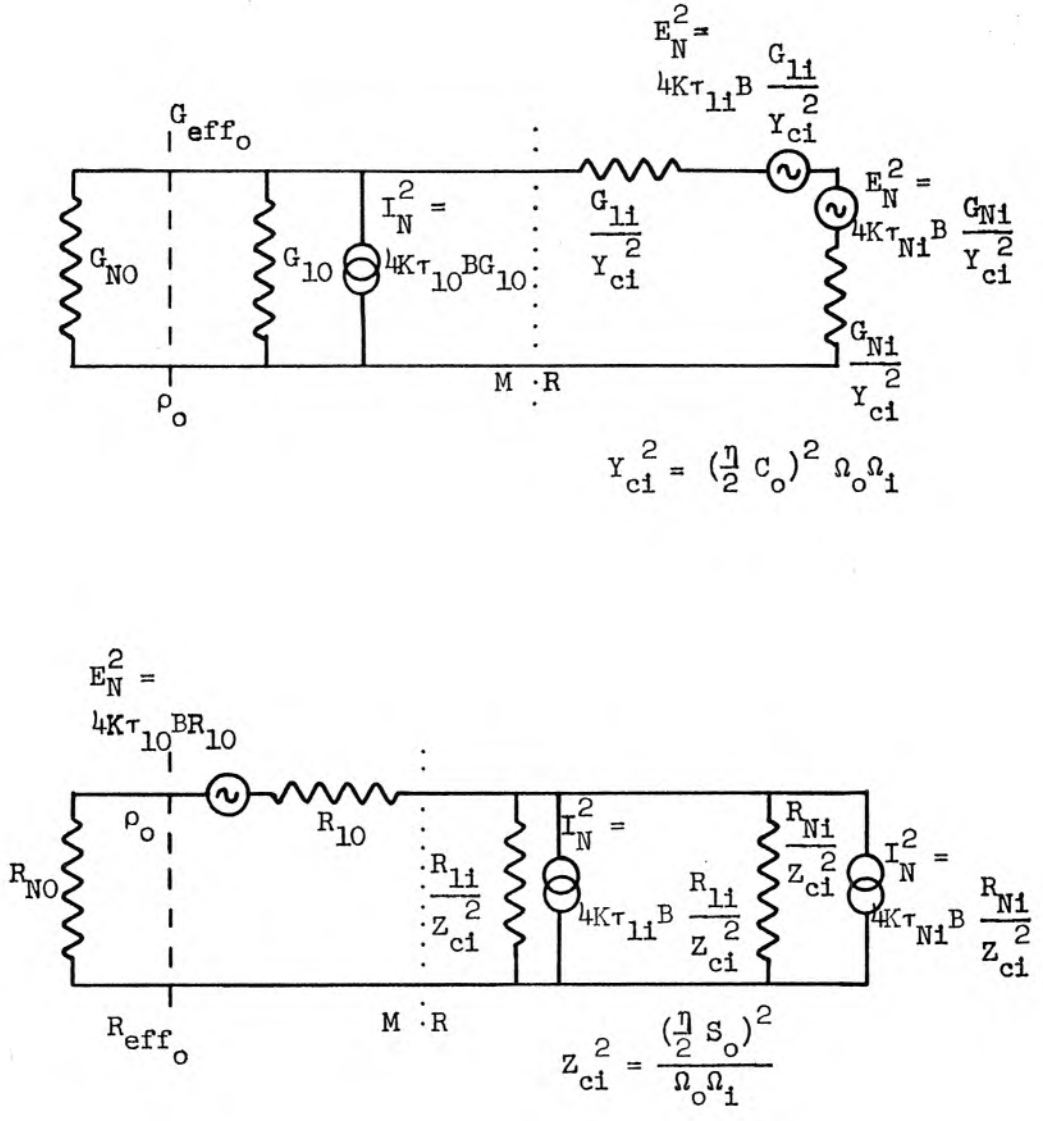

Figure 3.19 Midband equivalent circuits with noise generators derived from Figures 3.8 and 3.9

$$-G_{eff_c} = G_{10} - \frac{|Y_{c-1}|^2}{G_{1-1} + G_{N-1}} \tag{3.84}$$

This conductance has an effective temperature

$$\tau_{eff_c} = \frac{\left|\frac{\Omega_o}{\Omega_{-1}}\right| \times \frac{\tau_{1-1} G_{1-1} + \tau_{N-1} G_{N-1}}{G_{1-1} + G_{N-1}} + \frac{\tau_{10} G_{10}(G_{N-1} + G_{1-1})}{|Y_{c-1}|^2}}{\frac{G_{10}(G_{1-1} + G_{N-1})}{|Y_{c-1}|^2} - 1} \tag{3.85}$$

The results for the series derived circuit can be obtained by replacing all the above conductances with the comparable resistances.

The degenerate case needs separate consideration. Here G_{NO} and G_{N-1} represent the same elements physically, as do G_{10} and G_{1-1}. We hold to the equivalent circuit of Figure 3.19, however, and consider ω_o to represent frequencies below $\Omega_p/2$ and ω_{-1} to represent frequencies above $\Omega_p/2$. Since the actual physical output response of the amplifier to a signal at ω_o is the amplified signal plus the idler contribution at $\omega_{-1} = \omega_o - \Omega_p/2$, the power gain between any element and the load is double that predicted from the equivalent circuit. This does not change the ratio of power out due to G_{10} and G_{1-1} to amplified thermal power from the source in G_{NO}. The main thing to be decided is how to treat the noise from G_{N-1}. When it is not known whether the signal to be amplified is above or below $\Omega_p/2$, G_{N-1} represents increased signal gathering capability. In noise figure calculations, therefore, τ_{1-1} of equation 3.85 should be set to zero. The noise figure may then be

calculated assuming that the noise power available from the source is $2K\tau B$ rather than $1K\tau B$, effectively decreasing the noise figure of the degenerate amplifier compared to a comparable nondegenerate amplifier with $\tau_{1-1} = 0$. When, however, it is known that the signal presented to the amplifier is definitely below $\Omega_p/2$, G_{N-1} represents a noise source without signal gathering capability and must be treated as such.

Figure 3.19 may be used equally well to calculate the noise figure of transmission amplifiers at midband. One calculates the transmission gain between G_{NO}, G_{10}, and $-G_{1-1}/|Y_{c-1}|^2$ as well as the reflection gain between $-G_{N-1}/|Y_{c-1}|^2$ and itself. Using the power available from each element and the gain from the element to $-G_{N-1}/|Y_{c-1}|^2$, one may readily construct the noise figure. The procedure is equally useful for the non-inverting upconverter if the negative signs are removed. The full equations will not be given here.

For the parametric amplifier synthesis techniques given in previous sections in which the elements G_{1-1} and G_{10} were included, the midband noise figure calculation is nearly correct over the whole passband. For those synthesis techniques which do not so readily adjust themselves to the inclusion of the losses in the nonlinear reactance, the midband result must be used cautiously.

Without going into any more detail, one may still say from Figure 3.19 or equation 3.85 that for the production of a minimum noise amplifier, there is an optimum choice for G_{N-1}. This choice will depend very much on the temperature of G_{N-1} relative to G_{1-1}. If τ_{N-1} is higher than τ_{1-1}, the minimum noise will be obtained for rather

small G_{N-1}. If, however, τ_{N-1} is lower than τ_{1-1}, a larger value of G_{N-1} will be chosen. Thus the problem of simultaneous optimization of bandwidth and noise figure is a complicated one. The problem is best approached by trying to find optimum bandwidth syntheses under the assumption that G_{N-1} is predetermined. It is hoped that the fundamental information about parametric amplifiers given in this chapter will in the future be an aid to finding solutions to this very general but also very complicated problem.

CHAPTER IV

SYNTHESIS OF NEGATIVE RESISTANCE AMPLIFIERS WITH SEVERAL ACTIVE ELEMENTS BY PREDISTORTION

When amplifier bandwidth greater than that obtainable with a single active element is desired, it is necessary to find methods of cascading active elements in such a way that the net gain bandwidth capability increases. It has already been mentioned that amplifiers with circulators can be directly cascaded and that bilateral constant resistance stages are being considered by Carlin (6). An interesting approximate approach to the design of such stages is synthesis based on insertion of negative conductance elements in the arms of a quarter-wave coupled hybrid. This was proposed by Autler (25) and has been successfully used by Sie (26,27). An idealized equivalent circuit of such an amplifier stage is shown in Figure 4.1. Each stage requires two matched active elements. The power gain is equal to the reflection gain at either of the negative conductances, and therefore the gain per tunnel diode has the integral limitation

$$\int_0^\infty \ell n \, P_G^{1/2} \, d\omega = \frac{\pi}{2} \frac{G_T}{C_T} \tag{4.1}$$

Such stages may be individually widebanded in a way very similar to that given in Chapter II or they may be used in a stagger tuned cascade. The extent to which the circuit approximates a constant resistance section, however, does depend on the approximation with which a quarter wave hybrid can be built and widebanded.

This chapter will deal with amplifiers whose effective active

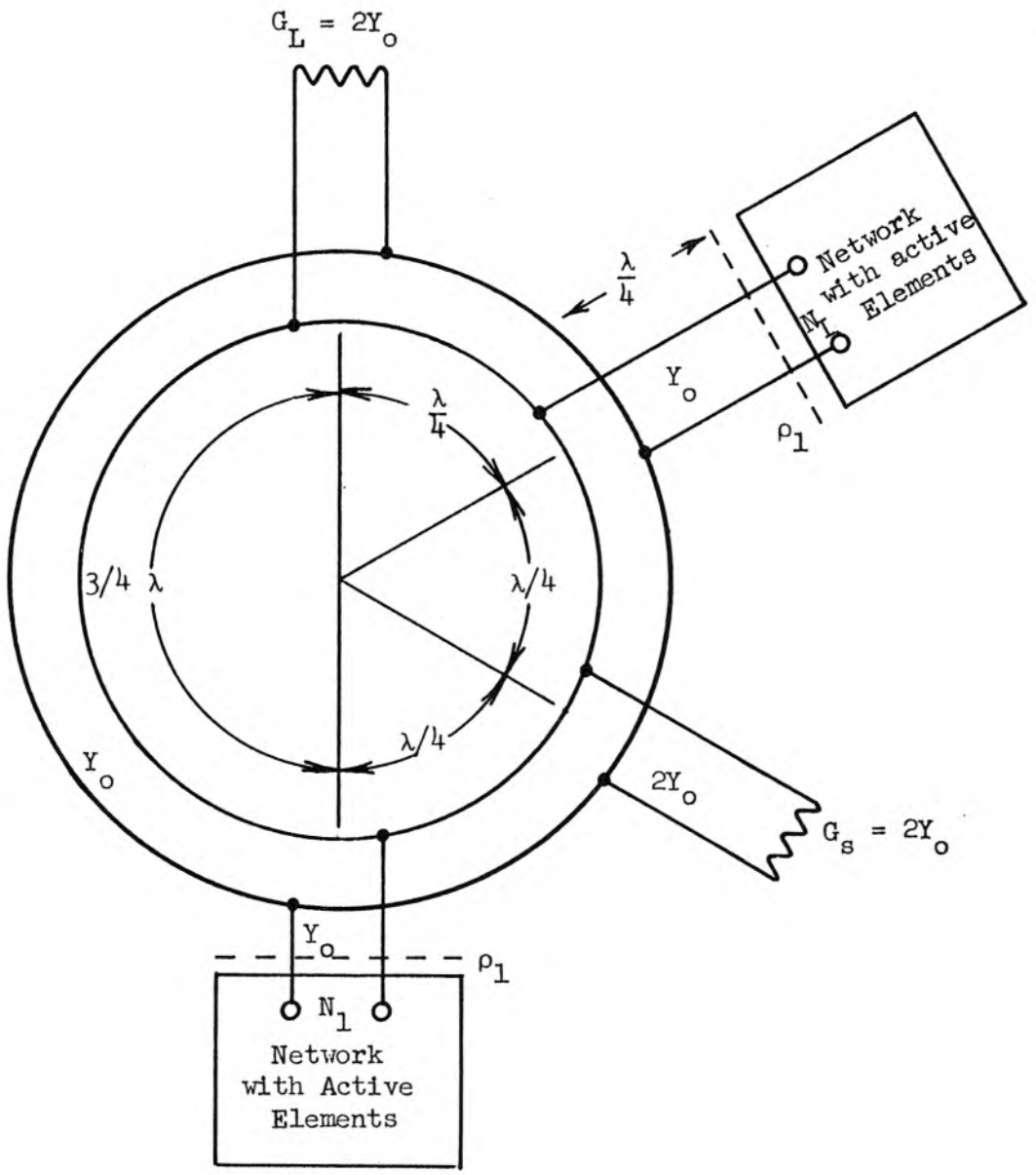

Figure 4.1 Quarter wave coupled hybrid network for approximating a constant resistance amplifier stage, $P_G = |\rho_1|^2$

elements are negative conductances in parallel with capacitors and negative resistances in series with inductances. Only configurations which are analyzable on the basis of the negative uniform loss low pass ladder with resistive terminations as shown in Figure 4.2 will be considered explicitly for synthesis. Recognizing that the immittance of each lossy element $i\omega L_i + R_i$ or $i\omega C_i + G_i$ can be written as

$$sL_i\Big|_{i\omega + \frac{R_i}{L_i}} \qquad \text{or} \qquad sC_i\Big|_{i\omega + \frac{G_i}{C_i}} \tag{4.2}$$

it can easily be seen that when all the reactances have the same loss or dissipation factor, G/C, analytic response functions of s are simply related to the lossless response functions by the transformation $s \rightarrow s + \frac{G}{C}$. The technique of precompensating lossless response functions so that this transformation yields a desired lossy response is called predistortion. Its use in negative resistance amplifier synthesis was suggested by Weinberg (7). Figure 4.3 shows predistorted Butterworth poles for an $N = 3$ network with negative loss elements.

Weinberg has also suggested synthesis using the Darlington (28) procedure for relating lossless to lossy response when the inductors do not have the same dissipation factor as the capacitors. The method is only applicable to analytic network functions which do not depend on terminations. Two transformations of s are required; one shifting s by the average loss factor of the two kinds of elements; the second shifting s^2 by the square of half the difference in loss factors. The complexity of the double transformation and the fact that it cannot be used on transmission gain response functions make it rather difficult to apply in amplifier

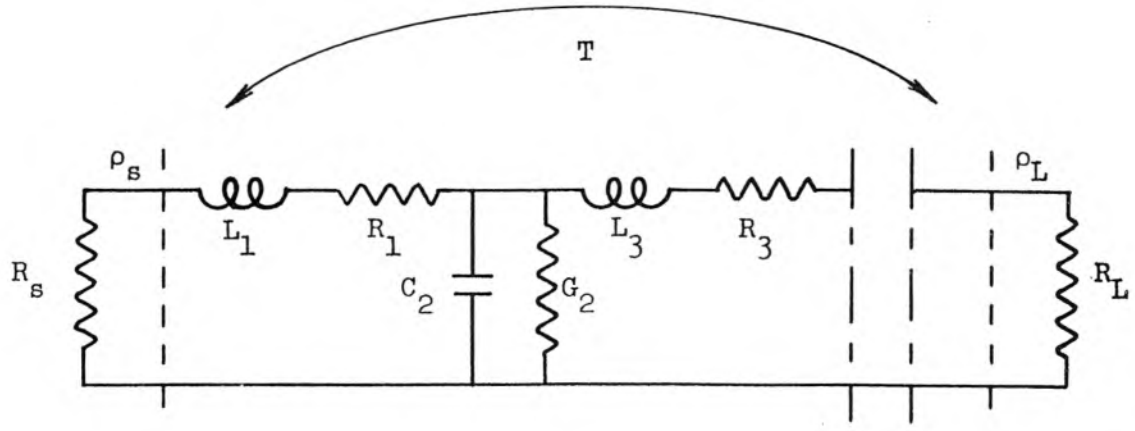

Figure 4.2 A lossy resistance terminated, low pass ladder network

Lossless ; $G_i = R_i = 0$

Uniform Loss ; All $G_i/C_i = R_i/L_i = G/C$

Darlington
Non-uniform Loss:; All $G_i/C_i = G/C$, all $R_i/L_i = R/L$

Iterative with lossless and matching sections; all L_i, C_i, G_i, and R_i from m to p are equal, all other G_i and R_i are zero.

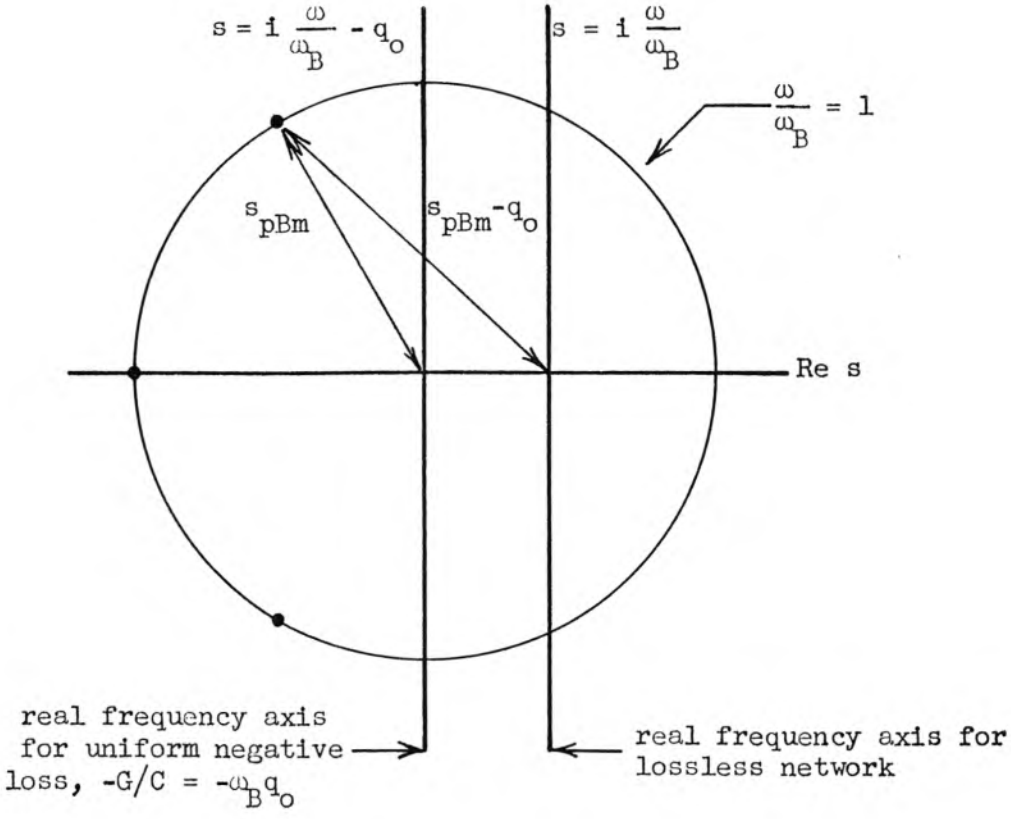

Figure 4.3 Illustrating N = 3 Butterworth poles predistorted for uniform negative loss, $-G/C = -q_o\omega_B$

synthesis.

A third synthesis method for multi-element amplifiers is to imbed identical reactance limited active elements in an iterative or periodic network. The characteristic impedance and transfer constant of such a network are easily calculated from image parameter theory. The transfer constant is not generally well behaved, becoming large at the band edges. The characteristic impedance is also badly behaved at the band edges. It becomes passively unrealizable and cannot be approximated in these regions. The problem of designing passive terminations to limit band edge gain peaks and guarantee stability is a difficult one. It must be solved by trial and error.

4.1 Integral Limitations and Noise Figure

An interesting integral limitation will be developed below for cascade two-port networks. It will show, in a sense, that the bandwidth limitation of transmission amplifiers designed by any of the above methods is the sum of the bandwidth limitations of the active elements. We consider a resistance terminated two-port network made up of lossy two-port stages of the general types shown in Figure 4.4. The divisions are made so that each stage is as simple as possible but with the restriction that for infinite s the two admittances seen by breaking the network at a junction are not both zero or both infinity. We will consider the ratio of the lossy transmission gain $T'(s)$ to the lossless transmission gain $T(s)$. The latter may have zeros on the $s = i\omega$ axis and poles in the LHP. We restrict $T'(s)$ also to have LHP poles. Each zero of $T'(s)$ and $T(s)$ can be causally related to a single stage such as a shunt inductance, series capacitance, parallel resonant series branch or series resonant shunt branch. The difference in the real parts of corresponding zeros of $T'(s)$ and $T(s)$ is always equal to the sum of loss factors of the elements causing the zero. Thus for a section with shunt inductance L_i in series with $-R_i$, $T(s)$ has a zero at $s = 0$ and $T'(s)$ has a zero at $s = + R_i/L_i$.

The ratio of lossy transmission to lossless transmission can be written as

$$\frac{T'(s)}{T(s)} = \pi_m \left(\frac{s - s_{pm}}{s - s'_{pm}}\right) \pi_n \left(\frac{s - s'_{on}}{s - s_{on}}\right) \tag{4.3}$$

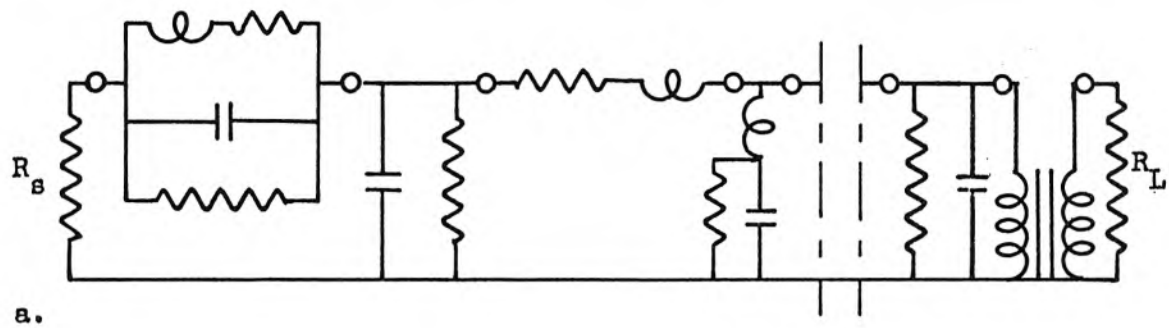

a.

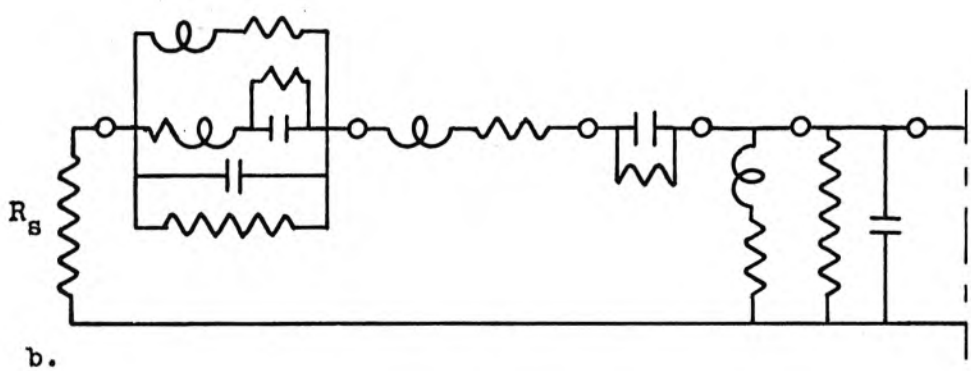

b.

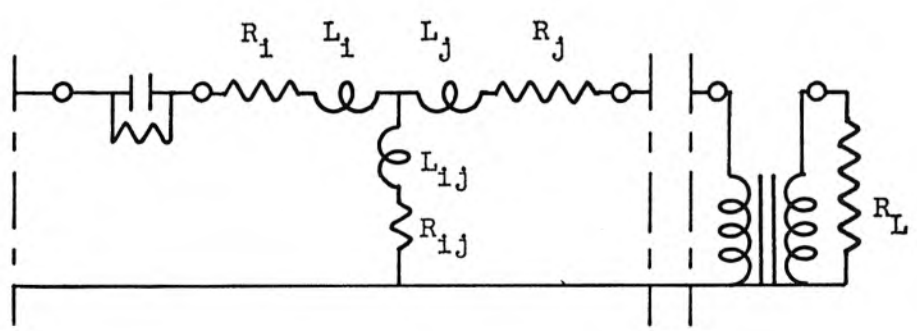

4.4 General low pass and bandpass lossy filter sections

Integrating $\ell n \frac{T'(s)}{T(s)}$ on the $s = i\omega$ axis and closing the contour about the RHP, we have

$$\int_0^\infty \ell n \frac{T'(\omega)}{T(\omega)} d\omega = \frac{\pi}{2}\left(\sum_m (s'_{pm} - s_{pm}) - \sum_n (s'_{on} - s_{on}) \right) + \pi \sum_{RHP_n} (s'_{on} - s_{on}) \tag{4.4}$$

The first two summations can be calculated with the successive use of the transmission formula for cascade two ports

$T_{12}(s) = \frac{T_1(s)\, T_2(s)}{1 - \rho_1(s)\, \rho_2(s)}$ in which T_{12}, T_1, T_2, ρ_1, and ρ_2 are defined in Chapter III, Figure 3.15.

Writing $\ell n \frac{T_{12}(s)}{T'_{12}(s)} = \ell n \frac{T_1(s)}{T'_1(s)} + \ell n \frac{T_2}{T'_2(s)} + \ell n \frac{1 - \rho'_1(s)\, \rho'_2(s)}{1 - \rho_1(s)\, \rho_2(s)}$ one may equate the asymptotic dependence of the two sides of the equation for large s. Because of the division of sections made on the network in Figure 4.4, the asymptotic values of $\rho'_1\, \rho'_2$ and $\rho_1 \rho_2$ are never -1 ; in addition, it can be directly shown that $\ell n \frac{1 - \rho'_1(s)\, \rho'_2(s)}{1 - \rho_1(s)\, \rho_2(s)}$ is of the form $1 - \frac{0}{s} + \frac{K_2}{s^2} + \cdots$. The asymptotic dependences of the other terms above have non-zero coefficients for the 1/s terms. These coefficients are equal to the summation of zero minus pole shifts and, equating them, one has

$$\sum_{n12} (s_{on12} - s'_{on12}) - \sum_{m12} (s_{pm12} - s'_{pm12}) =$$

$$\sum_{n1} (s_{on1} - s'_{on1}) + \sum_{n2} (s_{on2} - s'_{on2}) - \sum_{m1} (s_{pm1} - s'_{pm1}) - \sum_{m2} (s_{pm2} - s'_{pm2}) \tag{4.5}$$

The successive application of equation 4.5 in analyzing a network such as in Figure 4.4 can directly prove that the first two summations in equation 4.4 are equal to the total of the corresponding summations for the simple two-port sections. These latter are easy to calculate. For example, in the low pass network of Figure 4.2 for which there are no transmission zeros, the pole shifts of the individual sections are equal to the loss factors of the individual elements. For this network

$$\int_0^\infty \ln \frac{T'(\omega)}{T(\omega)} \, d\omega = -\frac{\pi}{2} \sum_i \left(\frac{G_i}{C_i} + \frac{R_i}{L_i} \right) \tag{4.6}$$

It can be shown that loss in elements which cause transmission zeros contributes nothing to the first two summations in equation 4.4. Those zero-causing elements which have negative loss factors $\left.\frac{R_i}{L_i}\right|_{-0}$ or $\left.\frac{G_i}{C_i}\right|_{-0}$ do, however, contribute to the third summation.

$$\sum_{RHP_n} (s'_{on} - s_{on}) = -\sum \left(\left.\frac{R_i}{L_i}\right|_{-0} + \left.\frac{G_i}{C_i}\right|_{-0} \right) \tag{4.7}$$

In general, half of the integral of $\ln \frac{T'(\omega)}{T(\omega)} \, d\omega$ due to these loss elements falls in the frequency range where $T(\omega)$ is very small, i.e., the region of a zero of $T(\omega)$. The actual contribution of these elements to the gain in the region where $T(\omega)$ is not small is thus essentially the same as given in equation 4.6 for pole producing elements. There is no term in equation 4.7 for positive losses which shift real axis zeros into the LHP. Such elements make $|T'(\omega)/T(\omega)| > 1$ near zeros of $T(\omega)$ and $|T'(\omega)/T(\omega)| < 1$ near poles of $T(\omega)$. The net effect on the integral is zero. Sections which have three reactances of the same kind such as the L_i, L_j, L_{ij} section in Figure 4.4, arise

in the coupled resonator configuration. The contribution to $\ell n \left|\frac{T'(\omega)}{T(\omega)}\right| d\omega$ from the zero shift in this section falls in the frequency range of the zero of $T(\omega)$ and is generally not useful for gain. The contribution elsewhere due to losses R_i, R_j, and R_{ij} can be evaluated in terms of an effective loss factor for the section.

$$\left.\frac{R}{L}\right|_{\text{eff } ij} = \frac{R_i}{L_i + \frac{L_{ij} L_j}{L_{ij} + L_j}} + \frac{R_j}{L_j + \frac{L_{ij} L_i}{L_i + L_{ij}}} + \frac{R_{ij}}{L_{ij} + \frac{L_i L_j}{L_i + L_j}} \qquad (4.8)$$

In most cases L_{ij} is much less than L_i and L_j, and R_{ij} has only a small contribution to $\left.\frac{R}{L}\right|_{\text{eff } ij}$.

From the above theory one can write an exact integral limitation on $\left|\frac{T'(\omega)}{T(\omega)}\right|$ in terms of the loss factors of the network elements. A simpler but slightly approximate integral relation which takes into account only contributions of losses to the passband gain and not to the gain near the zeros of $T(\omega)$ can also be written from the above theory. This limitation has more meaning in the synthesis problem.

$$\int_0^\infty \ell n \left|\frac{T'(\omega)}{T(\omega)}\right| d\omega = -\frac{\pi}{2} \sum \left(\frac{G_i}{C_i} + \frac{R_i}{L_i}\right) + \left.\frac{R}{L}\right|_{\text{eff } ij} \qquad (4.9)$$

not including regions near zeros of $T(\omega)$ — including zero-causing elements — contributions from coupling sections

The various methods of synthesis, uniform predistortion, non-uniform predistortion, and iterative design, differ in the number of passive elements required for a fixed number of active elements. They differ in how near unity $T(\omega)$ can be maintained over the amplification band.

They may differ in the possibility that $\ell n\left|\frac{T'(\omega)}{T(\omega)}\right|$ may change sign over the range of ω. For instance, networks with uniform negative loss have $\left|\frac{T'(\omega)}{T(\omega)}\right| > 1$ for all ω. The maximum bandwidth for flat gain T'_o is obtained if $T(\omega) = 1$ in the passband and has a limitation on the characteristic bandwidth ω_c, $\omega_c = \pi N \frac{G}{C} \frac{1}{\ell n T'_o}$. On the other hand, the one and two active element transmission amplifiers considered in Chapter II may definitely have $\left|\frac{T'(\omega)}{T(\omega)}\right| < 1$ outside the passband. The above limitation on ω_c does not hold for these amplifiers. The situation for non-uniform loss and iterative design is not yet known. It is expected, however, that in these we will in general have $\left|\frac{T'(\omega)}{T(\omega)}\right| > 1$ for all ω. Thus while in the sense of equation 4.9 the integral bandwidth capability of active networks designed by the three methods mentioned is the sum of the loss factors of the active elements, the above differences make a detailed comparison difficult.

For the uniformly negative lossy low pass ladder network, integral limitations can also be found on the reflection coefficients at the terminations. For equal loss factors $-\frac{G}{C}$

$$\frac{\rho'_L}{\rho_L} = \pi_m \left(\frac{s - s_{om} - \frac{G}{C}}{s - s_{pm} - \frac{G}{C}}\right)\left(\frac{s - s_{pm}}{s - s_{om}}\right) \quad ; \quad \frac{\rho'_s}{\rho_s} = \pi_m \left(\frac{s + s_{om} - \frac{G}{C}}{s + s_{pm} - \frac{G}{C}}\right)\left(\frac{s - s_{pm}}{s - s_{om}}\right) \qquad (4.10)$$

where the s_{om} are the zeros of ρ_L. The logarithms of these functions are to be integrated around the RHP. Only the RHP singularities will contribute and these must be identified. Positive s_{om} will lead to RHP poles and zeros of ρ'_L/ρ_L. Negative s_{om} give RHP poles and zeros of ρ'_s/ρ_s. RHP singularities are also possible for ρ'_L/ρ_L when $-G/C$ is less than negative s_{om}, and for ρ'_s/ρ_s when G/C is greater than

positive s_{om}. For stability s_{pm} and $s_{pm} + \frac{G}{C}$ cannot be in the RHP. We find that

$$\int_0^\infty \ell n \left| \frac{\rho_L'(\omega)}{\rho_L(\omega)} \right| d\omega = N_L \pi \frac{G}{C} + K_L$$

$$\int_0^\infty \ell n \left| \frac{\rho'_s(\omega)}{\rho_s(\omega)} \right| d\omega = N_s \pi \frac{G}{C} + K_s \qquad (4.11)$$

N_L = number of RHP zeros of ρ_L

N_s = number of RHP zeros of ρ_s

$N_s + N_L = N_o$ = number of network reactive elements

$K_L = \pi \sum_{xL} s_{oxL} + \frac{G}{C}$, where s_{oxL} are LHP zeros of ρ_L located between the $s = i\omega$ and $s = i\omega - \frac{G}{C}$ axes.

If one of the network terminations, say R_L , is infinite or zero, making $T = 0$, $T' = 0$, $\rho_L = 1$, $\rho_L' = 1$ and $\rho_s = 1$, equations 4.11 give an integral limitation of the uniform negative loss ladder as a reflection amplifier.

$$\int_0^\infty \ell n \left| \rho_s'(\omega) \right|^2 d\omega = 2N \pi \frac{G}{C} \qquad (4.12)$$

If a transmission amplifier such as the general configuration in Figure 4.2 contains only negative resistance or conductance elements and these all have the same negative effective temperature, $-\tau_T$, the noise figure can be calculated directly from a knowledge of the load reflection coefficients, ρ_L' , and the transmission gain T' by using

the reciprocity theorem. The ratio of noise power out due to the i^{th} element to noise power available from the i^{th} element is equal to the transmission gain between the load and the i^{th} element.

$$\frac{P_{out\ i}}{-K\tau_{Ti}\ df} = \frac{\text{Power dissipated in } G_i \text{ or } R_i}{\text{Power available from } R_L}$$

Therefore, for all elements at the same temperature $-\tau_T$,

$$\sum_i P_{out\ i} = -K\tau_T\ df\ \frac{\text{Power dissipated in all negative elements}}{\text{Power available from } R_L} .$$

Applying conservation of energy to the circuit, one sees that the power dissipated in all negative elements is negative and equal to the negative of the power dissipated in R_S plus the power reflected back into R_L minus the original power available from R_L . Inserting this into the usual definition of noise figure and including the reflected load noise we have

$$F = 1 + \frac{\tau_T}{\tau_s}\left(\frac{|T'|^2 + |\rho_L'|^2 - 1}{|T'|^2}\right) + \frac{\tau_L}{\tau_s}\ \frac{(\rho_L' - 1)(\rho_L'^{*} - 1) - 1}{|T'|^2} \qquad (4.13)$$

This discussion of noise figure has been placed before a detailed consideration of the synthesis technique to illustrate the following important point: The noise figure of the unilateral amplifier in which all active elements have the same noise temperature depends critically on the reflection coefficient at the load end. It does not depend at all on the reflection coefficient at the signal generator. In the synthesis of a multi-element amplifier by the predistortion technique, the zeros of the two reflection coefficients can be chosen rather arbitrarily.

The choice which minimizes ρ_L' also minimizes the noise figure, but will simultaneously maximize ρ_s' .

4.2 Uniform Predistortion Synthesis of Tunnel Diode Bandpass Amplifiers

The tunnel diode is not directly compatible with the circuit of Figure 4.2. The coupled resonator bandpass equivalents of Figure 4.2, however, do accommodate active elements which are all of the same kind. The resonators may be drawn as parallel capacitance, inductance and negative conductance when the tunnel diode inductance is itself negligible. Otherwise, series equivalents of the tunnel diode as given in section 2.8 can be fitted into a coupled resonator configuration with series resonators. The coupled resonator with negative uniform loss resonators can probably be synthesized by direct predistortion of the poles of a coupled resonator configuration. In this section, however, we will rely on the equivalence between low pass ladders and the coupled resonator bandpass configuration which was established in Chapter II.

We consider, then, as an equivalent representation of a physically realizable bandpass configuration, the circuit of Figure 4.2. Both the capacitance negative conductance branches and the inductance negative resistance branches represent tunnel diodes with all R_i/L_i and G_i/C_i equal to $-G_T/C_T$. G_T may also include any extraneous positive losses in the physical circuit and has a negative effective temperature $-\tau_T$ as shown in the introduction to Chapter II.

The uniform negative predistortion technique will now be applied to the low pass equivalent circuit in Figure 4.2 with uniform negative loss. Butterworth and Tchebysheff response with $\epsilon = 1$ are explicitly

chosen in this work, but the method is quite general and linear phase or any other response whose poles are known can be used. The poles of the response function of a lossless ladder network are chosen to be the pole configuration of the desired gain response but shifted to the left by an amount G_T/C_T . By equation 4.2 the subsequent evaluation of the real frequency performance of the uniform loss network is made on the $s = i\omega - \frac{G_T}{C_T}$ axis giving the desired response. Figure 4.3 shows a typical predistorted Butterworth pole configuration and the distorted real frequency axis. The diagram is normalized to ω_B and the normalized pole shift is $q_o = \frac{G_T}{\omega_B C_T}$. A similar normalization, $q_o = \frac{G_T}{\omega_T C_T}$, will be used for the Tchebysheff response.

The lossless transmission response may be evaluated on the $s = i\frac{\omega}{\omega_B}$ or $s = i\frac{\omega}{\omega_T}$ axis as

$$|T(\omega)|^2 = T_o^2 \pi_m \frac{|s_{pm} - q_o|^2}{\left|s - s_{pm} + q_o\right|^2_{i\frac{\omega}{\omega_B}}} \tag{4.14}$$

in which the s_{pm} are now the normalized LHP pole locations given by equations 2.15 through 2.18. The gain with negative loss is evaluated on the $s = i\frac{\omega}{\omega_B} - q_o$ axis as

$$|T'(\omega)|^2 = T_o^2 \pi_m \frac{|s_{pm} - q_o|^2}{\left|s - s_{pm}\right|^2_{i\frac{\omega}{\omega_B}}} \tag{4.15}$$

The normalization factor T_o^2 controls the realizability of the lossless network with passive components and terminations. For the completely

passive network to exist, the lossless transmission gain must be less than unity, $|T(\omega)|^2 \leq 1$, all ω. For the Butterworth and odd N Tchebysheff response, the maximum of $|T(\omega)|^2$ occurs at $\omega = 0$ and $T_{o\ max}^2 = 1$. For even Tchebysheff response this is not true for very small q_o, but has been found to apply in all cases in which the average gain $|T|^2$ is greater than $4\epsilon^2$. For our purposes such is always the case, and we take $T_o^2 \leq 1$.

The actual transmission gain $|T'|^2$ can now be evaluated from equation 4.15. For a given q_o the gain is maximum for $T_o^2 = 1$. The reflection zero positions will vary with T_o^2, however, and some $T_o^2 < 1$ may make a better overall amplifier. The midband gain increase $\left|T_o'/T_o\right|$ as a function of q_o can be found approximately for the Butterworth case. Here

$$s_{pB_m} = e^{i\theta_m} = e^{i\left(\frac{\pi}{2} + \frac{2m+1}{2N}\pi\right)}, \quad m = 0 \text{ to } N-1 \tag{4.16}$$

$$\ell n \left|\frac{T_o'}{T_o}\right|_B^2 = \sum_m 2\ell n \left(1 + \frac{q_o}{e^{i\theta_m}}\right)$$

$$\ell n \left(1 + \frac{q_o}{e^{i\theta_m}}\right) \cong \frac{q_o}{e^{i\theta_m}} \tag{4.17}$$

$$\ell n \left|\frac{T_o'}{T_o}\right|_B^2 \cong 2q_o \sum_m e^{-i\theta_m} \tag{4.18}$$

$\sum_m e^{-i\theta_m}$ is the summation of the Butterworth poles and is given by $1/\sin\frac{\pi}{2N}$. Then

$$\ell n \left|\frac{T_o'}{T_o}\right|^2 \cong \frac{2q_o}{\sin\frac{\pi}{2N}} = \frac{2G_T}{\omega_B C_T} \frac{1}{\sin\frac{\pi}{2N}} \tag{4.19}$$

For large N

$$\ell n \left|\frac{T'_o}{T_o}\right|^2_B = \frac{4}{\pi} N \frac{G_T}{\omega_B C_T} \tag{4.20}$$

No approximation has been found for the analogous Tchebysheff relation. The average value of the Tchebysheff gain increase $\left|\frac{T'_o}{T_o}\right|^2_{\epsilon=1}$ and $\left|\frac{T'_o}{T_o}\right|_B$ have been calculated numerically for various q_o and N. The results are shown in Figures 4.5 and 4.6. Equation 4.20 holds fairly well for $N > 2$ and the Butterworth curves are asymptotic to $\ell n \left|\frac{T'_o}{T_o}\right|^2_B = .4\pi N q_o$. The Tchebysheff curves for $N > 2$ are given fairly well by

$$\ell n \left|\frac{T'_o}{T_o}\right|^2_{\epsilon=1} = .6n\pi\ q_o \tag{4.21}$$

Figure 4.7 shows $\omega_c \frac{C_T}{G_T} = \frac{1}{q_o}$ plotted against N for $\left|\frac{T'_o}{T_o}\right|^2_B$ and $\left|\frac{T}{T_o}\right|^2_{\epsilon=1} = 100$. The ultimate flat gain limitation from equation 4.6 $C_T\omega_c/G_T = \frac{N\pi}{\ell n\ 100}$ is also shown.

It is important to compute the zeros of the reflection coefficients from the predistorted poles. The zero positions are required not only to continue the synthesis procedure to the point of calculating the elements of the low pass equivalents but also for computing reflection gain which enters into the noise figure and to test the sensitivity of the network to errors. The zeros of

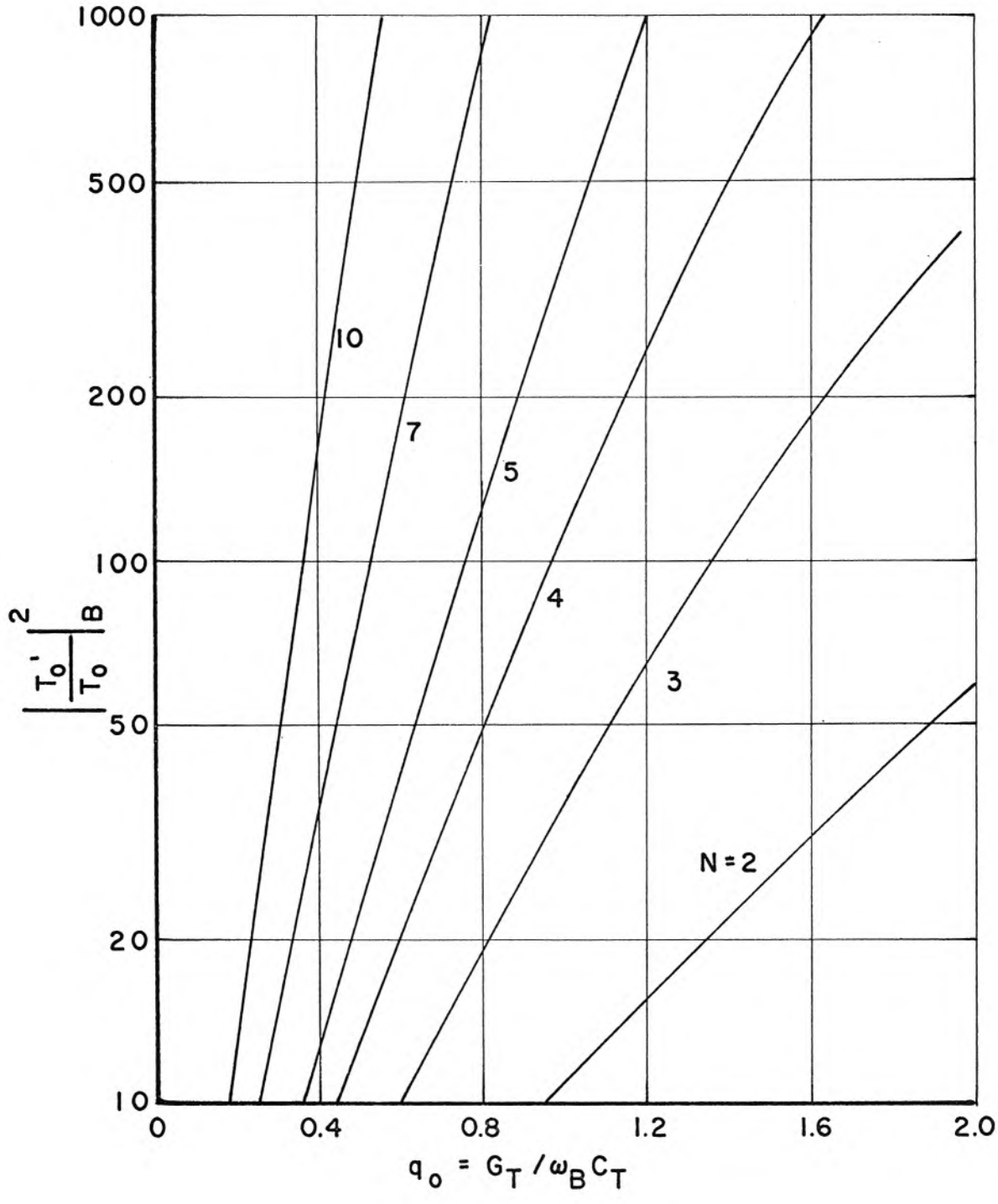

Figure 4.5 Normalized Midband power gain for predistorted N-pole Butterworth response versus $q_o = G_T/\omega_B C_T$

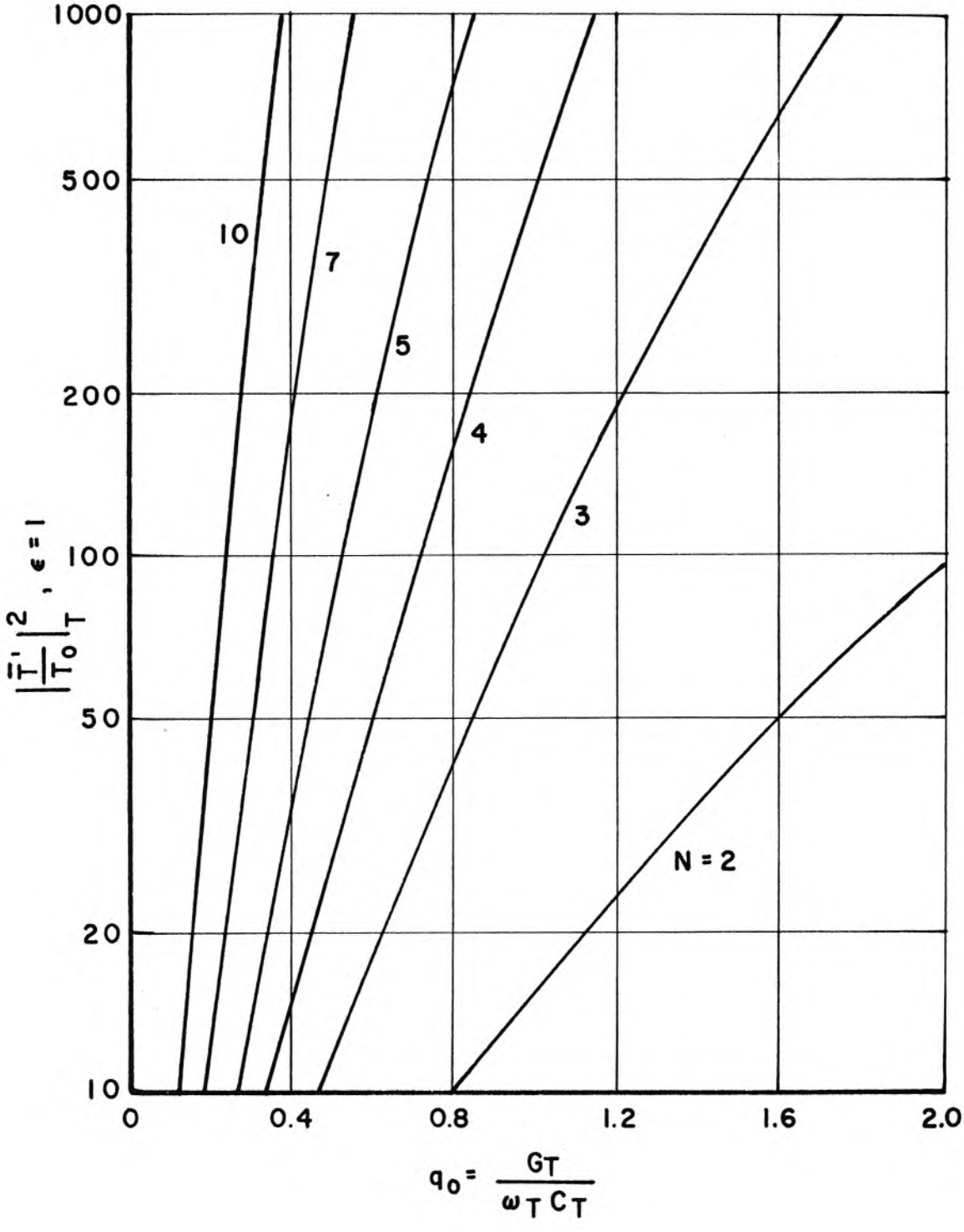

Figure 4.6 Normalized average power gain for predistorted N-pole 3 db ripple Tchebysheff response versus $q_o = G_T/\omega_T C_T$.

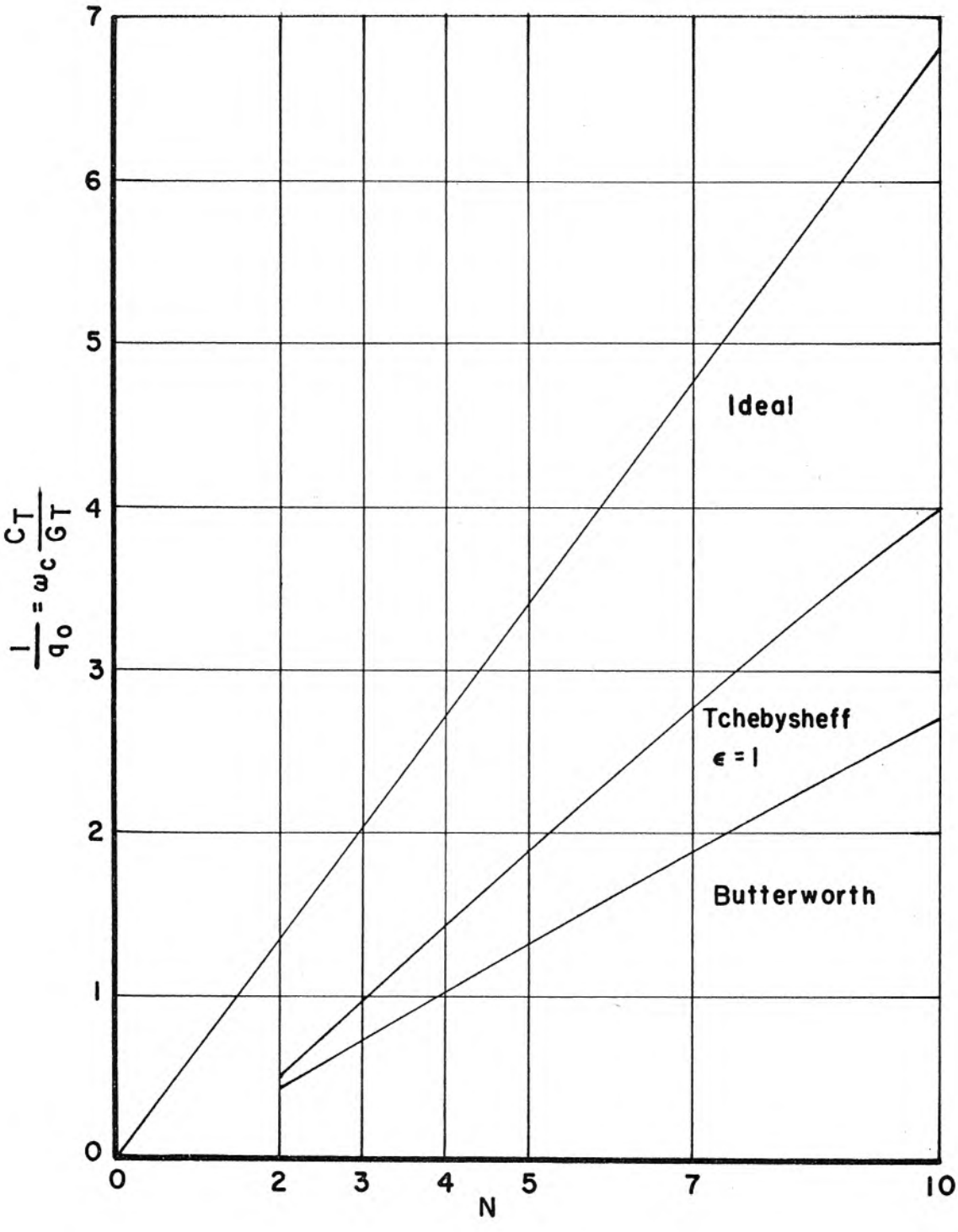

Figure 4.7 Normalized characteristic bandwidth versus N for Butterworth, Tchebysheff and ideal responses giving 20 db average gain.

$$\rho(s)\,\rho(-s) = 1 - T(s)\,T(-s) =$$

$$\frac{\pi_m(s - s_{pm} + q_o)(-s - s_{pm} + q_o) - T_o^2\,\pi_m\,|s_{pm} - q_o|^2}{\pi_m(s - s_{pm} + q_o)(-s - s_{pm} + q_o)} \qquad (4.22)$$

are the full zero complement of both reflection coefficients ρ_L and ρ_s. The zeros of ρ_L can be chosen from these in an arbitrary fashion as long as only one of each real conjugate pair is taken and complex conjugate symmetry is maintained. The remaining zeros belong to ρ_s. Unless otherwise specified, ρ_L will be assumed here to have only LHP zeros. When $T_o^2 = 1$, there is always a pair of roots of equation 4.22 at $s = 0$. These move rapidly toward $\pm q_o$ as T_o^2 is decreased. As T_o^2 goes to zero, the LHP zeros approach the poles. Figure 4.8a shows the Butterworth LHP pole distribution predistorted so that $\left|\frac{T_o'}{T_o}\right|_B^2 = 100$ for $N = 4$. One set of reflection zeros for $T_o^2 = 1,\ 1/\sqrt{2}$, and $1/2$ are shown in the LHP. This choice gives minimum reflection coefficient ρ_L' on the $s = i\frac{\omega}{\omega_B} - q_o$ axis. Figure 4.8b shows the reflection zeros in the RHP corresponding to the reflection at the opposite termination. The reflection coefficient at any point $s = i\omega - q_o$ is the product of the distances to the zeros divided by the product of the distances to the poles. It can be seen that the reflection gain with zeros in the LHP, $|\rho_L'|^2$, is on the order of unity. The reflection gain for zeros in the RHP, $|\rho_s'|^2$, is on the order or higher than $\left|\frac{T'}{T_o}\right|^2$. This situation has been found in all the cases computed. Figure 4.9a,b shows the analogous case for the Tchebysheff 3 db ripple response with $N = 4$, $\left|\frac{T'}{T_o}\right|^2 = 100$. The ratio of $|\rho_s'|^2$ to $\left|\frac{T'}{T_o}\right|^2$ is in general larger for Tchebysheff response.

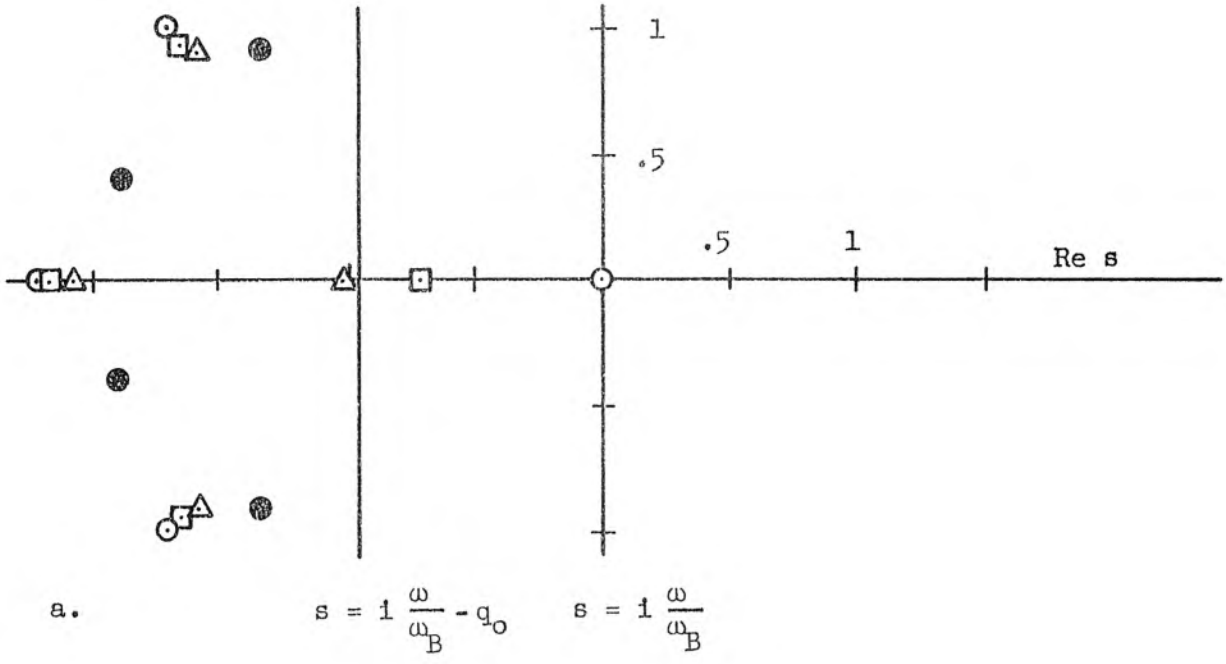

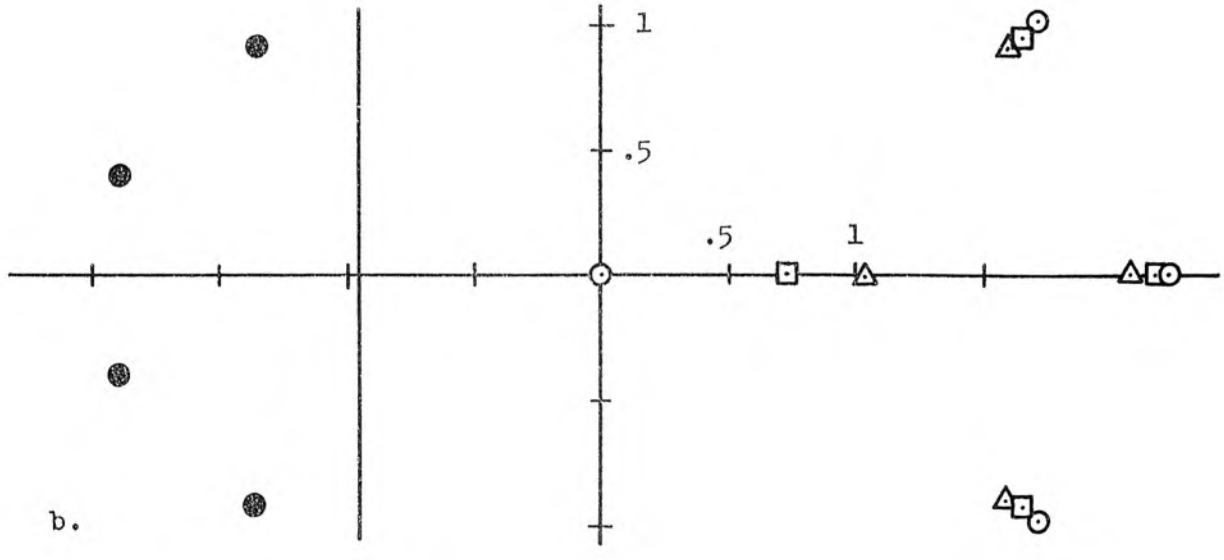

○ zeros for $T_o^2 = 1$

□ zeros for $T_o^2 = 1/\sqrt{2}$

△ zeros for $T_o^2 = 1/2$

● poles

Figure 4.8 Butterworth predistorted pole distribution for $N = 4$, $\left|\frac{T_o'}{T_o}\right|_B^2 = 100$ and LHP and RHP reflection zeros

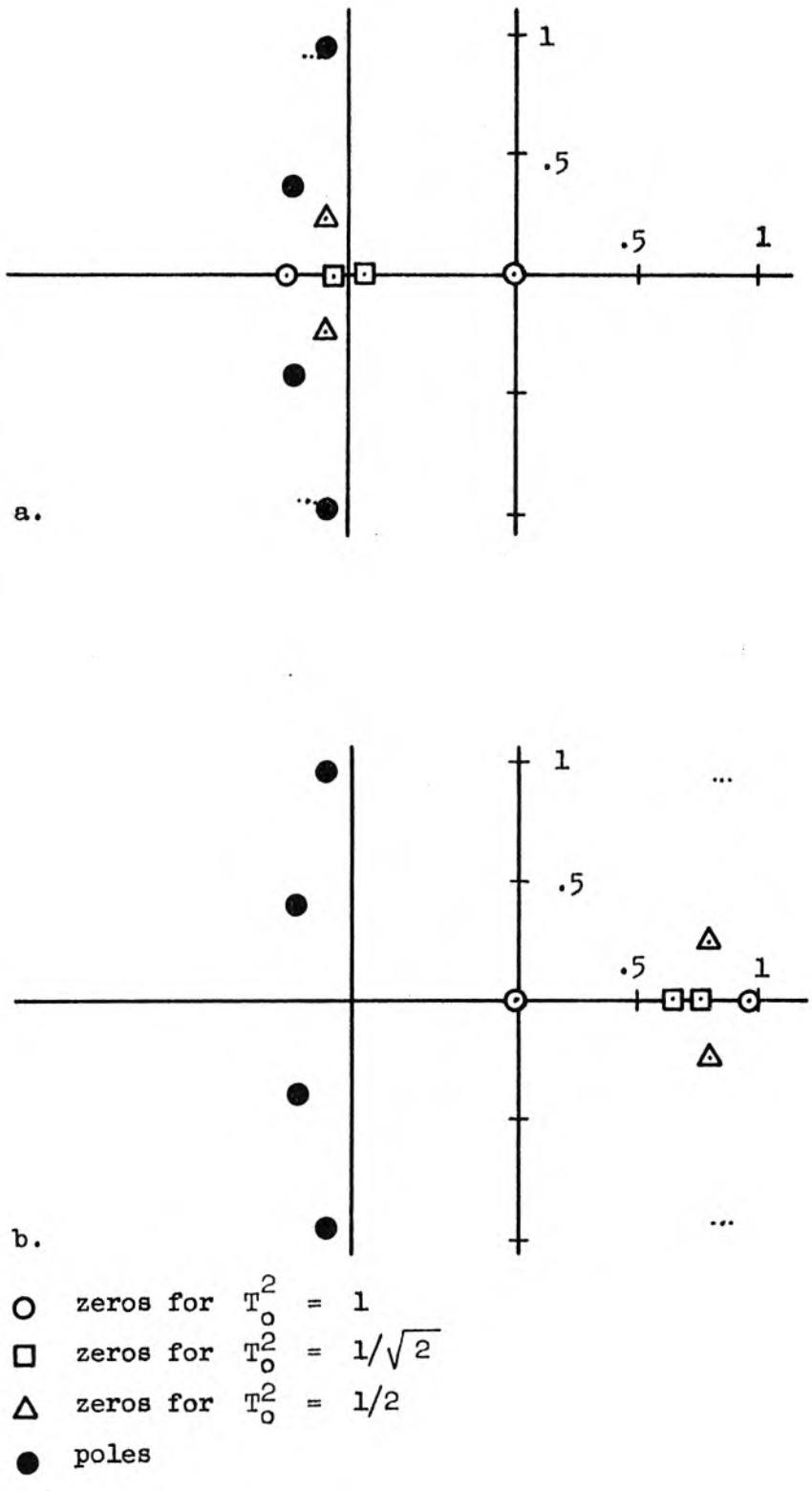

Figure 4.9 Tchebysheff predistorted pole distribution for N = 4, $\left|\frac{T'}{T_o}\right|^2_{\epsilon=1} = 100$. LHP and RHP reflection zeros

While the magnitudes of the reflection coefficients at the two terminations may be equalized somewhat by other choices of the zero distributions, the product of these reflection gains is invariant and when averaged over the band is generally greater than $\left|\frac{\overline{T}'}{T_o}\right|^2$.

The sensitivity to variation of a termination may be predicted from equation 4.23 below.

$$T_{12}(s) = \frac{T_1(s)\, T_2(s)}{1 - \rho_1(s)\, \rho_2(s)} \tag{4.23}$$

where T_1 is the calculated transmission for the correct termination G_o ; T_{12} is the transmission to termination G_1 which is different from G_o ;

$$\rho_2 = \frac{G_o - G_1}{G_o + G_1} \quad \text{is the reflection between } G_o \text{ and } G_1 \tag{4.24}$$

and

$$T_2 = \frac{2\sqrt{G_1 G_o}}{G_o + G_1} \quad \text{is the transmission between } G_o \text{ and } G_1 \,. \tag{4.25}$$

As long as $\rho_1\rho_2$ remains less than unity at all frequencies, the poles will remain in the left half plane, and the transmission reduction factor is given by

$$\frac{T_{12}(\omega)}{T_1(\omega)} = \frac{2\sqrt{G_1\, G_o}}{(G_o + G_1) - (G_o - G_1)\rho_1(\omega)} \tag{4.26}$$

When $\rho_1(\omega)$ is not large, T_{12}/T_1 is rather insensitive to $G_o - G_1$.

The reflection coefficient $|\rho'_L|$ whose zeros and poles are shown in Figures 4.8a and 4.9a is generally less than or on the order of unity, not only over the passband, but also outside it. Having zeros in the LHP only, ρ_L obeys the integral limitation

$$\int_0^\infty \ell n \left| \frac{\rho'_L(\omega)}{\rho_L(\omega)} \right| d\omega = K_L \tag{4.27}$$

K_L is given in equation 4.11 and may be zero if T_o^2 is chosen small enough so that ρ_L has no zeros between the $s = i\omega \pm q_o$ axes. At the other termination ρ'_s, which has only RHP zeros, is generally larger than unity everywhere and obeys the limitation

$$\int_0^\infty \ell n \left| \frac{\rho'_s(\omega)}{\rho_s(\omega)} \right| d\omega = N\pi q_o + K_s \tag{4.28}$$

The amplifier is rather sensitive to an error in this termination.

The sensitivities to variation of the terminations as well as the respective reflection coefficients may be equalized somewhat by some other choice of the zero distribution at the expense of the noise figure. In general, the sensitivities to source and load variation of these multi-element amplifier designs seems to be about the same as for a single active element amplifier having the same noise figure contribution from reflected load noise. The only great advantage of these particular multi-element designs then is that the bandwidth increases directly with the number of active elements specified.

It is apparent from the previous section that for minimizing the

product of the reflection coefficients at both terminations or for obtaining maximum bandwidth capability per active element, predistorted Butterworth or Tchebysheff response may not be the best choices. The two objectives above are not completely compatible. From equation 4.9 one can see that for maximizing the amplification bandwidth, $T(\omega)$ should be unity over the band. This would require the zeros of $\rho(s)\,\rho(-s)$ to be near the passband region of the $s = i\omega$ axis. From equation 4.11 it can be seen that this choice of zeros would give rather large K_L and K_G. In general the introduction of uniform loss in a network whose lossless reflection zeros are near the passband region of the $s = i\omega$ axis leads to a gain response severely peaked at the band edges. While the reflections are low over most of the active passband, so is the gain.

A possible approach to the problem of minimizing both reflection coefficients simultaneously is to find lossless response functions, all of whose zeros lie on the $s = i\omega \pm G/C$ axes, and whose poles lead to reasonably flat and stable $T'(\omega)$ on the distorted real frequency axes. Such response functions are not known. They may, of course, be generated by trial and error; that is, by choosing zeros and generating the poles from the relation $\rho(s)\,\rho(-s) + T(s)\,T(-s) = 1$. Some complexity may be removed by demanding that the network be even ordered with dual symmetry about the center. The search is then limited to finding a reflection coefficient $\rho(s)$ whose zeros lie in real conjugate pairs and whose poles have the desired properties. Such a reflection coefficient can be written in terms of the properties of the half network, thus simplifying the order of the problem.

There is no assurance that pole zero distributions which give low

ρ'_L and ρ'_s and well behaved T' can be found nor that the resulting bandwidth will be reasonably close to the ultimate theoretically obtainable. Nevertheless, the search for such distributions may be a good way of approaching an optimum synthesis of multi-element networks.

The synthesis results of this section can also be used in the construction of multi-element reflection amplifiers having approximately Tchebysheff or Butterworth reflection response. We consider the reflection zeros obtained from equation 4.22 when T_o^2 goes to zero. The LHP zeros can be seen to fall directly on the LHP poles, and the RHP zeros are the real conjugates of the LHP zeros. The reflection coefficient which has LHP zeros and poles has magnitude unity on both the $s = i\omega$ and $s = i\omega - \frac{G}{C}$ axes. This means that the synthesized resistance for this termination is either zero or infinity. The reflection coefficient with RHP zeros evaluated on the $s = i\omega$ axis also has unity magnitude. This reflection coefficient is large, however, when evaluated on the $s = i\omega - \frac{G}{C}$ axis. Its magnitude at midband can be evaluated from Figures 4.5 and 4.6 reading the ordinate as $|\rho'|_o$ rather than $\left|\frac{T'}{T_o}\right|^2$. The reflection poles, being much closer to the $s = i\omega - \frac{G}{C}$ axis than the zeros, are more important in determining the actual response shape. The reflection response shapes for Butterworth and Tchebysheff predistorted poles are therefore approximately Butterworth or Tchebysheff.

4.3 Predistortion Synthesis of Multi-element Parametric Amplifiers

The uniform predistortion synthesis technique used for tunnel diode amplifiers in the previous section can also be applied to parametric amplifiers if, as in Chapter III, normal modes can be found in which the effects of the time varying elements are describable in terms of real admittances at two frequencies. In this section we consider requirements for the isolation of such normal modes in multi-element amplifiers. Only time varying capacitors will be used here, but the approach is easily generalizable to networks containing other types of time varying reactances either alone or in combination. One may guess that the symmetry conditions for the multi-element network will be essentially the same as required for the degenerate and pseudo-degenerate syntheses of Chapter III.

We consider a network containing time varying elements $C_i\left(1 + \eta_i \cos(\omega_p t + \theta_{pi})\right)$ in parallel with effective loss conductances G_{oi} and G_{-li} at the two band center frequencies Ω_o and Ω_{-l}. Such networks are shown in Figure 4.10. Across each of these elements will appear voltages $V_{oi}\, e^{i\omega_o t}$ and $V_{-li}\, e^{-\omega_{-l} t}$. Neglecting other frequencies, the current through each of these elements is

$$I_{oi}\, e^{i\omega_o t} + I_{-li}\, e^{i\omega_{-l} t} =$$

$$(G_{oi} V_{oi} + i\omega_o C_i V_{oi} + \frac{\eta_i}{2} i\omega_o C_i V_{-li}\, e^{i\theta_{pi}}) e^{i\omega_o t}$$

$$+ (G_{-li} V_{-li} + i\omega_{-l} C_i V_{-li} + \frac{\eta_i}{2} i\omega_o C_i V_{oi}\, e^{-i\theta_p i})\, e^{i\omega_{-l} t} \qquad (4.29)$$

Then

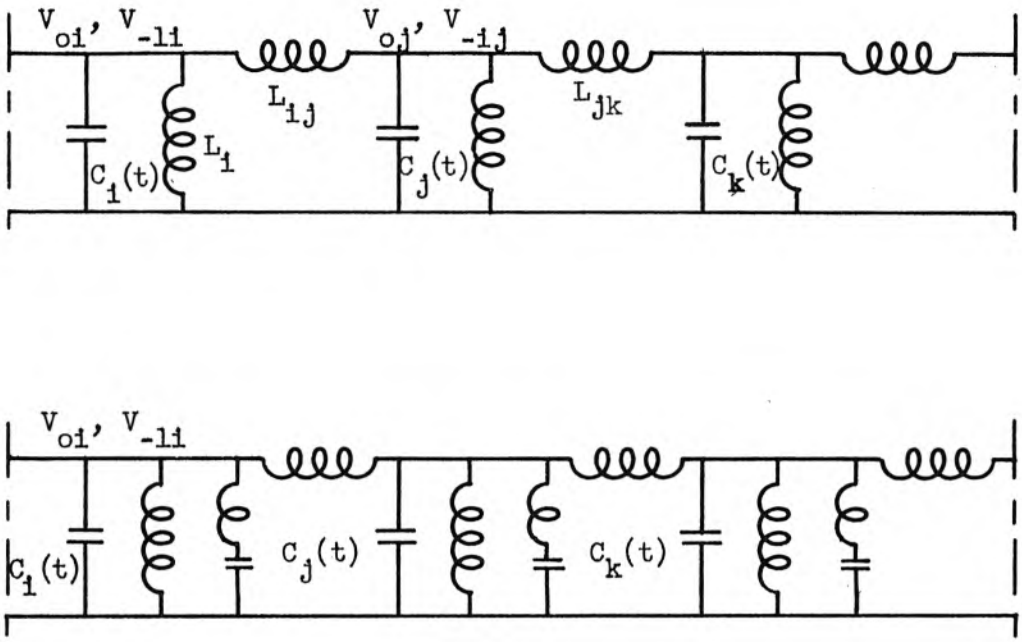

Figure 4.10 Possible degenerate and non-degenerate parametric amplifier configurations containing time varying capacitances $C_i(1 + \eta_i \cos \Omega_p t + \theta_p i)$

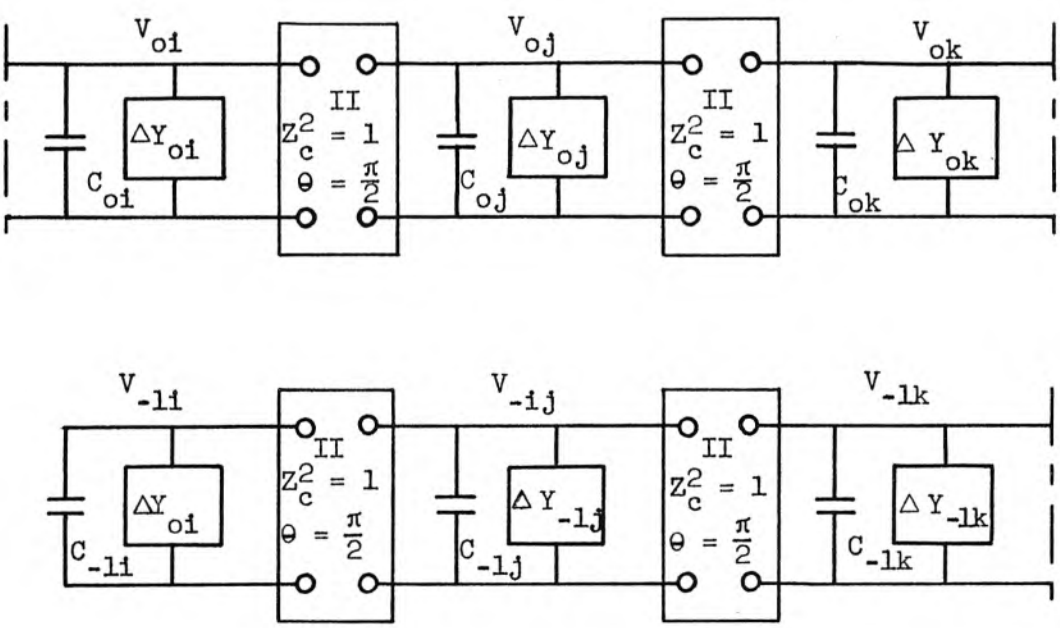

Figure 4.11 Required ω_o and ω_{-1} equivalent circuits for isolation of modes with real ΔY_o and ΔY_i

$$\frac{I_{oi}}{V_{oi}} = i\omega_o C_i + \Delta Y_{oi} =$$

$$i\omega_o C_i + G_{oi} + i\omega_o C_i \frac{\eta_i}{2} \frac{V_{-1i}}{V_{oi}} e^{i\theta_{pi}}$$

$$\frac{I_{-1i}}{V_{-1i}} = i\omega_{-1} C_i + \Delta Y_{-1i} =$$

$$i\omega_{-1} C_i + G_{-1i} + i\omega_{-1} C_i \frac{\eta_i}{2} \frac{V_{oi}}{V_{-1i}} e^{-i\theta_{pi}} \qquad (4.30)$$

To achieve the pseudo-degenerate symmetry requirements we demand that two low pass equivalent circuits can be drawn whose low pass properties are analogues of the Ω_o and Ω_{-1} centered properties of the physical network. Such analogues of Figure 4.10 are shown in Figure 4.11. The variable

$$s = i(\omega_o - \Omega_o) = i(\omega_{-1} - \Omega_{-1}) \qquad (4.31)$$

is used as in Chapter III. The elements C_{oi} and C_{-1i} are presumably again related to reactance slopes in the two band network and have the same product limitation as found in Chapter III. The circuits of Figure 4.10 can be made identical with the equivalent circuits of Figure 4.11 in the narrow band limit.

When the Ω_o and Ω_{-1} networks of Figure 4.11 are identical except for an admittance level ratio $C_{-1i} = BC_{oi}$, and a possible difference in the sign of the $\pi/2$ radians phase shift in the impedance inverters, the choice $\Delta Y_{-1i} = B\Delta Y_{oi}$ can be seen to be consistent with the choice ΔY_{-1i} and ΔY_{oi} real if and only if $\theta_{pj} - \theta_{pi}$ is

equal to the sum of the phase shifts of the Ω_o and Ω_{-1} impedance inverters connecting the i^{th} and j^{th} elements. For the circuits shown in Figure 4.10 and 4.11, $\theta_{pj} - \theta_{pi}$ must be $\pm\pi$. Had the series coupling branch in Figure 4.10 been chosen to resonate between Ω_o and $|\Omega_{-1}|$ such that the effective coupling were inductive in one band and capacitive in the other, the required $\theta_{pj} - \theta_{pi}$ would be zero.

Having found configuration conditions which lead to real ΔY_i, one may now calculate these admittances for the two modes. The excitation of each mode by a generator at Ω_o or Ω_{-1} can also be computed. The effective loss factors $\frac{2\Delta Y_{oi}}{C_{oi}}$ and $\frac{2\Delta Y_{-1i}}{C_{-1i}}$ are required to be equal. The factors of two were inserted in the above expressions so that these loss factors when inserted in the theory of previous sections give the correct Ω_o or Ω_{-1} bandwidth for C_{oi} and C_{-1i} defined on a reactance slope basis. Neglecting the variation of ω_{-1} and ω_o across the bands as in Chapter II, we have

$$\frac{G}{C}\, i\overline{+} = \frac{2G_{oi} + i\Omega_o C_i \eta_i \frac{V_{-1}}{V_o}}{C_{oi}} = \frac{2G_{-1i} - i|\Omega_{-1}| C_i \eta_i \frac{V_o}{V_{-1}}}{C_{-1i}} \tag{4.32}$$

$$\left.\frac{V_{-1}}{V_o}\right|_{\overline{+}} = -\frac{G_{oi} + \frac{G_{-1i}}{B}}{i\Omega_o C_i \eta_i} \overline{+} \frac{1}{i}\sqrt{\frac{(G_{oi} - \frac{G_{-1i}}{B})^2}{(\Omega_o C_i \eta_i)^2} + \left|\frac{\Omega_{-1}}{\Omega_o}\right| \frac{1}{B}} \tag{4.33}$$

where the minus signs refer to the mode with negative loss factors and consequent transmission gain.

$$\left.\frac{G}{C}\right|_{i\,\mp} = \frac{G_{oi}}{C_{oi}} + \frac{G_{-1i}}{C_{-1i}} \mp \sqrt{\left(\frac{G_{oi}}{C_{oi}} - \frac{G_{-1i}}{C_{-1i}}\right)^2 + \frac{\eta_i^2 C_i^2 / |\Omega_o \Omega_{-1}|}{C_{oi} C_{-1i}}} \tag{4.34}$$

The effective terminations in Figure 4.10 and the terminations shown in Figures 4.11 at Ω_o and Ω_{-1} must also be in the ratio $G_o/G_{-1} = 1/B$ if these modes found above are to exist. A current generator at ω_o couples to both the amplification and attenuation mode. The ratio of the excitations is

$$\frac{I_{in\,o-}}{I_{in\,o+}} = -\frac{\left.\frac{V_o}{V_{-1}}\right|_-}{\left.\frac{V_o}{V_{-1}}\right|_+} \tag{4.35}$$

and the fractional efficiency of input power coupling to the amplification mode is

$$A_{o-} = \left|\frac{I_{in\,o-}}{I_{in\,o-} + I_{mo+}}\right|^2 = \left|\frac{\left.\frac{V_o}{V_{-1}}\right|_-}{\left.\frac{V_o}{V_{-1}}\right|_- - \left.\frac{V_o}{V_{-1}}\right|_+}\right|^2 \tag{4.36}$$

A_{o+}, A_{-1-}, and A_{-1+} are simply obtained from equation 4.36 by change of subscripts.

When the $\left.\frac{G}{C}\right|_i$ as given in equation 4.34 are the same for all sections of the parametric amplifier network, a uniform predistortion synthesis is possible and the results of section 4.2 are directly applicable. Equation 4.34 is, however, applicable for non-uniform loss synthesis also.

When it is not necessary to include the attenuating mode in noise figure calculations, an effective temperature can be written for the effective negative conductance at ω_o .

$$\tau_{i\ eff}\Big|_{\omega_o} = A_{o-}\frac{G_{oi}/C_{oi}}{\frac{G}{2C}\Big|_{i-}}\tau_{oi} + A_{-1-}\left|\frac{V_o}{V_{-1}}\right|^2_{-}\frac{1}{B}\frac{G_{-1i}/C_{-1i}}{\frac{G}{2C}\Big|_{i-}}\tau_{-1i} \qquad (4.37)$$

For $G_{oi}/C_{oi} = G_{-1i}/C_{-1i}$, this becomes

$$\tau_{i\ eff}\Big|_{\omega_o} = \frac{1}{4}\left(\frac{G_{oi}/C_{oi}}{\frac{G}{2C}\Big|_{i-}}\right)\left(\tau_{oi} + \left|\frac{\Omega_o}{\Omega_{-1}}\right|\tau_{-1i}\right) \qquad (4.38)$$

This noise temperature may be used in the noise figure calculations of section 4.1. The noiseless attenuations A_{0-} and A_{-1-} as well as noise from the Ω_{-1} terminations must also be accounted for in the noise figure.

The consideration of conditions under which multi-element parametric amplifiers can be designed by negative loss factor synthesis techniques appears to place very tight symmetry conditions on the properties of the physical circuit. These tight conditions are probably more necessary for the mathematics of the synthesis than for the actual amplifier. It is expected that in physical amplifier configurations such as the network of Figure 4.10 which only approximate the required symmetry, exact mode voltage ratios V_o/V_{-1} can be found which are imaginary at the band centers and which are elsewhere slightly rotated in phase. This adds reactance of the same sign to ΔY_o and ΔY_{-1} tending to restore the symmetry. A small rotation of V_o/V_{-1} does not change the effective G/C to first order. It is very difficult to calculate these effects exactly, however, or to give limits on the asymmetries which will not greatly alter first order predicted response.

CHAPTER V

SUMMARY AND SUGGESTIONS FOR FURTHER WORK

Fundamental bandwidth limitations of the tunnel diode and similar reactance limited negative conductances have been established in Chapter II. The consideration of lossless ladder networks terminated in such elements has been shown to yield syntheses of amplifiers whose bandwidths approach these limits as rapidly as possible as the number of passive circuit components is increased. In addition to synthesis in terms of low pass networks, several questions of practical importance have been raised and answered, such as: the limitations imposed by a second essential reactance in the active element equivalent circuit; warm up stability; and the relations between the low pass ladder and simple bandpass networks.

There are still two large areas in the general problem of tunnel diodes in ladder networks whose consideration may lead to useful and interesting information. One is the general consideration of the capabilities of tunnel diodes appearing elsewhere than in network terminations. The problem has only been touched upon in Chapter IV, where a new integral theorem was derived and in which special case configurations analyzable on a uniform loss basis were discussed. The general problem and even the special case of a single tunnel diode imbedded in a passively terminated ladder network are much more difficult to solve. The simple synthesis procedures used in this work cannot be applied. The second problem area suggested by this work is the consideration of the tunnel diode terminated ladder network whose elements are uniformly

lossy. The transmission amplifiers of Chapter II can be synthesized to give Butterworth or Tchebysheff response by predistortion under these conditions. There is, however, no guarantee that these response functions will be best suited to simultaneous optimization of bandwidth and noise figure. The reflection amplifiers in Chapter II cannot be synthesized to give exact Tchebysheff or Butterworth response by predistortion. New response functions must be found which have desirable characteristics from three possible points of view, band shaping, bandwidth, and noise figure.

In Chapter III fundamental bandwidth limitations of three-frequency nonlinear reactance amplifiers have been derived in a somewhat less general or rigorous way than for tunnel diode amplifiers. These limitations were found to be of two types: a limitation on the minimum product of the two reactance slope parameters obtained in resonating the D.C. reactance at two frequencies, and the limitation which this product imposes on the bandwidth of the idealized active element with no D.C. reactance. With the exception of the degenerate parametric amplifier synthesis the syntheses given in Chapter III are somewhat inadequate. They are not optimum in a sense of approaching the ultimate bandwidth most rapidly as a function of network complexity. They do not allow the independent specification of the ratios of signal to idler load impedance and the first signal to idler reactance slopes. Thus, while some progress has been made here on the general problem of nonlinear reactance amplifier synthesis, there is still much work left to be done. Further work in this area should attempt to remove the above difficulties. In addition, it may be profitable to reconsider the basic symmetry assumptions made in Chapter III and either prove or disprove that this of all

possible physically realizable assumptions leads to the greatest bandwidth limit and the fastest approach to this limit as a function of network complexity.

In Chapter IV multi-element tunnel diode and parametric amplifier configurations which could be analyzed by reverse predistortion were considered. The objects of choosing such configurations were achieved. It was shown that amplifiers whose bandwidth increased almost linearly with the number of components are obtainable, and syntheses giving sixty percent of the maximum bandwidth obtainable with uniform negative loss configurations were demonstrated. A significant problem with the transmission amplifier synthesis as performed in Chapter IV was the resultant high reflection coefficients. It was shown that the reflection coefficient could be reduced to about unity at the load termination, minimizing the noise figure, but only at the expense of raising the reflection coefficient at the input termination. This results in high sensitivity to a change in the source impedance. It was proposed that this difficulty might be removed by a better choice of transmission function. It is possible that this difficulty does not arise in synthesis by the Darlington method of non-uniform predistortion. Both of these approaches to multi-element amplifier design need further consideration.

Throughout this work certain approximations or distortions have been necessary to describe the simplest physical amplifier configurations in terms of the simple low pass network. These have been mostly pointed out already in the text. There has been no mention, however, of the circuitry required to provide excitation in the form of D.C. bias or pump power to the active elements, or the effects which this circuitry

might have on other properties of the active elements.

Ideally speaking, excitation can be applied through extremely narrow band, high Q filters whose presence should not affect the properties of the signal circuit. In practice, the exciting circuitry can usually be designed so that its effects can be treated as perturbations to elements already required by the signal circuit. In a good design these perturbations should not occur as changes in the essential reactance of the active elements, since this may reduce bandwidth capability, nor as lossy elements which may deteriorate noise performance.

The excitation problem, like most of the approximations made in this work, will have to be considered on a single case basis. These "cases", however, need not be so restrictive as to imply the design of a specific special purpose amplifier. The present work has attempted to treat amplifiers in any frequency range. The words "wide band" and "narrow band" have been used here with no quantitative values attached to them. There is much specific synthesis information which can be compiled when the frequency range, and therefore the characteristics of available elements both active and passive, are known. There is much still to be said about configurations and their desirability, expecially in relation to constructional problems. There are approximations to be removed, many of which can be treated when the frequency range and fractional bandwidth are known.

It appears likely that such "common denominators" can be used as a basis for obtaining further design information for tunnel diode and variable reactance amplifiers. It is hoped that the information given here and the methods employed will pave the way for the future compilation of true design data for these devices.

References

1. L. Esaki, "New Phenomenon in Narrow Ge p-n Junctions", Phys. Rev. 109, p. 603 , January 15, 1958.

2. H. S. Sommers, Jr., "Tunnel Diodes as High-Frequency Devices", Proc. IRE 47, 1201-1206, July 1959.

3. T. Yajima and L. Esaki, "Excess Noise in Narrow Germanium p-n Junctions" Jour.Phys. Soc.Japan, Vol.13, 1281-1287, Nov. 1958.

4. H. Bode, Network Analysis and Feedback Amplifier Design, D. Van Nostrand Co., Inc. 1945, pages 365-367.

5. D. C. Youla and L. I. Smilen, "Optimum Negative Resistance Amplifiers" presented at the Polytechnic Institute of Brooklyn Microwave Research Institute Symposium on Active Networks and Feedback Systems, New York City, New York, April 1960.

6. H. J. Carlin and D. C. Youla, "Network Synthesis with Negative Resistors", presented at the Polytechnic Institute of Brooklyn Microwave Research Institute Symposium on Active Networks and Feedback Systems, New York, New York, April 1960.

7. L. Weinberg, "Synthesis Using Tunnel Diodes and Masers", to be published.

8. J. M. Manley and H. E. Rowe, Some General Properties of Nonlinear Elements, Part I--General Energy Relations", Proc. IRE 44, 404-413, April 1956.

9. R. M. Fano, "Theoretical Limitations on the Broadband Matching of Arbitrary Impedances", Jour. Franklin Inst. 249, 57-83, Jan. 1950, and continued on 139-154, February 1950.

10. E. A. Guillemin, Introductory Circuit Theory, John Wiley and Sons Inc. (1953) 148-153.

11. E. A. Guillemin, Synthesis of Passive Networks, John Wiley and Sons, Inc. (1957), 73-95, 445-465, 587-619.

12. L. Weinberg, "A,B,C,D-Network Design Easy as Pie", Proc. N.E.C. XIII October 1957.

13. V. Belevitch, "Tchebysheff Filters and Amplifier Networks", Wireless Eng. 28, 106-110, April 1952.

14. L. Weinberg, "Network Design by Use of Modern Synthesis Techniques and Tables", Tech. Memo. 427, Hughes Research Laboratories; also published in Proc. N.E.C. XII, 1956.

15. E. Green, "Synthesis of Ladder Networks to give Butterworth or Chebyshev Response in the Passband", Proc.IEE 101, Part IV Monographs 1954, 192-203.

16. E. W. Sard, "Gain-Bandwidth Performance of Maximally Flat Negative-Conductance Amplifiers", presented at the Polytechnic Inst. of Brooklyn Microwave Research Institute Symposium on Active Networks and Feedback Systems, New York, New York, April 1960.

17. Reference Data for Radio Engineers, fourth edition. International Telephone and Telegraph Corporation 1956, 214-221.

18. S. B. Cohn, "Direct Coupled Resonator Filters", Proc. IRE 45, 187-196, Feb. 1957.

19. H. Seidel and G. F. Herrman, "Circuit Aspects of Parametric Amplifiers", 1959 IRE Wescon Convention Record, Part 2, Circuit Theory, 83-90.

20. G. L. Matthaei, "A Study of the Optimum Design of Wideband Parametric Amplifiers and Upconverters" presented at the PGMTT Symposium, Coronado, California, May 1960.

21. C. A. Desoer, "Steady State Transmission through a Network Containing a Single Time Varying Element", Univ. of California, Inst. of Engineering Research 221, Series 60, Dec. 22, 1958; or ASTIA No. AD210 388.

22. D. Leenov, "Gain and Noise Figure of a Variable Capacitance Up-Converter", BSTJ 37, 989-1008, July 1958.

23. H. Bode, Network Analysis and Feedback Amplifier Design, D. Van Nostrand Co., Inc. 1945, pages 137-169.

24. L. Weinberg, "Explicit Formulas for Tchebysheff and Butterworth Ladder Networks, 1957 IRE Convention Rec., Part 2, 200-209.

25. S. H. Autler, "Proposal for a Maser Amplifier without Nonreciprocal Elements", Proc. IRE 46, 1880-1881, Nov. 1958.

26. J. Sie, "Absolutely Stable Hybrid Coupled Tunnel-Diode Amplifiers", Proc. IRE 48, 1321, July 1960.

27. J. Sie and S. Weisbaum, "Noise Figure of Receiver Systems Using Parametric Amplifiers", 1959 IRE Convention Rec., Part 3, 141-157.

28. S. Darlington, "Synthesis of Reactance 4-Poles which Produce Prescribed Insertion Loss Characteristics", J. Math Phys. 18, 336-340, Sept. 1939.

29. W. Johnson, Transmission Lines and Networks, McGraw-Hill Book Co., Inc. (1950), 271-289.

Nonr 220(13)

DISTRIBUTION LIST

Chief of Naval Research 2
Navy Department - CODE 427
Washington 25, D. C.

Director, Naval Research Lab.
Washington 25, D. C.
Attn: CODE 5240 1
CODE 7130 1
CODE 2000 6
CODE 5430 1

Commanding Officer 1
ONR Branch Office
1000 Geary Street
San Francisco, California

Scientific Liaison Officer 25
ONR, London
c/o Navy 100, Box 39, FPO
New York, New York

Commanding Officer 1
ONR Branch Office
1030 E. Green Street
Pasadena, California

Commanding Officer 1
ONR Branch Office
The John Crerar Library Bldg.
86 E. Randolph Street
Chicago, 1, Illinois

Commanding Officer 1
ONR Branch Office
346 Broadway
New york 13, New York

Officer-in-Charge 3
Office of Naval Research
Navy No. 100
Fleet Post Office
New York, New York

Chief, Bureau Aeronautics EL4 1
Navy Department EL43 1
Washington 25, D.C. EL45 1

Chief, Bureau of Ordnance
Navy Department Re 4 1
Washington 25, D. C. Re 9 1

Chief of Naval Operations Op 20X 1
Navy Department Op 421 1
Washington 25, D.C. Op 55 1

Director, Naval Ordnance Lab. 1
White Oak, Maryland

Director, Naval Electronics Lab 1
San Diego 52, California

Dept. of Electronics Physics 1
U.S.Naval Post Grad. School
Monterey, California

Commander Code 366 1
Naval Air Missile Test Center
Point Mugu, California

U.S. Naval Proving Ground 1
Attn: W. H. Benson
Dahlgren, Virginia

Commander 1
U.S.Naval Air Development Center
Johnsville, Pennsylvania

Committee on Electronics 1
Research and Development Board
Department of Defense
Washington 25, D. C.

Director, Natl. Bureau of Stds. 1
Washington 25, D. C.
Attn: Div.14.0 CRPL, Librarian

Commanding Officer 1
Engineering Res.and Dev. Lab.
Fort Belvoir, Virginia

Ballistics Research Labs. 2
Aberdeen Proving Ground
Maryland
Attn: D.W.H. Delsasso

Chief, Ordnance Develop. Div. 2
Natl. Bureau of Standards
Connecticut Av, VanNess St, NW
Washington 25, D. C.

Commanding Officer 1
Frankford Arsenal
Bridesburg, Philadelphia, Pa.

Thermionics Branch 5
Signal Corps Eng. Labs.
Evans Signal Lab, Bldg. 42
Belmar, New Jersey

Commanding General 1
Air Research and Dev. Command
ATTN: RDSBTL(Hq.Tech.Library)
Andrews Air Force Base
Washington 25, D. C.

Commanding General WCLC 1
Wright Air Devel.Center WCLRC 1
Wright-Patterson AF Base, Ohio

Commanding General CRRE 1
AF Cambridge Research Center
230 Albany Street
Cambridge 39, Massachusetts

Commanding General RCRW 1
Rome Air Development Center
Griffiss Air Force Base
Rome, New York

Commander 5
Armed Services Tech. Info.
ATTN; TIPDR
Arlington Hall Station
Arlington 12, Virginia

Director CR4582 1
Air University Library
Maxwell AF Base, Alabama

Chief, Western Division 1
Air Research and Devel.Command
Office of Scientific Research
P.O.Box 2035, Pasadena, Calif.

Microwave Laboratory 1
Stanford University
Stanford, California
Attn: F.V.L. Pindar

University of Michigan 1
Electron Tube Laboratory
Ann Arbor, Michigan
Attn: J. Rowe

Mr. John S. McCullough 1
Eitel-McCullough, Inc.
San Bruno, California

Johns Hopkins University 1
Radiation Laboratory
1315 St. Paul Street
Baltimore 2, Maryland
Attn: M. Poole, Librarian

Cascade Research 1
5245 San Fernando Road
Los Angeles 39, California

Engineering Library 1
Stanford University
Stanford, California

Research Lab.of Electronics 1
Massachusetts Inst. of Tech.
Cambridge 39, Massachusetts

Sloane Physics Laboratory 1
Yale University
New Haven, Connecticut
Attn: R. Beringer

Mr. H. J. Reich 1
Department of Elec. Eng.
Yale University
New Haven, Connecticut

Electron Tube Section 1
Electrical Engineering Dept.
University of Illinois
Champaign, Illinois

Chairman, Div. of Elec. Eng. 1
University of California
Berkeley 4, California

Technical Report Collection 1
303A, Pierce Hall
Harvard University
Cambridge 38, Massachusetts

Laboratory for Insulation Res. 1
Massachusetts Inst. of Tech.
Cambridge 39, Massachusetts
Attn: A. von Hippel

Chief, West Coast Office
Signal Corps Eng. Labs.
75 So. Grand Avenue
Pasadena, 2, California

Periodicals Librarian 1
General Library
California Inst. of Technology

Lincoln Laboratory 1
Massachusetts Inst. of Tech.
Cambridge 39, Massachusetts

Signal Corps Resident Engineer 1
Electronic Defense Lab.
P.O. Box 205
Mountain View, California

Cornell Aeronautical Laboratory 1
Cornell Research Foundation
Buffalo 21, New York

Director, Electronics Defense 1
Engineering Research Inst.
University of Michigan
Ann Arbor, Michigan

Georgia Inst. of Technology 1
Atlanta, Georgia
Attn: Librarian

Fred D. Wilimek 1
Varian Associates
611 Hansen Way
Palo Alto, California

John Dyer 1
Airborne Instrument Laboratory
Mineola, L.I., New York

Bell Telephone Laboratories
Murray Hill, New Jersey
Attn: J. R. Pierce 1

Hughes Aircraft Company 1
Culver City, California
Attn: Mr.Milek, Tech.Librarian

RCA Laboratories 1
Princeton, New Jersey
Attn: Dr.W.M.Webster

Federal Tele. Laboratories
500 Washington Avenue
Nutley, New Jersey
Attn: W. Derrick 1
K. Wing 1

Technical Library 1
G.E. Microwave Laboratory
601 California Avenue
Palo Alto, California

Columbia Radiation Laboratory 1
538 W. 120th Street
New York 27, New York

Countermeasures Laboratory 1
Gilfillan Brothers, Inc
1815 Venice Boulevard
Los Angeles, California

The Rand Corporation 1
1700 Main Street
Santa Monica, California
Attn: Librarian

Technical Library 1
Research and Development Board
Pentagon Building
Washington 25, D. C.

Motorola Riverside Res. Lab. 1
8330 Indiana Avenue
Riverside, California
Attn: Mr. John Byrne

Chief, Bureau of Ships 816 1
Department of the Navy 820 1
Washington, D. C. 840 1

Advisory Group on Electron Tubes 1
346 Broadway (8th Floor)
New York 13, New York

Supervisor of Research Lab. 1
Electrical Engineering Bldg.
Purdue University
Lafayette, Indiana

W. E. Lear 1
University of Florida
Department of Electrical Eng.
Gainesville, Florida

W. E. Lear 1
University of Florida
Department of Electrical Eng.
Gainesville, Florida

Director Electronics Defense 1
Engineering Research Inst.
University of Michigan
Ann Arbor, Michigan

Cornell Aeronautical Lab 1
Cornell Research Foundation
Buffalo 21, New York

Director, Microwave Res.Inst. 1
Polytechnic Inst.of Brooklyn
55 Johnson Street
Brooklyn 1, New York

University of Washington
Department of Elec. Eng.
Seattle, Washington
ATTN: E. A. Harrison 1
A. V. Eastman 1

University of Colorado 1
Department of Elec. Eng.
Boulder, Colorado

University of Colorado 1
Engineering Experiment Sta.
Boulder, Colorado
ATTN: W. G. Worcester

Electrical Engineering Dept. 1
Princeton University
Princeton, New Jersey

Professor W. P. Dyke 1
Linfield College
McMinnville, Oregon

Research Lab.of Electronics 1
Chalmers Institute of Tech.
Gothenburg, Sweden
ATTN: Librarian

Columbia Radiation Lab. 1
538 W. 120th Street
New York 27, New York

Mr. John S. McCullough 1
Eitel-McCullough, Inc.
San Bruno, California

Cascade Research 1
5245 San Fernando Road
Los Angeles 39, California

Fred D. Wilimek 1
Varian Associates
611 Hansen Way
Palo Alto, California

John Dyer 1
Airborne Instrument Lab
Mineola, New York

Bell Telephone Laboratories 1
Murray Hill, New Jersey
ATTN: J. R. Pierce

Hughes Aircraft Company 1
Culver City, California
ATTN: Mr. Milek, Librarian

Hughes Aircraft Company 1
Microwave Laboratory
Culver City, California
ATTN: Dr. A. D. Berk

Bell Telephone Laboratories 1
Technical Information Library
463 W. Street
New York 14, New York

RCA Laboratories 1
Princeton, New Jersey
ATTN: Dr. W. M. Webster

Federal Telecommunic. Labs 1
500 Washington Avenue
Nutley, New Jersey
ATTN: W. Derrick
K. Wing 1

Countermeasures Laboratory 1
Gilfillan Brothers, Inc.
1815 Venice Boulevard
Los Angeles, California

The Rand Corporation 1
1700 Main Street
Santa Monica, California
ATTN: Librarian

Motorola Riverside Res. Lab. 1
8330 Indiana Avenue
Riverside, California
ATTN: Mr. John Byrne

Ramo-Wooldridge Corporation 1
Control Systems Division
P.O. Box 900B
Hawthorne, California
ATTN: Librarian

Microwave Physics Laboratory 1
Sylvania Electric Products
P. O. Box 1296
Mountain View, California

Dr. J. E. Shepherd 1
Sperry Gyroscope Company
Great Neck, New York

W. L. Maxson Corporation 1
460 West 34th Street
New York 1, New York
ATTN: M. Simpson

Bertram G. Ryland, Manager 1
Spencer Laboratory
Raytheon Manufacturing Co.
Burlington, Massachusetts

Westinghouse Electric Corp. 1
Electronic Tube Division
Elmira, New York
ATTN: Mr. S.S.King, Librarian

Mr. Gilbert Kelton 1
Security Officer
Philips Laboratories
Irvington-on-Hudson, New York

R. E. McGuire, Librarian 1
Boeing Airplane Company
P.O. Box 3707
Seattle 24, Washington

Dr. Donald W. Kerst 1
General Atomic
P. O. Box 608
San Diego, California

Image Instruments, Inc. 1
2300 Washington Street
Newton Lower Falls 62, Mass.

Sylvania Electric Prod. Inc. 1
Waltham, Massachusetts
ATTN: Charles A. Thornhill

Research Division Library 1
Raytheon Company
28 Seyon Street
Waltham 54, Massachusetts

ITT Laboratories 1
15151 Bledsoe Street
San Fernando, California

Technical Research Group Inc. 1
2 Aerial Way
Syosset, New York

American Systems Incorporated 1
3412 Century Boulevard
Inglewood, California
ATTN: M. D. Adcock

Microwave Physics Laboratory 1
Sylvania Electric Products
P.O. Box 1296
Mountain View, California

U. S. Atomic Energy Commission 1
Tech. Information Service Ext.
P.O. Box 62
Oak Ridge, Tennessee